ISSN 8755-6839

SCIENCE OF TSUNAMI HAZARDS

Journal of Tsunami Society International

Volume 36 **Number 4** **2017**

Andrey Kozelkov [1,2)], Valentin Efremov [3)], Andrey Kurkin [2,4)], Efim Pelinovsky [2,5)], Nataliya Tarasova [1)] & Dmitry Strelets [6)]

1) Russian Federal Nuclear Center, All-Russian Scientific Research Institute of Experimental Physics, Sarov, **RUSSIA**
2) Nizhny Novgorod State Technical University named after R. E. Alekseev, Nizhny Novgorod, **RUSSIA**
3) Joint Stock Company 'Instrument Engineering Design Bureau named after Academician A.G. Shipunov', Tula, **RUSSIA**
4) Institute of Space Technologies, Peoples' Friendship University of Russia, Moscow, **RUSSIA**
5) Institute of Applied Physics, Nizhny Novgorod, **RUSSIA**
6) Moscow Aviation Institute, Moscow, **RUSSIA**

Theofilos Toulkeridis [1]*, Kervin Chunga [2], Willington Rentería [3], Fabian Rodriguez [1,4], Fernando Mato [1], Sissy Nikolaou [5], Mario Cruz D´Howitt [1], Davide Besenzon [6], Hugo Ruiz , Humberto Parra [1] and Xavier Vera-Grunauer [7,8]

[7]Facultad de Ingeniería, Universidad [1]Universidad de las Fuerzas Armadas ESPE, Sangolquí, **ECUADOR**
[2]Universidad Estatal Península Santa Elena, Facultad de Ciencias de la Ingeniería, La Libertad, **ECUADOR**
[3]Instituto Oceanográfico de la Armada del Ecuador (INOCAR), Guayaquil, **ECUADOR**
[4]Pontificia Universidad Católica del Ecuador (PUCE), Facultad de Economía, Quito, **ECUADOR**
[5]WSP Parsons Brinckerhoff, New York City, **USA**
[6]Escuela Superior Politecnica del Litoral, Facultad de Ingeniería en Ciencias de la Tierra, Guayaquil, **ECUADOR**
Católica de Santiago de Guayaquil (UCSG), Guayaquil, **ECUADOR**
[8]Geoestudios, SA, Guayaquil, **ECUADOR**

Alexandr RASSADIN [1], Artem TUGARYOV [1], Broneslav KISELMAN [1], Raissa MAZOVA1 AND Leopold LOBKOVSKY [2]

[1] R.E.Alekseev Nizhny Novgorod State Technical University, Nizhny Novgorod, **RUSSIA**
[2]P.P.ShirshovInstitute of Oceanology, Russian Academy of Sciences, Moscow, **RUSSIA**

WWW.TSUNAMISOCIETY.ORG

TSUNAMI SOCIETY INTERNATIONAL, 1741 Ala Moana Blvd. #70, Honolulu, HI 96815, USA.

SCIENCE OF TSUNAMI HAZARDS is a CERTIFIED OPEN ACCESS Journal included in the prestigious international academic journal database DOAJ, maintained by the University of Lund in Sweden with the support of the European Union. SCIENCE OF TSUNAMI HAZARDS is also preserved, archived and disseminated by the National Library, The Hague, NETHERLANDS, the Library of Congress, Washington D.C., USA, the Electronic Library of Los Alamos, National Laboratory, New Mexico, USA, the EBSCO Publishing databases and ELSEVIER Publishing in Amsterdam. The vast dissemination gives the journal additional global exposure and readership in 90% of the academic institutions worldwide, including nation-wide access to databases in more than 70 countries.

OBJECTIVE: Tsunami Society International publishes this interdisciplinary journal to increase and disseminate knowledge about tsunamis and their hazards.

Submit manuscripts of research papers, notes or letters to the Editor. If a research paper is accepted for publication the author(s) must submit a scan-ready manuscript, a Doc, TeX or a PDF file in the journal format. Issues of the journal are published electronically in PDF format. There is a minimal publication fee for authors who are members of Tsunami Society International for three years and slightly higher for non-members. Tsunami Society International members are notified by e-mail when a new issue is available. Permission to use figures, tables and brief excerpts from this journal in scientific and educational works is granted provided that the source is acknowledged.

Recent and all past journal issues are available at: http://www.TsunamiSociety.org CD-ROMs of past volumes may be purchased by contacting Tsunami Society International at postmaster@tsunamisociety.org Issues of the journal from 1982 thru 2005 are also available in PDF format at the U.S. Los Alamos National Laboratory Library http://epubs.lanl.gov/tsunami/

ISSN 8755-6839

SCIENCE OF TSUNAMI HAZARDS

Journal of Tsunami Society International

Volume 36 Number 4 2017

THREE-DIMENSIONAL NUMERICAL SIMULATION OF TSUNAMI WAVES BASED ON THE NAVIER-STOKES EQUATIONS

Andrey Kozelkov[1,2], Valentin Efremov[3], Andrey Kurkin[2,4], Efim Pelinovsky[2,5], NataliyaTarasova[1] & Dmitry Strelets[6]

1) Russian Federal Nuclear Center, All-Russian Scientific Research Institute of Experimental Physics, Sarov, Russia

2) Nizhny Novgorod State Technical University named after R. E. Alekseev, Nizhny Novgorod, Russia

3) Joint Stock Company 'Instrument Engineering Design Bureau named after Academician A.G. Shipunov', Tula, Russia

4) Institute of Space Technologies, Peoples' Friendship University of Russia, Moscow, Russia

5) Institute of Applied Physics, Nizhny Novgorod, Russia

6) Moscow Aviation Institute, Moscow, Russia

ABSTRACT

A numerical algorithm of solving the three-dimensional system of Navier-Stokes equations to simulate free surface waves and flows with gravity is presented. The main problem here is to ensure that the gravity force is properly accounted in the presence of discontinuities in the medium density. The task is made more complicated due the use of unstructured computational grids with collocated placement of unknown quantities and splitting algorithms based on SIMPLE-type methods. To obtain correctly the hydrostatic pressure, it is suggested that the contribution of the gravitational force in the equation for pressure should be distinguished explicitly; the latter being calculated by using the solution of the two-phase medium gravitational balance problem. To ensure the balance of the gravity force and the pressure gradient in the case of rest an algorithm in which the pressure gradient in the equation of motion is replaced by a modification considering the gravitational force action is suggested. This method is demonstrated by the example of tsunami wave propagation in the real water area of the World Ocean.

1. INTRODUCTION

At present, there are several methods used for modeling multiphase flows with a free surface, which differ in the way the latter is calculated. The first method is based on the 'Lagrangian' approach, in which a free surface is tracked either by moving the grid nodes or by particles (Shuvalov et al., 2012). The second method is based on the 'Euler' approach, in which special markers are introduced to track the free surface. Either particles (Lucy, 1977) or spatial marker functions (Harlow and Welch, 1965; Daly, 1969; Hirt and Nichols, 1981) that obey the convective transfer equation can act in the role of the above-mentioned markers. The second method is the most applicable in practice. It uses the volume fraction of fluid (VOF – Volume-of-fluid) as a marker function (Hirt and Nichols, 1981; Ubbink, 1977). The fluid-gas system in this approach is regarded as a single one-velocity medium with variable physical properties. This method is easily generalized is case of arbitrary unstructured grids and an arbitrary number of phases (Ubbink, 1977).

The determining force for waves and fluid flows with a free surface is the gravity force. The gravity force experiences a discontinuity on the free surface. It happens due to a sharp change in the medium density, resulting in a rupture in the pressure gradient magnitude, which in the case of the medium rest completely balanced the action of gravitational forces (Landau and Lifshitz, 1987).

The construction of a numerical algorithm correctly taken into account the gravity force and the pressure gradient value calculations is a non-trivial task. This is especially true for grids with a 'collocated' arrangement of unknown quantities, which is mainly used in practice, but leads to a weak coupling between the velocity and pressure fields (Ferziger and Peric, 2002; Jasak, 1996). Using the collocated arrangement of unknown quantities implies pressure and velocity determination in the same place (usually the cell center), leading to the appearance of even-odd oscillations, which can be eliminated by the use of the Rhie-Chow type method (Rhie and Chow, 1983). Papers (Gu et al., 1991; Mencinger, 2012; Majumdar, 1988) deal with the construction of a numerical algorithm ensuring the absence of numerical oscillations in the case of non-homogeneous gravity field. The volume force in the momentum conservation equation, in which the gravity force can act as the volume force, is analyzed in (Khrabry et al., 2010). To exclude oscillations in the velocity and pressure fields, it is proposed to use a correction of the Phie-Chow type (Rhie and Chow, 1983). However, this paper does not discuss problems with a strong discontinuity in the volume force field when arises the problem of the correct pressure gradient calculation, the value of which must completely balance the volume force when the medium is at rest. The theoretical analysis of the gravity force allowance is presented in (Mencinger, 2012). In addition to ideas borrowed from (Gu et al., 1991), an expression to interpolate the volume force and pressure on the inner faces of the computational grid, which provides the state of balance, is proposed. However, the considered examples demonstrate only the absence of oscillations in the velocity field but not the analysis of the obtained free surface forms. Similarly, when using arbitrary unstructured grids, the effectiveness of the algorithm is not considered. In (Khrabry et al., 2010), is presented an effective scheme to calculate the pressure gradient in the presence of gravitational forces. The scheme is based on the interpolation of the pressure gradient value with the medium density in the adjacent cells taken into account. This algorithm allows eliminating non-physical oscillations in the velocity field near the free surface. The algorithm efficiency, however, is demonstrated only on the orthogonal grids whose lines are parallel to the gravity direction.

This paper formulates a new algorithm to construct the pressure equation based on the Rhie-Chow method. The algorithm is constructed by replacing the gravity force by its direct discrete analogue in the equation. The expressions for a direct discrete analogue are formulated on the basis of hydrostatic approximation, which provides a correct pressure field on an arbitrary unstructured grid. To ensure the balance of the gravity force and the pressure gradient when the medium is at rest, an algorithm based on the replacement of the pressure gradient in the equation of motion by its modification considering the gravity action is proposed. The effectiveness of the proposed solution is explored on the example of the numerical simulation of tsunami wave propagation.

2. THE 3D NUMERICAL ALGORITHM

The VOF method unifies the continuity and the momentum conservation equations for all phases and solves for the resulting medium, whose properties linearly depend on the volume fraction of each phase.

The general system of multiphase medium equations has the form (Ferziger and Peric, 2002):

$$\begin{cases} \rho\dfrac{\partial u_i}{\partial t}+\dfrac{\partial \rho u_i u_j}{\partial x_j}-u_i\dfrac{\partial \rho u_j}{\partial x_j}=-\dfrac{\partial p}{\partial x_i}+\dfrac{\partial}{\partial x_j}\left(\mu\left(\dfrac{\partial u_i}{\partial x_j}+\dfrac{\partial u_j}{\partial x_i}\right)\right)+\rho g_i, \\ \dfrac{\partial u_i}{\partial x_i}=0, \\ \dfrac{\partial F_j}{\partial t}+u_i\dfrac{\partial F_j}{\partial x_j}=0,\ \ j=1\ldots N-1,\ \ F_N=1-\sum\limits_{j=1}^{N-1}F_j, \end{cases} \quad , \tag{1}$$

where $\rho=\sum\limits_{j=1}^{N}F_j\rho_j$ is the medium resulting density, $\mu=\sum\limits_{j=1}^{N}F_j\mu_j$ is the resulting medium viscosity, p is the pressure, u_i is the velocity component vector, N is the number of phases in the problem, F_j is the phase j volume fraction, g_i is the gravity vector. In the system (1), the equation of motion is written in the form giving the best results in the numerical solution of problems with a free surface (Landau and Lifshitz, 1987).

To solve the system (1), the classical SIMPLE/PISO-type splitting algorithms (Ubbink, 1997; Ferziger and Peric, 2002; Jasak, 1996) are used, as well as the completely implicit algorithm (Chen, Z.J., Przekwas, 2010; Darwish et al., 2009; Kozelkov et al., 2016b), the common feature of which is the derivation of the pressure equation by substituting a discrete analogue of the equation for the velocity into equation continuity. The present paper considers a discrete analogue of the velocity calculation equation with a purpose of formulating an algorithm allowing us to obtain a correct hydrostatic pressure in the cell centers in the case of the density field discontinuity. With finite-volume discretization this algorithm takes the form:

$$a_{PP}u_{i,P} + \sum_k a_{PN}u_{i,N} = R_{i,P} - \left(\frac{\partial p}{\partial x_i}\right)_P V_P + \rho g_i V_P\,, \tag{2}$$

where a_{PP} is the diagonal coefficient for the P cell, a_{PN} is the coefficient at the velocity value in the cell N adjacent to the face k, the summation is done over all internal faces, V_P is the cell volume (Fig. 1).

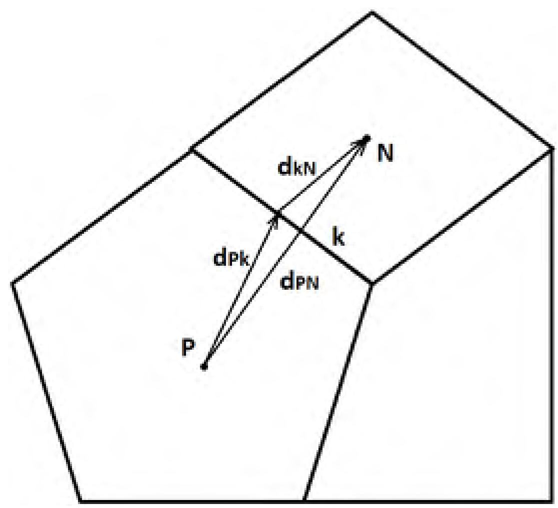

Figure 1. Two adjacent cells of the computational grid

From equation (2), the flow velocity is expressed as:

$$u_{i,P} = \frac{1}{a_{PP}}\left(R_{i,P} - \sum_k a_{PN}u_{i,N}\right) - \frac{V_P}{a_{PP}}\left(\frac{\partial p}{\partial x_i}\right)_P + \frac{V_P}{a_{PP}}\rho g_i = H_{i,P} - \frac{V_P}{a_{PP}}\left(\frac{\partial p}{\partial x_i}\right)_P + \frac{V_P}{a_{PP}}\rho g_i\,. \tag{3}$$

The velocity on the face $u_{i,k}$ is calculated by interpolating the expression (3) from the cell centers to the center of the face k with the weight λ_k . Exception is made for the pressure gradient whose contribution is replaced by its direct discrete analogue (Ubbink, 1997; Mencinger, 2012). The obtained expression for the velocity is substituted into the discrete continuity equation (1):

$$\sum_k u_{i,k} n_i S_k = \sum_k \left[\acute{I}_{\ k} n_i S_k - A_k \frac{p_N - p_P}{d_{PN}} S_k + A_k \left(\rho g_i\right)_k n_i S_k \right] = 0\,, \tag{4}$$

where $\acute{I}_k = \lambda_k H_{i,P} + (1-\lambda_k) H_{i,N}$, $A_k = \lambda_k \frac{V_P}{a_{PP}} + (1-\lambda_k)\frac{V_N}{a_{NN}}$, $u_{i,k}$ is velocity on the face k, n_i is the normal of the face k, S_k is the area of the face, the summation being carried out over all the faces of the cell P. The weight λ_k in practice is determined in various ways, for example, starting from the geometric distances from the cell center to the face center (Jasak, 1996), the values of the diagonal coefficients a_{PP} and a_{NN} (Rhie and Chow, 1983), or $\lambda_k = 0.5$ is accepted.

Equation (4) determines the pressure field in the each cell centre. If the system is balanced, the pressure field must have a hydrostatic distribution (Landau and Lifshitz, 1987). In the presented equation entry for calculating the pressure (4) there is the gravity magnitude interpolated to the face – ρg_i. In order to determine its value, which allows us to obtain a correct pressure distribution, we consider a model one-dimensional problem of a resting system consisting of two fluids with different densities in the gravitational force field (Fig. 2).

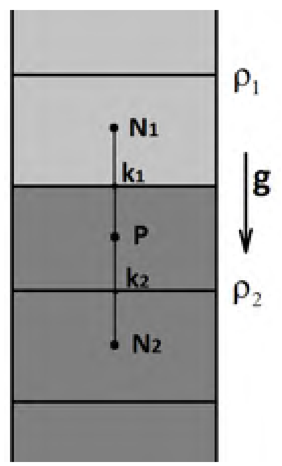

Figure 2.The system balance in the gravity field

In a state of balance, the velocities in the system are zero, so the equation for the pressure (4) takes the form:

$$A_{k_1}\left(\frac{p_{N_1} - p_P}{d_{PN_1}} - (\rho g)_{k_1} S_{k_1}\right) - A_{k_2}\left(\frac{p_{N_2} - p_P}{d_{PN_2}} - (\rho g)_{k_2} S_{k_2}\right) = 0. \quad (5)$$

The equation (5) shows that the term $(\rho g)_{k_1}$ determines the pressure drop between the cell centers P and N_1, and the term $(\rho g)_{k_1}$ does the same between the cell centers P and N_2. These pressure differences are calculated analytically (Landau and Lifshitz, 1987) under the assumption of a constant density within the cells:

$$p_{N_1} - p_P = g\left(d_{N_1 k_1}\rho_1 + d_{k_1 P}\rho_2\right), \tag{6}$$

where $d_{N_1 k_1}$ is the distance from the cell N_1 center to face k_1, $d_{k_1 P}$ is the distance from face k_1 to the cell P center.

Taking this into account, the equation (5) takes the form:

$$A_{k_1}\left(\frac{p_{N_1} - p_P}{d_{PN_1}} - g\frac{\left(d_{N_1 k_1}\rho_1 + d_{k_1 P}\rho_2\right)}{d_{PN_1}}\right) - A_{k_2}\left(\frac{p_{N_2} - p_P}{d_{PN_2}} - g\frac{\left(d_{N_2 k_2}\rho_1 + d_{k_2 P}\rho_2\right)}{d_{PN_2}}\right) = 0\,. \tag{7}$$

Obviously, the solution of the equation (7) leads to a pressure drop corresponding to the hydrostatic solution (6).

In the three-dimensional case, the hydrostatic pressure drop between the adjacent cells P and N is given by:

$$p_N - p_P = d_{i,Nk}g_i\rho_N + d_{i,kP}g_i\rho_P \quad . \tag{8}$$

Taking into account (8), the equation (4) can be written in the form:

$$\sum_k u_{i,k}n_i S_k = \sum_k \left[\acute{I}_{\,k} n_i S_k - A_k\frac{p_N - p_P}{d_{PN}}S_k + A_k d_{i,Nk}g_i\rho_N\right] = 0 \quad . \tag{9}$$

The equation (9) allows us to ensure the calculation of the correct hydrostatic pressure field in the cell centers for any method of interpolating the vector H_i on the face of the calculated model.

3. THE PRESSURE GRADIENT ALGORITHM CALCULATION

To balance gravity by the pressure gradient when the free surface is at rest, it is also necessary to ensure the correct pressure gradient calculation near the free surface. It was shown in (Mencinger, 2012) that the pressure gradient calculation done by conventional methods, for example, by the Gauss method (Jasak, 1996) or by the least squares method, leads to the incorrect result due to the existence of a pressure field kink in the free surface. To solve this problem, (Khrabry et al., 2010) suggests using the Gauss method with a modified expression to interpolate the pressure value on the inner faces of the cell P:

$$\left(\frac{\partial p}{\partial x_i}\right)_P = \frac{1}{V_P}\sum_k p_k S_{i,k}\,,$$

where

$$p_k = \xi\left(\frac{p_P d_{kN}\rho_N + p_N d_{Pk}\rho_P}{d_{kN}\rho_N + d_{Pk}\rho_P}\right) + (1-\xi)\left(\frac{p_P d_{kN} + p_N d_{Pk}}{d_{kN} + d_{Pk}}\right), \tag{10}$$

a $\xi = \cos^2\alpha$, α is the angle between the normal of the face k and the direction of the gravitational force. This approach allows us to estimate correctly the pressure gradient near the free surface in the case of using an orthogonal computational grid with grid lines parallel to the direction of the gravitational force. However, as shown below, the use of expression (10) in the case of an unstructured grid leads to an unsatisfactory result.

In this paper, we propose to use another method that allows obtaining good results on any computational grid type. The main idea of the method is as follows: it is not necessary to calculate the pressure gradient in order to solve the motion equation. For this purpose it is enough to calculate the expression representing the simultaneous contribution of the pressure gradient and the force of gravity. To calculate such an expression, we introduce the variable p^*, which is a modified pressure field:

$$\frac{\partial p^*}{\partial x_i} = \frac{\partial p}{\partial x_i} - \rho g_i\,. \tag{11}$$

To calculate the right-hand side of the equation (3) with the newly introduced variable, we write the integral expression (11) for the cell volume P:

$$\int\limits_{V_P} \frac{\partial p^*}{\partial x_i} dV = \int\limits_{V_P} \frac{\partial p}{\partial x_i} dV - \int\limits_{V_P} \rho g_i dV\,.$$

The transition to the surface integral gives:

$$\int\limits_{V_P} \frac{\partial p^*}{\partial x_i} dV = \int\limits_{S_P} (p - G) n_i dS\,, \tag{12}$$

where G is the antiderivative of the function ρg_i, which, assuming the density inside the cells constant, can be written as:

$$G = \rho g_i r_i + C,$$

where r_i is the radius vector, C is an arbitrary constant. The presence of the constant C allows us to select the reference point of the vector r_i in an arbitrary way, for the cell P we choose it in the center of the cell, then:

$$G = \rho g_i \left(r_i - r_{P,i} \right). \tag{13}$$

The substitution of (13) into (12) and finite-volume discretization (13) yields:

$$\int_{V_P} \frac{\partial p^*}{\partial x_i} dV = \int_{S_P} \left(p - \rho g_i \left(r_i - r_{P,i} \right) \right) n_i dS \approx \sum_k \left[p - \rho g_i \left(r_i - r_{P,i} \right) \right]_k n_{k,i} S_k \ .$$

The second term in the square brackets of the last expression is the contribution of hydrostatic pressure to the total pressure. This contribution is calculated with respect to the center of the cell P. At the center of the cell P it goes to zero, and at the center of the next cell N it is calculated according to the expression (8) which is used to compose the equation for pressure. Using the linear interpolation with weight λ_k to calculate the values on the face, we get:

$$\begin{aligned} \int_{V_P} \frac{\partial p^*}{\partial x_i} dV &\approx \sum_k \left[\lambda_k \left[p - \rho g_i \left(r_i - r_{P,i} \right) \right]_P + (1 - \lambda_k) \left[p - \rho g_i \left(r_i - r_{P,i} \right) \right]_N \right] n_{k,i} S_k = \\ &= \sum_k \left[\lambda_k p_P + (1 - \lambda_k) \left(p - d_{i,Nk} g_i \rho_N - d_{i,kP} g_i \rho_P \right)_N \right] n_{k,i} S_k . \end{aligned} \tag{14}$$

The physical meaning of the expression (14) is reduced to the fact that the gravitational force ρg_i subtracts from the pressure gradient only the part that it contributed when forming the equation for the pressure (9). This allows ensuring the pressure gradient and the force of gravity balance when the medium is at rest.

The numerical results demonstrated the effectiveness of the proposed numerical algorithms for calculating pressure and the pressure gradient in problems with a free surface are presented in (Efremov et al., 2017). Numerical experiments were carried out using the LOGOS code, which is intended for solving conjugate three-dimensional problems of convective heat and mass transfer, aerodynamics and hydrodynamics on parallel computers (Betelin et al., 2014; Deryugin et al., 2015). The LOGOS code successfully underwent verification and showed fairly good results in a series of various hydrodynamic problems, including non-stationary turbulent flow (Kozelkov et al., 2015a, 2015b, 2016b), as well as geophysical phenomena based on multiphase Navier-Stokes equations (Kozelkov et al., 2015c, 2015d, 2016a; 2016c).

4. MODELLING OF THE 2003 MONTSERRAT TSUNAMI

The presented method is of great significance when considering gravity in the numerical modeling of flows with a free surface. This significance is particularly evident in the modeling of tsunami wave propagation over large distances. In comparison with the size of the water area where tsunami wave propagates, the source is small enough: - a tsunami can spread thousands of kilometers, and the source size is only a few kilometers (for landslide tsunami) or several tens of kilometers (for tsunami of seismic origin). In this case, the ocean surface outside the tsunami wave zone should not fluctuate during the entire numerical calculation. In practice, numerical solution oscillations for a free surface are allowed to be much smaller than the amplitude of the propagating wave. Such numerical oscillations should not grow. The proposed method makes it possible to achieve a stable count and control of the numerical oscillation amplitude on arbitrary unstructured grids.

This method was used to model the 2003 tsunami generated by the pyroclastic flow descent into the water, resulting from the Soufriere volcano eruption on the island of Montserrat in the Caribbean Sea (Pelinovsky et al., 2004). In (Pelinovsky et al., 2004) two approaches were used to model it. In the first case, a hydrodynamic source in the form of a cone was used as the initial approximation, and the propagation was computed by using the shallow water code TUNAMI (Goto et at., 1997), recommended by UNESCO for tsunami studies. In the second case, the pyroclastic flow was generated using the model described in (Watts and Waythomas, 2003), and the wave propagation was computed using the FUNWAVE code (Kirby et al., 1998), based on the nonlinear-dispersion theory. Later, after adding a block to calculate various initial disturbances, this code was called GEOWAVE. A rather significant difference in the results obtained with the help of these approaches is shown in (Pelinovsky et al., 2004). This difference can be observed both in the fundamental wave height prediction and in the wave pattern as a whole. It should be noted that the use of the nonlinear-dispersion theory is the most appropriate. As the hydrodynamic source in the form of a cone (Fig. 3a) was used as the initial condition for both calculations in (Pelinovsky et al., 2004), the source generated by the model described in (Watts and Waythomas, 2003) is taken for an adequate comparison of the tsunami distribution. The source obtained by this model also has the form of a cone (Fig. 3b), the geometric parameters of which correspond to the descending pyroclastic flow. The initial tsunami wave amplitude in the source is 1.26 meters. The distance between the calculated grid nodes is equal to 500 meters.

Figure 4 shows the results of computations the tsunami propagation within the framework of the Navier-Stokes equations with the help of the LOGOS code in comparison with the calculation results employing the non-linear dispersion theory using the GEOWAVE code. As can be seen, the figures are almost identical qualitatively. The quantitative comparison of the tide gauge records presented in Fig. 5 can also be considered very satisfactory. The first incoming waves to the north-western part of the island of Guadeloupe and to the island of Antigua are almost identical. It can be seen that the first three waves are well predicted by both methods, although their heights are somewhat different. Subsequent waves are different to a greater extent, and the Navier-Stokes equations lead to a more pronounced vibrational character. The waves calculated from the nonlinear-dispersion model, however, are more rapidly damped. These differences can be associated with many factors and require additional research. These factors are primarily the models themselves; they are different and are solved by using various numerical approaches, namely, finite differences and finite volumes. Secondary factors include the grid model resolution and the numerical approximation schemes used

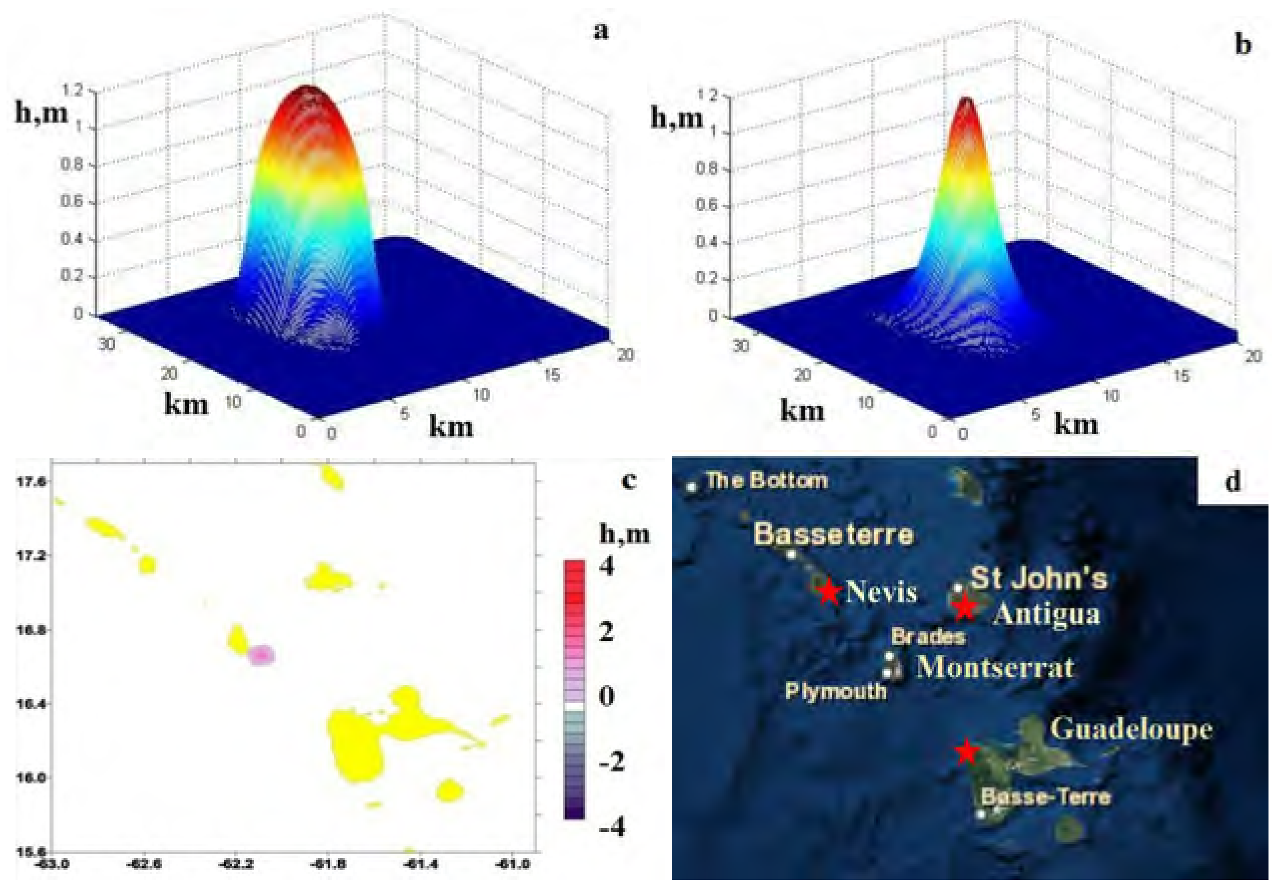

Figure 3. Initial tsunami disturbance: *a* – hydrodynamic source, *b* – the profile obtained by using the GEOWAVE code, *c* – calculation area, *d* – tide gauge positioning

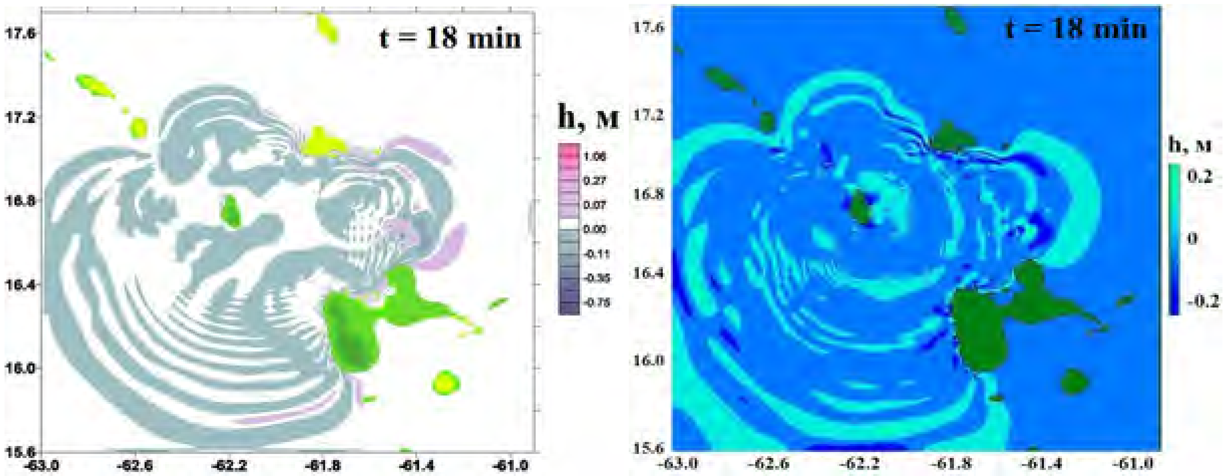

Figure 4. Tsunami propagation snapshots: GEOWAVE (left) and LOGO (right)

5. CONCLUSION

The given paper is concerned with the problem of constructing a numerical algorithm which ensures the correct calculation of the gravitational force and the pressure gradient value. The calculation is carried out in the case of medium density discontinuities, which are always present in the problems with a free surface. To obtain the correct field of hydrostatic pressure, when compiling the equation for pressure and its calculation, it is proposed to use the algorithm to isolate the gravity force contribution. In doing so, the solution of the problem of a two-phase medium gravitational equilibrium is used. The correct pressure gradient calculation in the event of gravitational force field discontinuities is ensured by using an algorithm that allows us to obtain good results on any computational grid type. The main idea of the algorithm consists in direct calculating the contribution of the pressure gradient and the gravity force to the equation of motion.

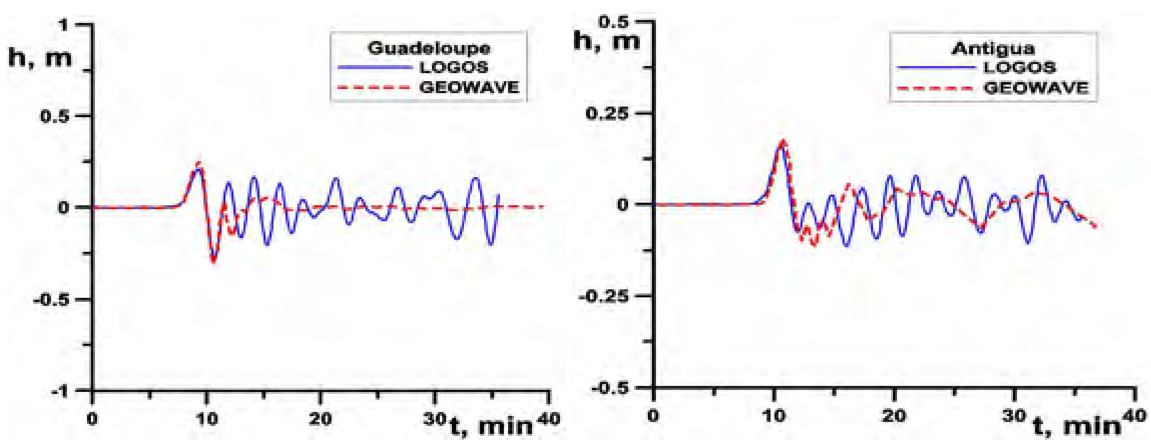

Figure 5. Comparison of tide gauge records on the islands of Guadeloupe and Antigua

The possibility of the proposed algorithm in tsunami problem use is demonstrated on the example of the tsunami simulation that occurred in the pyroclastic flow descent during the volcano eruption on the island of Montserrat in the Caribbean in 2003.

ACKNOWLEDGEMENTS

This study was initiated in the framework of the state task programme in the sphere of scientific activity of the Ministry of Education and Science of the Russian Federation (projects No.5.4568.2017/6.7 and No. 5.5176.2017/8.9), grant of the President of the Russian Federation NSh-6637.2016.5 and RFBR grants 16-01-00267, 15-45-02061 and 17-05-00067.

REFERENCES

1. Betelin, V.B., Shagaliev, R.M., Aksenov, S.V., Belyakov, I.M., Deryuguin, Yu.N., Kozelkov, A.S., Korchazhkin, D.A., Nikitin, V.F., Sarazov, A.V., and Zelenskiy, D.K. Mathematical simulation of hydrogen–oxygen combustion in rocket engines using LOGOS code. Acta Astronautica, 2014, vol. 96, 53-64.
2. Chen, Z.J., and Przekwas, A.J. A coupled pressure-based computational method for incompressible/compressible flows. Journal of Computational Physics, 2010, vol. 229, 9150-9165.
3. Daly, B.J. A technique for including surface tension effects in hydrodynamic calculations. J. Comput. Phys, 1969, vol. 4, 97-117.
4. Darwish, M., Sraj, I., and Moukalled, F. A coupled finite volume solver for the solution of incompressible flows on unstructured grids. Journal of Computational Physics, 2009, vol. 228, 180-201.
5. Deryugin, Yu.N., Zhuchkov, R.N., Zelenskiy, D.K., Kozelkov, A.S., Sarazov, A.V., Kudimov, N. F., Lipnickiy, Yu.M., Panasenko, A.V., and Safronov, A.V. Validation results for the LOGOS multifunction software package in solving problems of aerodynamics and gas dynamics for the lift-off and injection of launch vehicles. Mathematical Models and Computer Simulations, 2015, vol. 7, no. 2, 144-153.
6. Efremov, V.R., Kozelkov, A.S., Kornev, A.V., Kurkin, A.A., Kurulin, V.V., Strelets, D.Yu., and Tarasova, N.V. Method for taking into account gravity in free-surface flow simulation. Computational Mathematics and Mathematical Physics, 2017, vol. 57, no. 10, 1720-1733.
7. Ferziger, J.H., and Peric, M. Computational Method for Fluid Dynamics. Springer-Verlag. New York, 2002.
8. Goto, C., Ogawa, Y., Shuto, N., and Imamura, N. Numerical method of tsunami simulation with the leap-frog scheme (IUGG/IOC Time Project), IOC Manual, UNESCO, no. 35, 96 p., 1997.
9. Gu, C.Y., Taylor C., and Chin, J.H. Computation of flows with large body forces. Numerical Methods in Laminar and Turbulent Flow, Pineridge Press, Swansea, 1991, 294-305.
10. Harlow, F.H., and Welch, J.E. Numerical calculation of time-dependent viscous incompressible flow. Phys. Fluids. 1965, vol. 8, 2182-2189.
11. Hirt, C.W., and Nichols, B.D. Volume of fluid (VOF) method for the dynamics of free boundaries. Journal of computational physics. 1981, vol. 39, 201-226.

13. Jasak, H. Error Analysis and Estimation for the finite volume method with applications to fluid flows. PhD Thesis, Department of Mechanical Engineering, Imperial College, 1996.
14. Khrabry, A.I., Smirnov, E.M., and Zaytsev, D.K. Solving the Convective Transport Equation with Several High-Resolution Finite Volume Schemes: Test Computations. Computational Fluid Dynamics 2010 – Proceedings of the 6th International Conference on Computational Fluid Dynamics, ICCFD 2010, 535-540.
15. Kirby, J., Wei, G., Chen, Q., Kennedy, A., and Dalrymple, R. Fully Nonlinear Boussinesq Wave Model Documentation and Users Manual. Center for Applied Coastal Research Department of Civil Engineering University of Delaware, Newark DE 19716, Research Report №. CACR-98-06, 1998.
16. Kozelkov, A.S., Krutyakova, O.L., Kurkin, A.A., Kurulin, V.V., and Tyatyushkina, E.S. Zonal RANS–LES Approach Based on an Algebraic Reynolds Stress Model. Fluid Dynamics, 2015b, vol. 50, no. 5, 621-628.
17. Kozelkov, A.S., Kurkin, A.A., and Pelinovskii, E.N. Effect of the Angle of Water Entry of a Body on the Generated Wave Heights. Fluid Dynamics, 2016c, vol. 51, no. 2, 288-298.
18. Kozelkov, A.S., Kurkin, A.A., Pelinovskii, E.N., and Kurulin, V.V. Modeling the Cosmogenic Tsunami within the Framework of the Navier–Stokes Equations with Sources of Different Types. Fluid Dynamics, 2015c, vol. 50, no. 2, 306-313.
19. Kozelkov, A.S., Kurkin, A.A., Pelinovskii, E.N., Kurulin, V.V., and Tyatyushkina, E.S. Modeling the Disturbances in the Lake Chebarkul Caused by the Fall of the Meteorite in 2013. Fluid Dynamics, 2015d, vol. 50, no. 6, 134-149.
20. Kozelkov, A.S., Kurkin, A.A., Pelinovsky, E.N., Tyatyushkina, E.S., Kurulin, V.V., and Tarasova, N.V. Landslide-type tsunami modelling based on the Navier-Stokes Equations. Science of Tsunami Hazards, 2016a, vol. 35, no. 3, 106-144.
21. Kozelkov, A., Kurulin, V., Emelyanov, V., Tyatyushkina, E., and Volkov, K. Comparison of convective flux discretization schemes in detached-eddy simulation of turbulent flows on unstructured meshes. Journal of Scientific Computing, 2015a, no. 89, 1-16.
22. Kozelkov, A.S., Kurulin, V.V., Lashkin, S.V., Shagaliev, R.M., and Yalozo, A.V. Investigation of Supercomputer Capabilities for the Scalable Numerical Simulation of Computational Fluid Dynamics Problems in Industrial Applications. Computational Mathematics and Mathematical Physics, 2016b, vol. 56, no. 8, 1506-1516.
23. Landau, L.D., and Lifshitz, E.M. Fluid Mechanics, Second Edition. Pergamon Press, 1987.
24. Lucy, L.B. A numerical approach to the testing of the fission hypothesis, Astron. J., 1977, vol. 82 (12), 1013-1024.
25. Majumdar, S. Role of under-relaxation in momentum interpolation for calculation of flow with nonstaggered grids. Numer. Heat Transfer., 1988, vol. 13, 125-132.
26. Mencinger, J. An Alternative Finite Volume Discretization of Body Force Field on Collocated Grid. Finite Volume Method - Powerful Means of Engineering Design, 2012, 101-116.
27. Pelinovsky, E., Kozelkov, A., Zahibo, N., Dunkly, P., Edmonds, M., Herd, R., Talipova, T., and Nikolkina, I. Tsunami generated by the volcano eruption on July 12-13, 2003 at Montserrat, Lesser Antilles. Science of Tsunami Hazards, 2004, vol. 22, no. 1, 44-57.
28. Rhie, C.M., and Chow, W.L. Numerical study of the turbulent flow past an airfoil with trailing edge separation, AIAA Journal, 1983, vol. 21, 1525-1532.

29. Shuvalov, V.V., Dypvik, H., Kalleson, E., Setsa, R., and Riis, F. Modeling the 2.7 km in Diameter, Shallow Marine Ritland Impact Structure. Earth Moon Planets, 2012, no. 108, 175-188.
30. Ubbink, O. Numerical prediction of two fluid systems with sharp interfaces. PhD Thesis, Imperial College, 1997.
31. Watts, Ph., and Waythomas, C.F. Theoretical analysis of tsunami generation by pyroclastic flows. Journal of Geophysical Research, 2003, vol. 108(B12), 1-21.

ISSN 8755-6839

SCIENCE OF TSUNAMI HAZARDS

Journal of Tsunami Society International

Volume 36 Number 4 2017

THE 7.8 M_w EARTHQUAKE AND TSUNAMI OF 16th April 2016 IN ECUADOR: Seismic Evaluation, Geological Field Survey and Economic Implications

Theofilos Toulkeridis[1]*, Kervin Chunga[2], Willington Rentería[3], Fabian Rodriguez[1,4], Fernando Mato[1], Sissy Nikolaou[5], Mario Cruz D´Howitt[1], Davide Besenzon[6], Hugo Ruiz[1], Humberto Parra[1] and Xavier Vera-Grunauer[7,8]

[1]Universidad de las Fuerzas Armadas ESPE, Sangolquí, Ecuador
[2]Universidad Estatal Península Santa Elena, Facultad de Ciencias de la Ingeniería, La Libertad, Ecuador.
[3]Instituto Oceanográfico de la Armada del Ecuador (INOCAR), Guayaquil, Ecuador
[4]Pontificia Universidad Católica del Ecuador (PUCE), Facultad de Economía, Quito, Ecuador
[5]WSP Parsons Brinckerhoff, New York City, USA
[6]Escuela Superior Politecnica del Litoral, Facultad de Ingeniería en Ciencias de la Tierra, Guayaquil, Ecuador
[7]Facultad de Ingeniería, Universidad Católica de Santiago de Guayaquil (UCSG), Guayaquil, Ecuador
[8]Geoestudios, SA, Guayaquil, Ecuador

*Corresponding author: ttoulkeridis@espe.edu.ec

ABSTRACT

We evaluated the recent earthquake and tsunami responsible for considerable damage and 663 deaths due to a 7.8Mw movement on the 16th of April 2016. The seismic event filled tens of thousands in refugee camps and affected some two million persons directly. The potential of high losses and damage with a total of 29,672 properties, including family houses, is also given by the fact that the infrastructure of the fishing, tourism and other industries and the movement to live along the beaches, have been highly developed within the last decades along the Ecuadorian coasts. The geological survey and determination of field data were performed three days after the main seismic event, allowing to obtain 290 data coseismic effects on the ground that allowed to evaluate the maximum macroseismic intensities as well as the predominant geomorphological features.The results of these sampling stations allowed to reconstruct a geological map with isoseismals fields of intensities. With

all the compiled and recorded coseismic data in the field of higher macroseismic intensities, we proceeded to produce a map of intensities applying the definitions and degrees of the ESI 2007 scale. We also evaluated the distribution and intensities of the aftershocks demonstrating the spatial-temporal affinities. The occurred tsunami, although less destructive than previous in the same region has been documented with all details available.

The economical assessment included in this study concludes that this earthquake impacted a large part of a variety of coastal cities destroying between 70 and 80% of some close-by villages and cities with a distance of 140-150 km of the epicenter, which suffered damages of their buildings within 40 to 55%, in which lines of electricity transmission, infrastructure of water supply, hospitals, schools, private and public buildings, main roads and highways have been severely affected or even completely destroyed. The costs of the damages of the mentioned infrastructure are summing up an approximate loss of some 3.3 billion USD, being equivalent to 3.31 % of the Ecuadorian GDP. In addition to losses in infrastructure and properties, over 28 thousand jobs were lost and about 300 million US$ in trade and businesses.

Keywords: *Earthquake, Tsunami, seismic damage, economic losses, Ecuador*

1. INTRODUCTION

The deadliest of all natural hazards by death toll are earthquakes along with their secondary affects like tsunamis (Kahn, 2005; Anbarci et al., 2005; Raschky, 2008; Marano et al., 2010; Holzer and Savage, 2013). The recurrance of seismic events has been ~~studied~~ extensively ~~by~~ researched (e.g., McGuire, 1995; Shome et al., 1998; Ruff and Kanamori, 1980; McCaffrey, 2008). Earthquakes also generate tsunamis, either being in or close to masses of water, like lakes, seas or oceans, generating landslides or other types of massive mass movements or failures (Gutenberg, 1939; Pararas-Carayannis, 1967; Synolakis et al., 2002; Bardet et al., 2003; Gusiakov, 2005; Tinti et al., 2005; Pararas-Carayannis, 2006; 2010; 2012; 2014; Bryant, 2014). There is at least a dozen of known earthquakes and subsequent tsunamis that have claimed more than 100,000 lives. Among these, two single events in China caused more than 700,000 human losses (Butler et al., 1979; Chen, 1988; Gang, 1989; Hou et al., 1998; Gupta et al., 2001), and the 2004 seismically-induced tsunami claimed some 280,000 lives in Indonesia and neighbouring countries (Sieh, 2005; Ghobarah et al., 2006).

In Ecuador, around one dozens of tsunamis have been generated during the past two centuries, close-by or above the Colombian-Ecuadorian trench within the existing geodynamic setting shown on Fig. 1 (Berninghausen, 1962; Kanamori and McNally, 1982; Pararas-Carayannis, 2012). Moreover, recent bathymetric mapping detected submarine landslide scars of a steep-sided fracture zone named "Yaquína Fracture Zone" shown on Fig. 2, that is certainly capable of generating tsunamis (Collot et al., 2004; 2005; 2010; Ratzov et al., 2007; Collot et al., 2010; Ioualalen et al., 2011).

The focus of this paper is the evaluation of the M_w7.8 earthquake on the 16th of April 2016, which caused hundreds of deaths and considerable damage and generated a tsunami detected during its movement along the Ecuadorian shores.

2. GEODYNAMI SETTING OF ECUADOR AND SEISMOGENIC ORIGIN

Due to its geodynamic situation along the Pacific Rim, the coastal Ecuadorian continental platform is often the target of earthquake activity and subsequent tsunamis (Gusiakov, 2005; Pararas-Carayannis, 2012; Rodriguez et al., 2016). The active continental margin and associated subduction zone between the oceanic Nazca Plate with the continental South American and Caribbean Plates (Fig. 1), both separated by the Guayaquil-Caracas Mega Shear (Kellogg and Vega, 1995; Gutscher et al., 1999; Egbue and Kellog, 2010) give rise to tsunamis of tectonic, as well submarine landslide origin (Shepperd and Moberly, 1981; Pontoise and Monfret, 2004; Ratzov et al, 2007; 2010; Ioualalen et al., 2011; Pararas-Carayannis, 2012). The main seismic source in the Ecuadorian territory is the subduction zone, which is about 756 kilometers (km) long, at a distance between 60 and 150 km from the coastline of continental Ecuador.

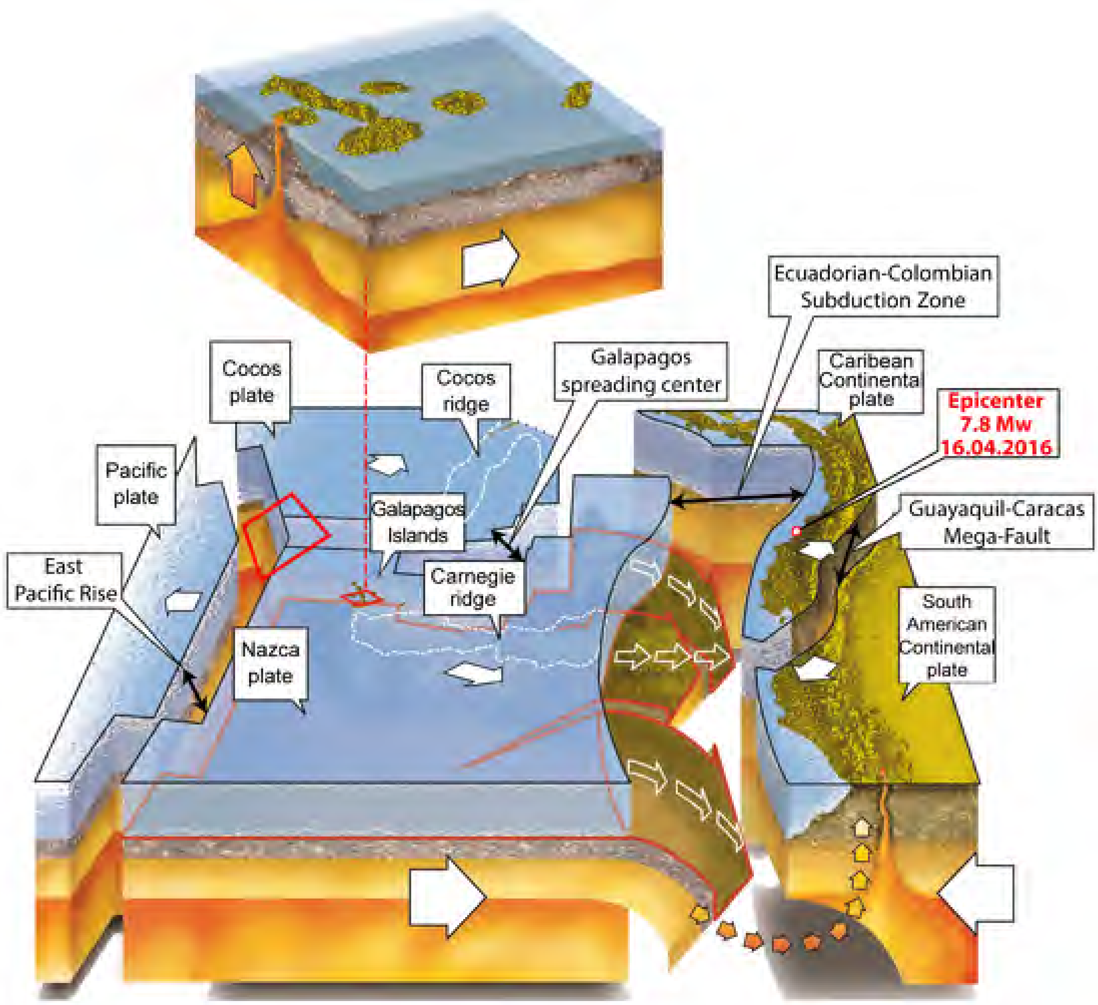

Fig. 1: Geodynamic setting of Ecuador, the Galapagos Islands and the Carnegie Ridge. Adapted from Toulkeridis, 2013 and Rodriguez et al., 2016.

Another origin of earthquakes and tsunamis has been credited to the Galápagos volcanism (Toulkeridis, 2011). The active Galápagos hotspot has produced several voluminous shield-volcanoes, most of which are inactive due to the ESE-movement of the overlying Nazca oceanic plate (Holden and Dietz 1972; Toulkeridis, 2011). The main Galápagos Islands are located south of the EW-trending Galápagos Spreading Center, east of the NS-trending East Pacific Rise, and approximately 1,000 km west of the Ecuadorian mainland.

The volcanic activity and subsequent plate drifting have generated two aseismic volcanic ridges: (i) the Cocos Ridge moving NE above the Cocos Plate and (ii) the Carnegie Ridge moving East above the Nazca Plate (Harpp et al., 2003). These submarine extinct volcanic ridges are the result of cooling/contraction reactions of magma, as they slowly sunk below the sea surface due to lack of magma supply, lithospheric movement and strong erosional processes (Fig. 1). With time, these ridges, as well as various microplates, have accreted on the South American continent (Reynaud et al., 1999; Harpp and White, 2001).

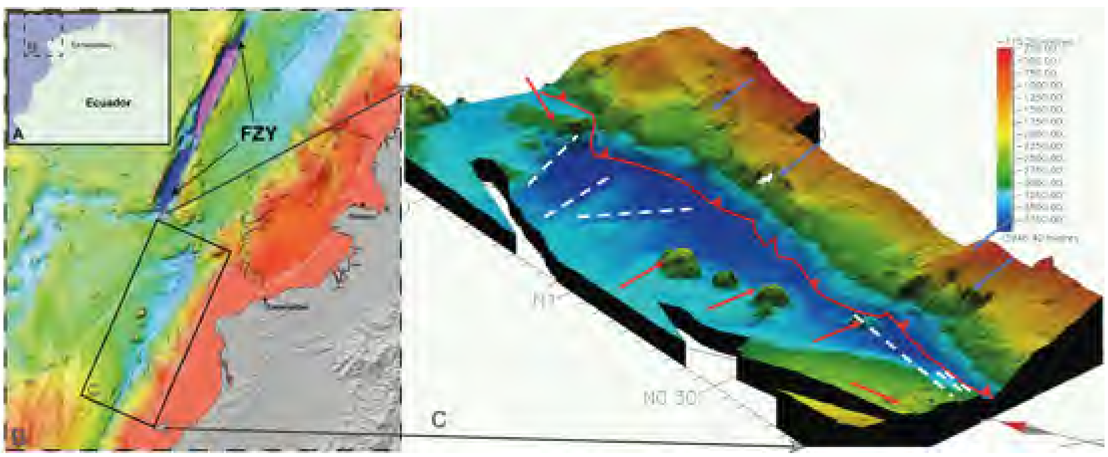

Fig. 2: (a) Detailed morphology of continetal rim of NW Ecuador. Inlet (b) shows the Fracture Zone of Yaquina (FZY) extension, and (c) highlights geodynamic aspects, such as deformation front between Nazca Oceanic and Carribean Continental Plates (red line), active faults at oceanic crust floor (white dashed lines), seamounts entering the subduction zone (red arrows), and scars of landslides, fissures and submarine debris (blue arrows). Adapted from Collot et al., 2010.

Nonetheless, such aseismic ridges, like Carnegie Ridge, may become an obstacle in the oblique subduction process by generating a potential valve of marine quakes within the subduction zone with earthquakes and occasionally tsunamis along the Ecuadorian coast (Pararas-Carayannis, 2012). The Carnegie Ridge collides towards the Ecuadorian continental margin with an average velocity of 5 cm/year at a latitude between 1°N and 2°S (Pilger, 1983).

From historic records of the last two centuries, the Ecuadorian shoreline has experienced strong, locally-generated earthquakes and marine quakes, with occasional triggering of tsunamis. On of these events was the great earthquake of 1906 with estimated M_w8.8 and 600-km long rupture area

(Rudolph and Szirtes, 1911; Kelleher, 1972; Beck and Ruff, 1984; Kanamori and McNally, 1982; Swenson and Beck, 1996; Pararas-Carayannis, 2012), with scarce evidence of paleo-tsunami deposits (Chunga and Toulkeridis, 2014). Other earthquakes with subsequent tsunamis along the Ecuador–Colombia subduction zone include the tsunamis of 1942 (M_w7.8), 1958 (M_w7.7) and 1979 (M_w8.2) within the 1906 rupture area (Collot et al., 2004). While the 1906 event caused the death of up to 1,500 persons in Ecuador and Colombia with an unknown financial damage to the existing infrastructure, the 1979 tsunami killed at least 807 persons in Colombia and destroyed approximately 10,000 homes, knocking out electric power and telephone lines (Pararas-Carayannis, 1980; USC&GS, 2016a).

Evaluation of the last marine quakes which generated tsunamis, suggests that the probability of a major or great earthquake in this margin region is highly likely, especially as there appears to be substantial strain accumulation in this region (Pararas-Carayannis, 2012). Considering that the last earthquake in 1979 did not release the amount of energy of the 1906 event, there is a high calculated probability of a tsunami of similar magnitude to that of 1906 in the near future, due to a potential earthquake within the Ecuadorian-Colombian trench. Based on historic evidence of tsunamis in Ecuador from the last 200 years, the estimated probability of a strike in 2015 reached 87% (Rodriguez et al., 2016). A potential future tsunami may be even more destructive than the one in the past if it occurs near high tide (Pararas-Carayannis, 2012). The risk exposure is greater since, in the last decades, the population density has increased along the shorelines and the infrastructure of the major industries of fishing and tourism is also concentrated along the shores.

3. GEOLOGICAL AND TECTONIC SETTING OF THE EPICENTRAL AREA AND IMPLICATIONS FOR SEISMIC WAVES

The rock deposits from Pedernales to Bahia de Caraquez are represented by tertiary geological formations (Oligocene to Miocene), with some minor recent rock formations like the Onzole and Borbon being of the Pliocene. The Dos Bocas and Villingota units belong to the Tosagua formation are the oldest sedimentary rocks in the epicentral area of the 2016 earthquake besides the basaltic basement. The Dos Bocas formation consists of brown, well stratified hard shales, with interbedded siltstones and fine to medium-grained sandstones, with minor thin abundant gypsum veinlets being fractures filling as well as thin sandstone and dolomite layers. This stratigraphic sequence is followed by the younger lithologic units of the Villingota Formation, which consists of thin layers of gray tuffaceous shales, being interbedded with some medium-grained yellow sandstones (Bristow and Hoffstetter, 1977; Baldock, 1982).

Rock appears broadly in the epicentral area and is well evident in slopes of hills of San Vicente and Bahia de Caraquez that have origin of the Onzole Formation (Stainforth, 1948). They consist of laminated siltstone interspersed with fine layers of sandstones and fracture fillings of gypsum. Some of the siltstone in the Onzole formation is underlying sandstones of the Borbon formation, while the base of the crust correspond to the Cretaceous basaltic formation of Piñon (Tschopp, 1948; Bristow y Hoffstetter, 1977; Feininger, 1980; Lebrat et al., 1987).

The Digital Terrain Model (DTM) interpretation of Fig. 3 demonstrates the existence of pronounced system of reverse faults with NNE-SSW directions, characterized by a component of dextral transcurrent. Possibly this system is related to the compressional forces acting on the coast, where clastic sedimentary rocks are dominant (Reyes and Michaud, 2012). In the study area, the faults observed do not evident NW-SE directions, except for a block located between Pedernales and Canaveral, limited by older regional faults of NNW-SSE directions that have been intersected by the predominant NNE-SSW fault system.

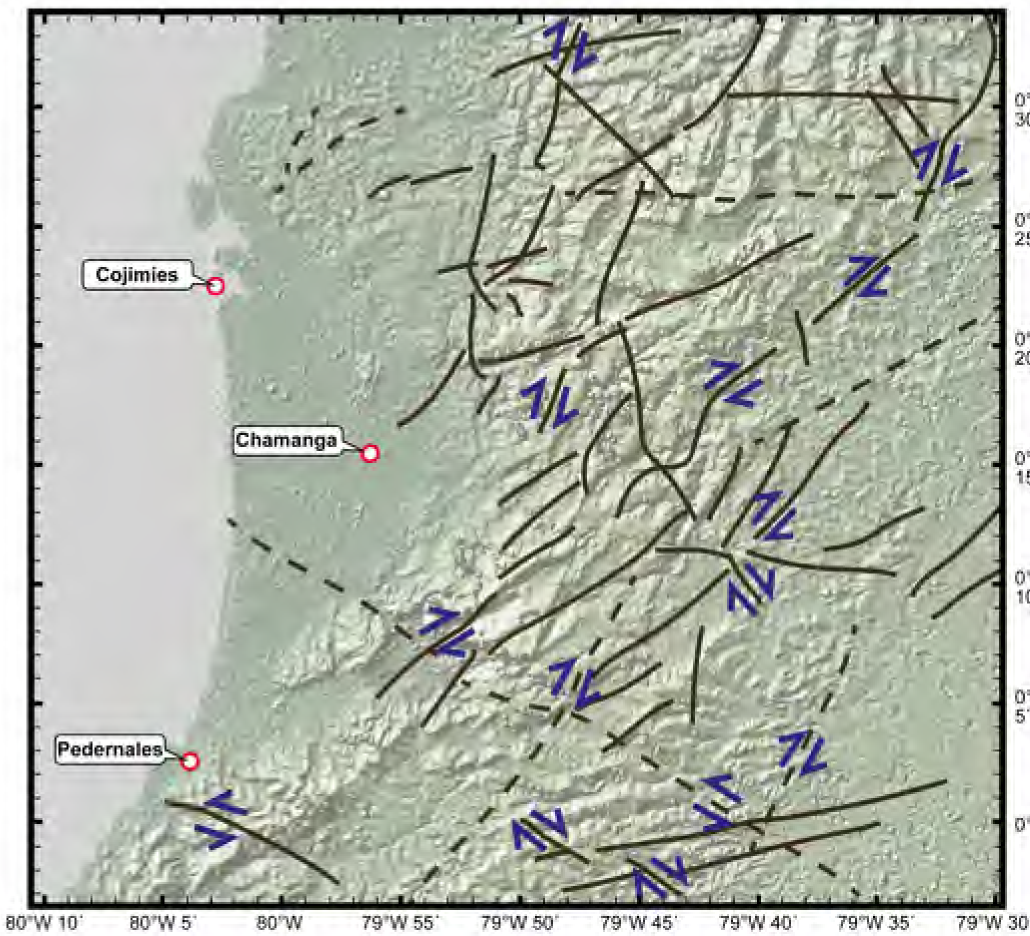

Fig. 3. Digital Terrain Model (DTM) with the schematic tectonic analysis of the Cordillera Costanera in the section Pedernales - Cojimíes.

The propagation of seismic waves differs in the various rock types, depending mainly on their stiffness and lithological consistency and thickness. Moreover, site amplification effects may be generated as the waves propage through the Holocene sediments (Sato et al., 2012). Geomorphologically, the epicentral area is formed by the supratidales coastal plains, areas of depressions between hills, plains of paleo-meander floodplain which can affect the intensity of the ground motions from both a topographic and geologic perspective (Chunga et al., 2016; Papanikolaou et al., 2010).

Watersheds of the coastal region of Manabi are characterized by alternating periods of erosion and sedimentation, with frequent alluvial fans deposited on hill tops. One of the main river structures is the basin of Portoviejo that is occupied by many villages. This basin is filled over time with soft or loose deposits (typical of Class E or F sites as per international codes) that may amplify the motion or become unstable or lose strength during a seismic event (Chunga et al., 2016). Regional seismic hazard studies have considered the geomorphological position of the watershed-axis and the direction of the seismogenic structure, and demonstrated that wave attenuation may be less prominent in the area of low-compacted alluvial deposits. The orientation of the watershed in the Manabi Province is heading from east to west, which is an unfavorable for the potential seismic effects.

4. THE EARTHQUAKE OF 16th APRIL 2016

In the late afternoon of Saturday, at 18:58:36 (UTC-05:00) local time, an earthquake with moment magnitude of M_w7.8 impacted the coastal Ecuador (Fig. 4) with epicenter 29 km SSE of the town of Muisne in the Esmeraldas province (Lat.: 0.353ºN; Long.: 79.925 ºW; USGS, 2016b), and hypocentral depth of 21 km. The event took the life of 663 people, moved tens of thousands in refugee camps and directly affected the lives of 2 million persons.

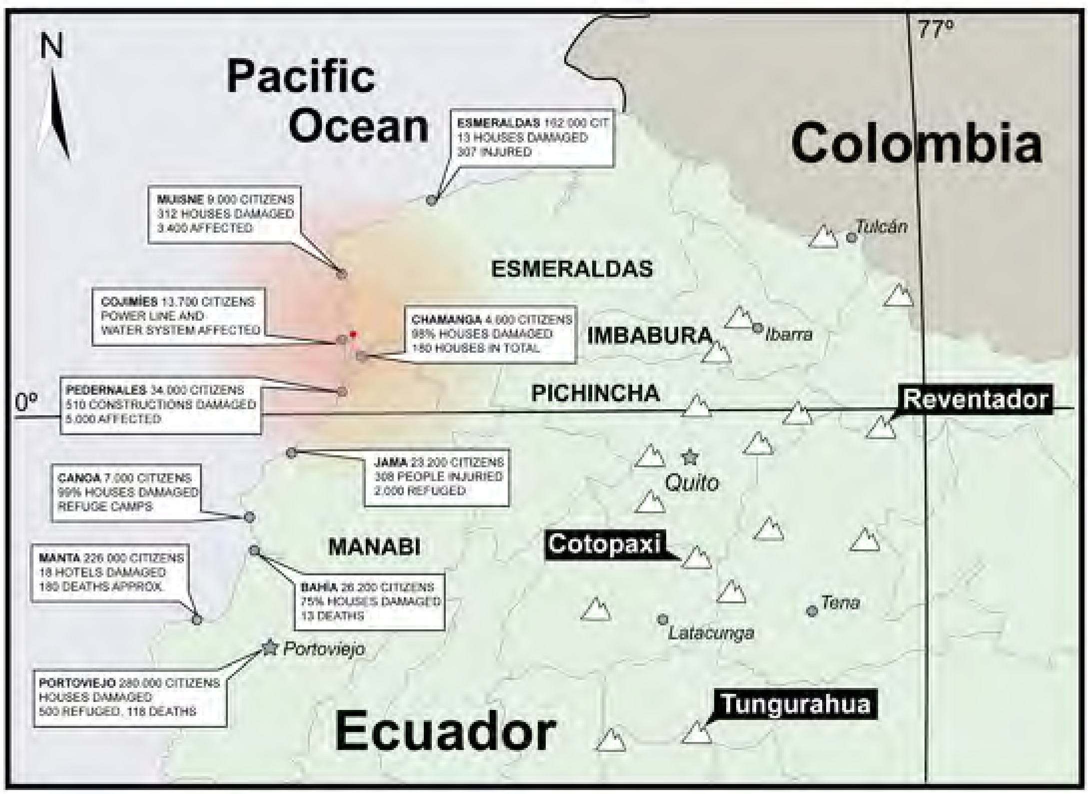

Fig. 4: Epicenter of the M_w7.8 earthquake (red dot) and selected damage observations in several coastal cities.

This earthquake has, in many aspects, similarities with the estimated M_w7.8 earthquake of May 14th, 1942, but the tsunami triggered by a submarine landslide or coseismic deformation did not have significant impact. However, if in the future the epicentral area is within the continental margin and the macroseismic intensity is higher than IX, it is likely to find evidence of underwater landslides (Michetti et al., 2007).

The earthquake impacted a large portions of several coastal cities, destroying between 70 and 80% of nearby villages and cities, Pedernales, Jama and Canoa (area of maximal macro-seismic intensities of IX to X), and cities within a distance of 140-150 km from the epicenter, like Chone, Portoviejo and Manta, which suffered building damage within 40 to 55%. As shown on Fig. 4, lines of electricity transmission, infrastructure of water supply, hospitals, schools, private and public buildings, main roads and highways were severely affected or completely destroyed. The cost estimate of the damage in the building stock and infrastructure were estimated at 3.3 billion USD (El Telegrafo, 2016; SENPLADES, 2016).

The mainshock was followed by 84 aftershocks with moment magnitude M_w between 3.8 and 6.8, recorded by the USGS in Ecuador (and hundreds by the IGEPN) until May 20th. The highest magnitudes were registered around the rupture zone with 86% of them during the first 10 days after the main shock (Toulkeridis et al., 2016; Tierra et al., 2017).

5. STATISTICAL EVALUATION AND GEOPHYSICAL CLUSTERING OF THE MAIN EARTHQUAKE AND AFTERSHOKS

A thorough understanding of the regional tectonics and the modeling of the rupture point to the second plane are essential in gaining insight to how the earthquake was generated. On the one hand, the earthquake occurred in an area where the subducting Nazca plate under the Caribean plate slides at a rate of 61 mm/year (Fig. 1). The focal mechanism of the main earthquake was a reverse fault with nodal planes given by the triads (strike, dip, rake) equal to (183°, 75°, 84°) and (26°, 16°, 113°) as reported by USGS (USGS, 2016b).

The location and mechanism are consistent with a subduction earthquake interface, sliding over an area approximately 160 km long and 60 km wide. On the other hand, the main earthquake was followed for weeks by a large number of seismic events generated (IGEPN, 2016a) , 678 of which were registered within the affected area until May 20th (IGEPN, 2016b) as shown on Fig. 5a. A large portion of these registered events, of about 88%, were not directly related to the rupture zone (USGS, 2016c), as indicated in Fig. 5b (USGS, 2016d). Furthermore, the spatial location uncertainty of the afterschocks reported by IGEPN (Figs. 5a, 6a,b, IGEPN, 2016a,b) dificults the study of the geodynamics of the subduction process (Fig. 7a), masking the existence of three distinct seismic clusters in such process (Fig. 7b): (1) Zone 0 (red), around Muisne; (2) Zone 1 (green) around Bahía Caraquez; and (3) Zone 3 (blue) around Manta.

The presence of such clusters has been demonstrated previously (Toulkeridis et al., 2016), by correlating the discovery of a clear pre-seismic environmental radiation with the spatio-temporal distribution of the USGS records. The methodology followed allows, with respect to the rupture process: (1) the association of seismic events with the main points of energy release; (2) a geophysical clustering of aftershocks; and (3) the identification of the geodynamic relationships between clusters since the time of the main shock.

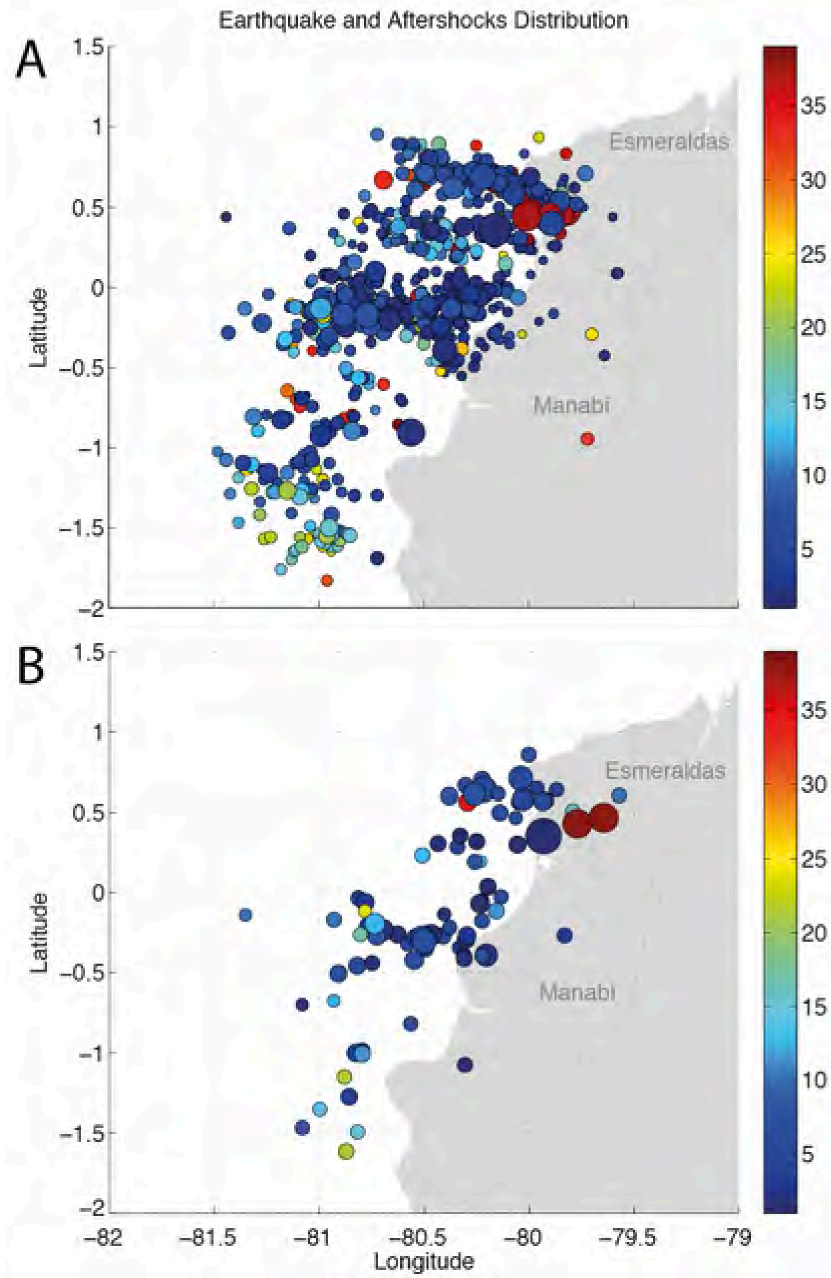

Fig. 5: Spatio-temporal distribution of the April 16, 2016 M_w7.8 Muisne, Ecuador Earthquake and aftershocks registered by IGEPN (a) and USGS (b) within the affected area [79.5W - 81.5W, 2S - 1N] from April 16th (dark blue) to May 20th (dark red).

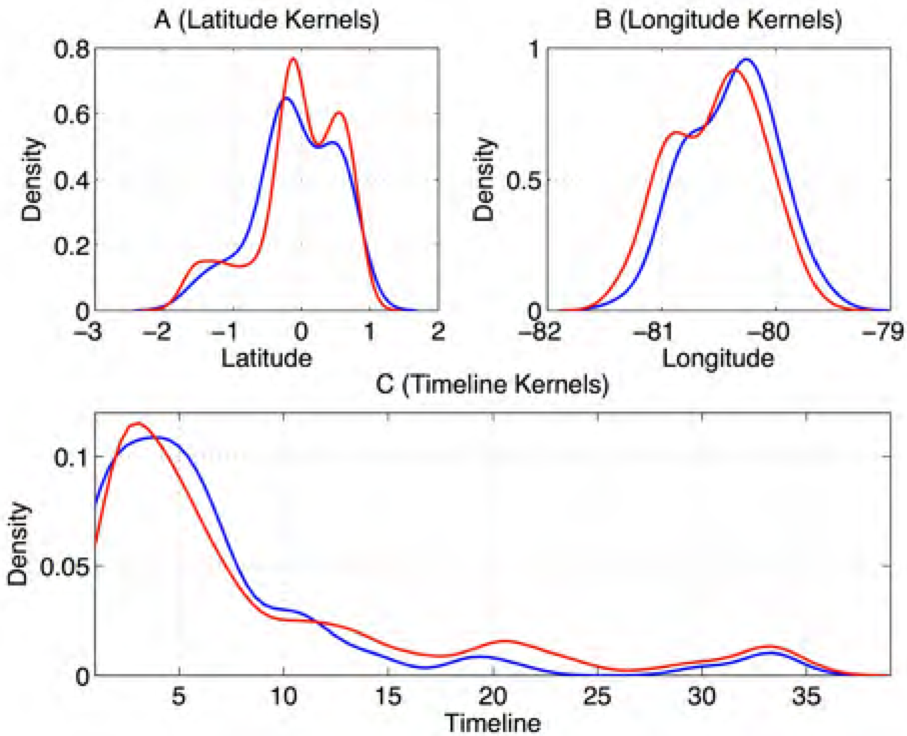

Fig. 6: Latitude (a) and Longitude (b) kernels distribution of the April 16, 2016 M_w7.8 Muisne, Ecuador Earthquake and aftershocks registered by IGEPN (red) and USGS (blue) within the affected area [79.5W - 81.5W, 2S - 1N]; (c) corresponding timeline kernels distribution. , Observations presented up to May 20th 2016.

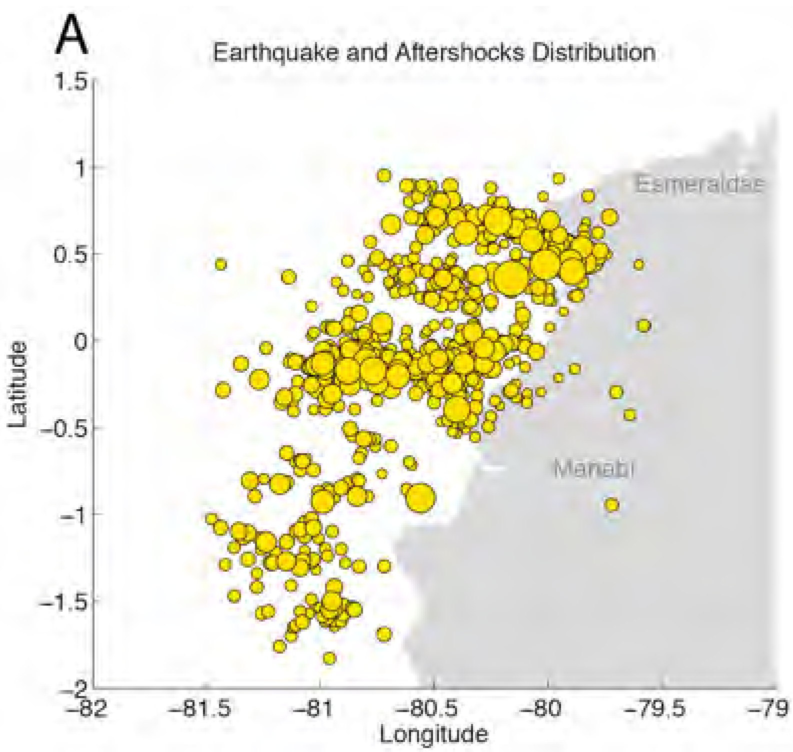

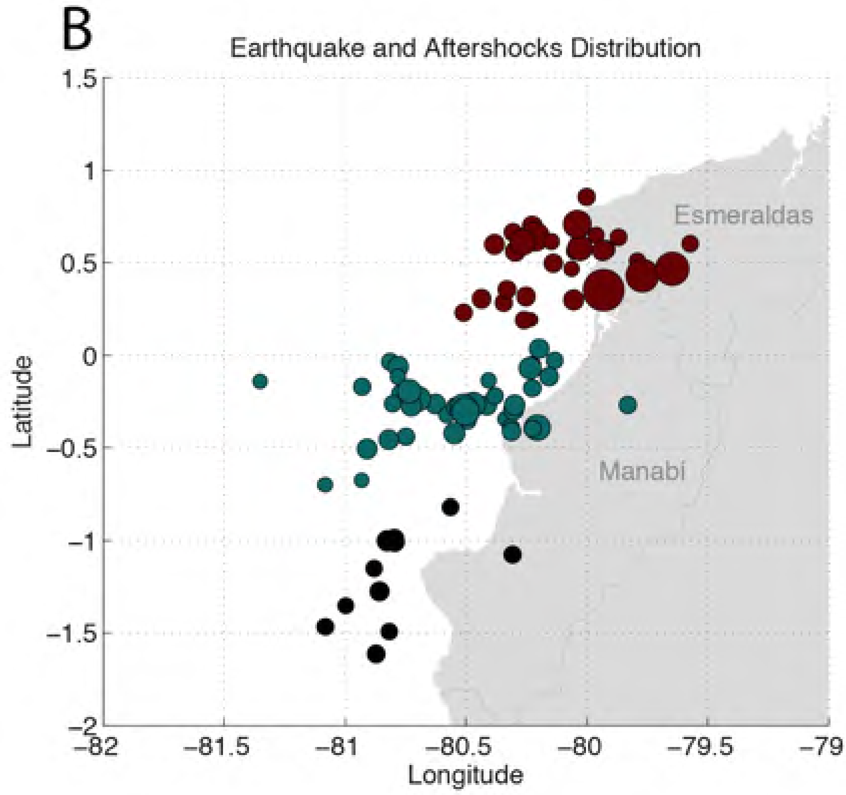

Fig. 7: (a) Spatial distribution of the April 16, 2016 M_w7.8 Muisne, Ecuador Earthquake and aftershocks registered by IGEPN; (b) geophysical clustering by means of the pre-seismic environmental radiation correlation with the spatio-temporal distribution of USGS data (Toulkeridis et al., 2016). Observations presented within the affected area [79.5W-81.5W, 2S-1N] up to May 20th, 2016.

5. SEISMIC HAZARD EVALUATION BASED ON THE CO-SEISMIC GEOLOGICAL DAMAGES

The geological survey and field data collection was performed within 3 days from the main seismic event, providing 290 data points of coseismic effects on the ground that allowed to evaluate the maximum macroseismic intensities and the predominant geomorphological features. The latter are important in evaluating site effects documented in Muisne, Pedernales, Jama, Canoeing, Chone, San Isidro, Manta, Portoviejo and Tosagua.

Aftershocks with M_w of 6.8 (02:57 a.m. local time) and 6.9 (11:46 a.m.) were recorded on May 18th, 2016, with hypocentral distance of 15 km. These events are associated with the same seismogenic structure responsible for the main M_w7.8 event and generated effects such as sinkholes, soil liquefaction with sand ejecta in Muisne and minor landslides in Pedernales and Mompiche. We evaluated the intensity through observations of damage to the environment, applying the macroseismic intensity scale ESI 2007 (Environmental Seismic Intensity; Michetti et al., 2007).

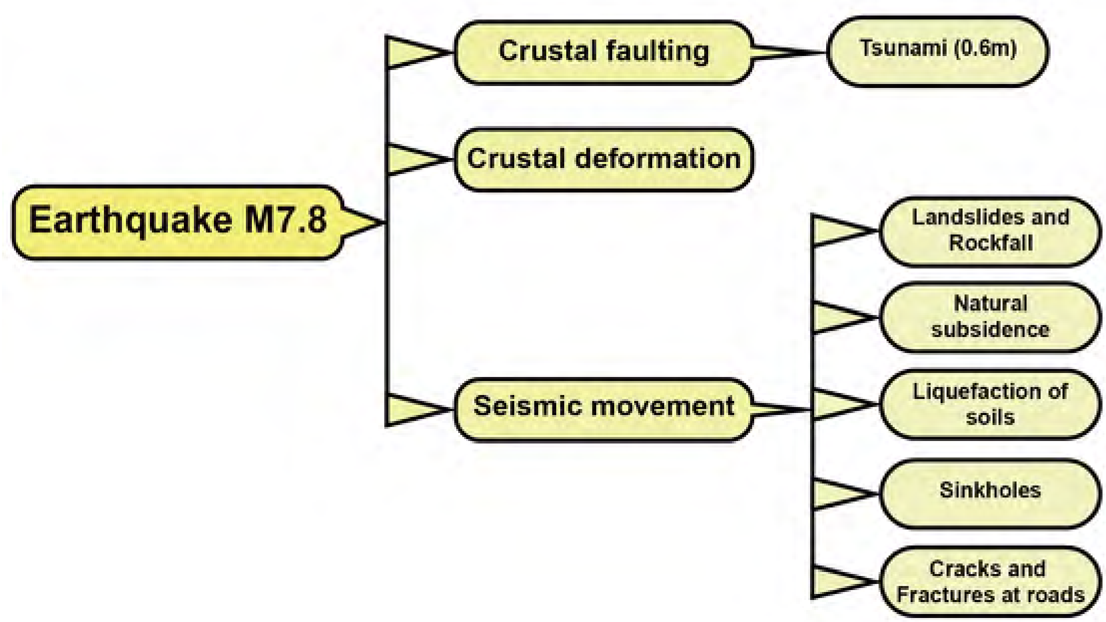

Fig. 8: Primary and secondary effects during and following the main M_w7.8 earthquake (Chunga et al., 2016).

In order to understand the isoseismal fields of macroseismic intensities and delineate the epicentral area of the main earthquake, the coseismic geological information has been compiled in the field based on (see Fig. 9): (a) landslides of natural and stabilized slopes, (b) cracks in natural field in the supratidal coastal plains and flood plains, (c) longitudinal and transverse fractures to the main axis of the concrete and paved roads, (d) sinkholes and soil liquefaction (e.g., sand ejecta and boils) formed in floodplains and areas of paleo-meander, (e) surface faulting with vertical and horizontal displacements (i.e., dextral shears) in hilly areas, (f) natural and anthropic subsidences in areas of depressions between hills and floodplains, (g) minor tsunami formed in the ocean with logs of a run-up height of less than 1 m. Field effects have been incorporated when the local seismic intensity is higher than VI. The implementation of the ESI 2007 scale (Michetti et al., 2007) has allowed to assign intensities based on evident ground effects in the different geomorphological settings of the Manabi and southern Esmeraldas provinces.

5.1 Geological mapping of features corresponding to an intensity of IX

Seismic effects in the epicentral area based on geomorphological features of supratidales coastal plains, floodplains, coastal terraces and depressions (filled areas) and between hills (Jama) were mapped. The supratidal areas experience wavy surface deformations, affecting buildings and streets (Figs. 9, 11). Some cobblestones were re-arranged as folds with vertical displacements from 8 to 10 cm recorded in Pedernales. Subsidence of cobblestone layers were commonly observed as shown on Fig. 10.

Fig. 9: Deformations along concrete-made road between Pedernales and Coaque, with diagonal and transverse fractures 10 to 14 cm wide. geomorphological floodplain features. ESI Intensity of IX and coordinates (UTM: 602.858mE 10.003.638mN).

Fig. 10: Wavy deformations on the beach boardwalk and streets of Pedernales, with re-arrangements of cobblestones in folds. ESI Intensity of IX to X and coordinates (UTM: 604.756mE 10.007.656mN).

Visible damage of the concrete road between Pedernales and Coaque included uplift internal steel beams that formed transverse fractures with openings of 8-15 cm (Fig. 9). In paved roads, the deformations generated bigger fractures, reaching 20 to 30 cm openings within transverse esruptur (Fig 11; Jama, UTM Coord. 584.676mE, 9.982.122mN.).

Fig. 11: Deformation in Jama paved road, with transversal fractures 20 to 30 cm wide and longitudinal fractures of 12 to 15 cm. Cracks observed in the free field soils reached 1 m. ESI Intensity of IX and coordinates (584.676mE 9.982.122mE).

In the natural terrain or soil of this area, crack openings reached 1 m. Such deformation characteristics were also observed in Pedernales and Coaque, but not towards the north, in Cojimies and Chamanga, confirming that the earthquake was felt strongly towards the south of the epicenter. In some other sites, the land appeared to have settled with apparent evidence of liquefaction in flooded areas and sand ejecta as shown on Fig. 12.

Fig. 12: Liquefaction evidence from GEER helicopter flyover of Manabí coast (Nikolaou et al., 2016), close to Jama (0º12'31.7"S, 80º15'22.5"W UTM coordinates 9976918.8N, 582762.5E).

5.2 Geological mapping of features corresponding to an intensity of VIII

Landslides and rockfalls of natural slopes were evident throughout the affected area (Fig. 13) with 126 reports out of 290 sampling stations. Stabilized slopes also reported damages in the epicentral area (Fig. 14), like in the northern side of Canoa, where part of a slope was deformed with a displacement escarpment. Field inspections indicated that the slope was likely not adequately stabilized, since the top did not have any stabilization work done and presented cracks and fissures with water runoff (Fig. 15).

Fig. 13: Satellite images of pre- and post-earthquake. In the hilly area of San Vicente, the displacement rate of active landslides was increased during the main earthquake. This hazard area may be re-activated during winter periods with high rainfall. Intensity ESI = VIII. Images courtesy of the Military Geographical Institute of Ecuador.

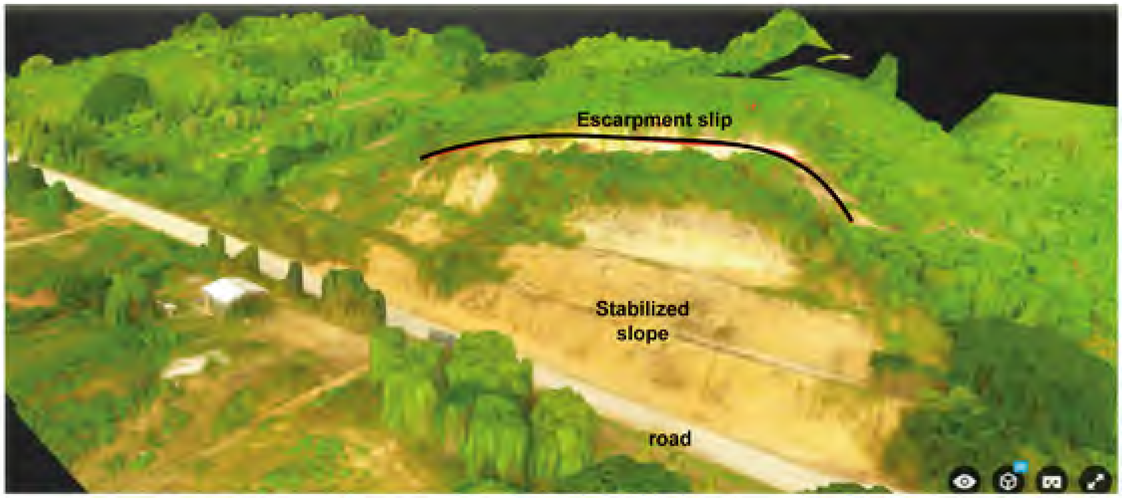

Fig. 14: Digital Terrain Model (DTM) from drone images, showing rotational slip on the road El Rosario - Canoa. Courtesy: Global Medical – SGR. Intensity ESI = VIII and coordinates (UTM: 561.268mE 9.952.722mN).

Fig. 15: Rotational slip in the road El Rosario – Canoa with evidence of escarpment at the slope and damages on the bicycle path and concrete road. Approximately 400 m^3 of material slipped (Chunga et al, 2016.). ESI Intensity = VIII and coordinates (UTM: 561.268mE 9.952.722mN).

In the accumulation zone at the lower part of some slopes, we documented between 800 to 10,000 m^3 of colluvium and debris, which affected some rails of the main paved and concrete roads. Rotational landslides in the filled areas between sections of slopes triggered lateral spreading. In the area of Boca de Briceno, the rocky mass of the hills showed fracturing or active jointing resulting to rock falls.

Fig. 16: Aerial photo of landslide on San Vicente-Canoa local road by GEER (Nikolaou et al., 2016). (GPS: 0°33' 5"S, 80°25'42"W UTM coordinates 9939051.9N, 563610.3E)

Fig. 17: Massive rockfall, which covered and destroyed completely the paved road with some 10,000 m^3 at Boca de Briceño. Intensity ESI = VIII, coordinates (561.647mE 9.944.416mN).

In the epicentral area, rock falls occurred in slopes of hills and filled areas or depressions between hills. Longitudinal, diagonal or transverse fractures of up to 25 cm were reported in Coaque, Jama and Canoes, San Isidro, Ricaurte, Bahia de Caraquez, Flavio Alfaro, Boca de Palmito, Pavon, Marco and San Clemente (Figs. 16 to 18). The sites farthest from the epicenter, but within the Manabi province, also reported multiple slides. In Esmeraldas, similar damage occured in Mompiche, Salima, Daule, Bellavista and Chamanga.

Fig. 18: Transcurrent displacement of ~35 cm on the paved road between San Vicente-San Isidro. Intensity ESI = VIII , coordinates (UTM: 573.419mE, 9.939.274mN).

In Crucita, vertical settlements and lateral deformations due to instability may be attributed to liquefaction, although surface manifestation of sand ejecta was not identified in reconnaissance. The assumed failure planes on Fig. 19 appear to be either along the interface between the embankment and the foundation soils (planar surface), or through the foundation soils. The latter, indicative of a more circular surface failure, may be due to liquefaction-induced softening that allowed the reduced-strength soil to shear during the earthquake (Nikolaou et al., 2016).

In Chamanga, several homes collapsed with evidence of 15-25 cm wide cracks due to lateral deformations in the supratidal coastal zone (Fig. 20) and bearing failures. In total we documented 65 sites in the cities and towns of Cojimies, Pedernales, Coaque, Jama, Canoeing, San Vicente, Bridge Mejia, Junin, San Isidro, Chone, Manta, Rocafuerte and Chamanga with similar damage patterns.

Fig. 19: Aerial view of embankment failure with assumed movement and failure modes marked with yellow at Mejia Bridge. Coord. UTM: 558.990mE 9.890.563mN. Intensity ESI = VIII. GEER-ATC report (Nikolaou et al., 2016).

Fig. 20: In Chamanga cracks in natural terrain with openings of 15 to 25 cm and collapses of buildings. Intensity ESI = VIII.Coordinates UTM: 616034mE 10009804mN.

Furthermore, soil liquefaction and sinkholes were observed along with sand boils in Muisne, Boca de Briceno and Tosagua (Figs. 21 to 24). The soil profile in these areas consists of sedimentary features formed in active and abandoned floodplains as well as paleo-surface meanders, which is combined with shallow ground water table. Observations of lateral spreading at river banks and road cuts on slopes included crack openings of up to 30 cm. In the central park of the island Muisne, a variety of sand boils (Figs. 17 and 18) between 50 cm to 80 cm in diameter were formed 1 minute after the main M_w7.8 earthquake, submerging two blocks of the park and leaving behind wavy deformation patterns in sidewalks, cobbles and streets. Similar phenomena were re-activated during the strong aftershocks of May 18th, 2016 (11:46 a.m) that reached M_w of 6.8.

Fig. 21: Liquefaction evidence in the central park of Muisne Island. Intensity ESI = VIII and coordinates (UTM: 609170mE 10067485mN).

Fig. 22: Sand boils with a diameter of 30 to 55 cm. 585364mE 9913357mN. Intensity ESI = VIII.

Fig. 23: Boca de Briceno Bridge liquefaction evidence in free-field and adjacent to embankment footing from GEER observations (Nikolaou et al., 2016) (GPS: 0°30'59"S, 80°26'31"W) UTM coordinates 9942920.8N, 562096.1E.

Fig. 24: Sinkhole at Tosagua village site with diameter of 2-3 m within floodplain and evidence of subsidence. Tosagua has been settling above an abandoned meander plain.

5.3 Geological mapping of features corresponding to an intensity of VII

From the 290 sampling stations, 73 had evidence of mass movements of landslides and rockfalls of natural slopes. The volume of accumulated material from unstable natural slopes has been estimated on the order of 50-250 m^3. In San Vicente, fallen rocks reached up to 1 m in diameter. On the slopes via San Isidro (UTM coordinates 586.049mE, 9.960.532mN), we documented the tree layer denudation phenomenon. Geomorphological features where these landslides effects were observed are in slopes and roadcuts of alluvial terraces at sites in Coaque, Jama, Canoeing, San Vicente, San Jacinto, Portoviejo, Pueblo Nuevo, Junin, Calceta, San Isidro, Zapallo, Tosagua, Flavio Alfaro, El Carmen, Boca de Palmito, El Achote, Puerto Cayo, Matiano, Manta, Jaramijó, Boca de Chila, Guachal, Chamanga and Cheve Abajo. Between Cube – Tacusa and Colope, several unstable slopes were observed, which were not affected by the main event, suggesting a recorded intensity with a lower degree of VII. Rockfall in coastal cliffs and damage to the protective wall in the beach area were not observed.

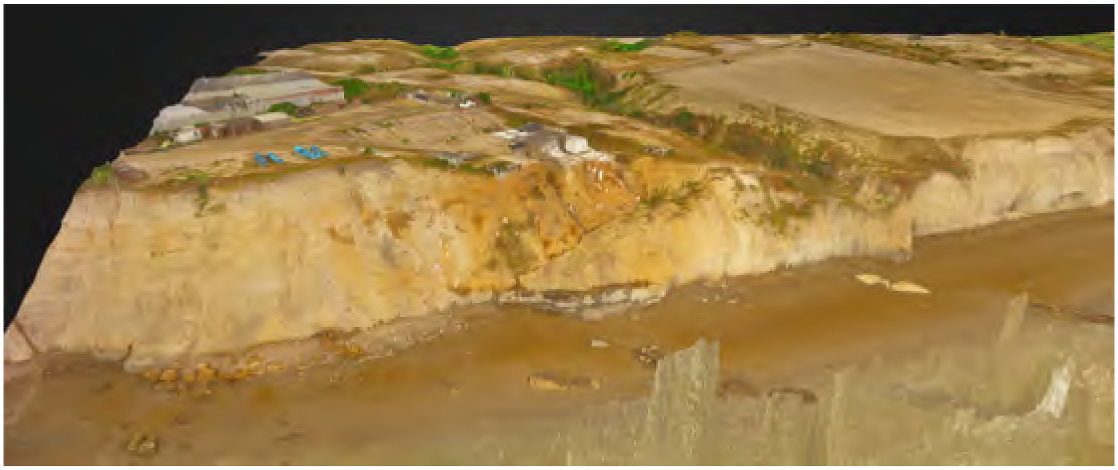

Fig. 25: Fissures in Jaramijó, rockfalls on unstable slopes of cliffs generating accumulated material of less than 150 m^3. Intensity ESI = VII. Image courtesy of Global Medical.

Fig. 26: Longitudinal fractures in middle of a paved road in Manta, with openings of 2 to 5 cm, lateral spreading. Coord. UTM: 531735mE 9894912mN.

Concrete roads did not suffer significant damage, in contrast to paved roads that experienced diagonal, tranversal and longitudinal fractures (relative to the road axis) with openings between 2 to 8 cm in sites like Portoviejo, Crucita, Junco - Cerecita, Jaramijó, Manta, San Mateo, San isidro, Mejia Bridge, Junin and Bahia de Caráquez, Cheve, Morascumbo and south of the city of Esmeraldas (UTM coordinates 614.372mE, 10016.254mN). Cracks in natural free-field soil reached widths of 10 cm in areas of floodplains such as Junin. Alluvial terraces and or abandoned flood plain areas experienced cracks of 2 to 4 cm wide, like in Manta and Crucita (Fig. 26). The most notable feature related to this macroseismic intensity, however, has been documented in the Bolvoni site in Portoviejo, where part of the river bank collapsed through rotational and lateral spreading movements causing partial damage to the bridge affecting parked vehicles were affected (Fig. 27). Figure 28 shows ground movements from a single vent in the pavement as recorded by the GEER-ATC team (Nikolaou et al., 2016). Eyewitness accounts indicate that water sprayed out of the ground as high as 1 m immediately following the ground shaking.

Fig. 27: Rotational and lateral ground deformations in the river margin, partial bridge collapse, easily eroded sandy material. Intensity ESI = VII. Bolvoni site, Portoviejo. 560261mE 9882769mN.

Fig. 28: Wall at Portoviejo Velboni site recorded by GEER-ATC (Nikolaou et al., 2016): Slope failure showing two primary slip surfaces and wall rotating, following the slope movement (GPS: 1°3'37.8"S, 80°27'29.3"W).

Fig. 29: Rio Chico: Settlement and rotation of block in foreground and circular global failure in background recorded by GEER-ATC (Nikolaou et al., 2016). (GPS: 0° 58' 36.6" S, 80° 25' 23.7" W).

At the margins of coastal plains of beaches, evidence of lateral spreading was noted through the deformation of cobblestones in the seawall as seen in Bahia de Caraquez, where cracks parallel to the coastline reached openings of 20 cm (coord. UTM: 564.133mE, 9.932.734mN). Damage on bridges by vertical displacement (10 to 15 cm) on the lateral side of the roads were caused by the formation of lateral spreading (Fig. 29). Cracks associated with this phenomenon reached openings of 20 to 25 cm (e.g., floodplain of Calceta, UTM Coord. 593.178mE, 9.906.222mN). Evidence of lateral spreading has been reported in San Mateo, Piedra Larga, Chone, Calceta, Jaramijó, Sesme, Pavon, Mate, Muisne, San Isidro, Portoviejo and Bahia de Caraquez.

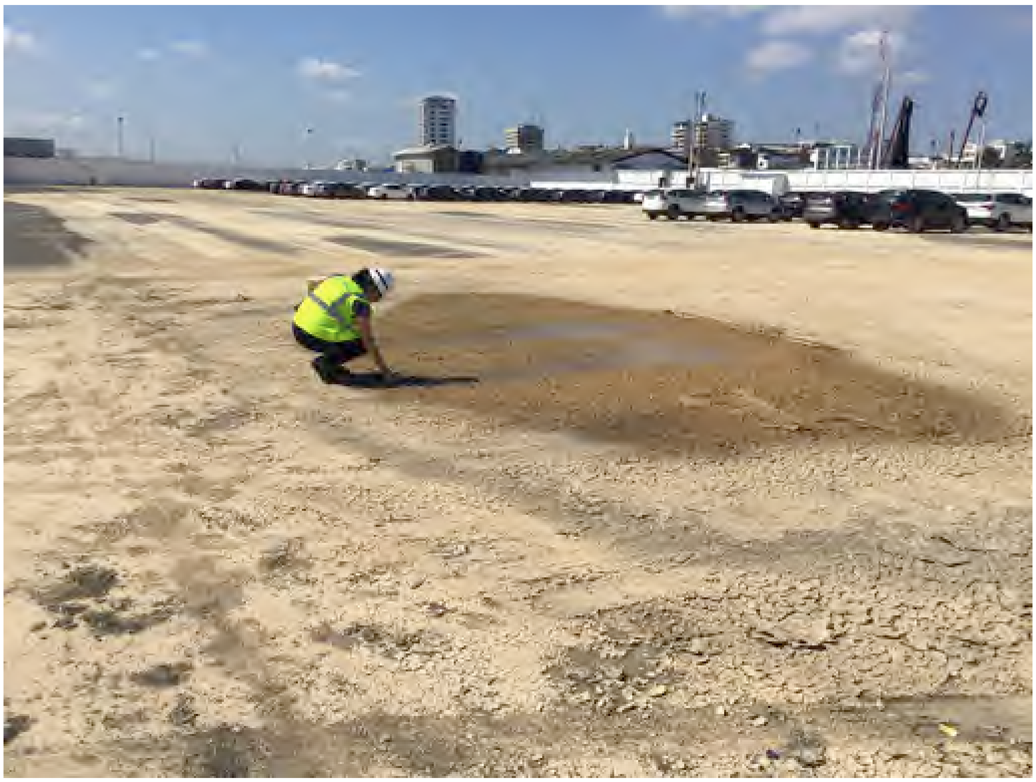

Fig. 30: Concentrated sand blow in the center of pavement in the Manta Port parking area (GPS: 0°56'27.6"S, 80°43'29.4"W). (Nikolaou et al., 2016)

Soil liquefaction in alluvial plains such as this observed by GEER-ATC (Nikolaou et al., 2016) at the parking lot of the Manta Port affected networks and induced collapses in Manta where lateral spread was also observed (UTM coord: 605.574mE, 9.925.484mN and 606.894mE, 9.928.506mN). In Chone, subsidence due to soil liquefaction in alluvial terraces has been recorded (UTM Coord. 598.218mE, 9.921.753mN).

Referring to damage sites with lower intensities, such as landslides with less than 50 m^3 and minor fractures with openings of 1 cm or less in paved roads, were assigned with and intensity degree of VI, where the evidences in the field are sporadic.

The results of these sampling stations were used to reconstruct a geological map with isoseismals fields of intensities. With the compiled and recorded coseismic data in the field of higher macroseismic intensities, we wer able to produce a map of intensities by applying the definitions and scale of the ESI 2007 scale (Fig. 31).

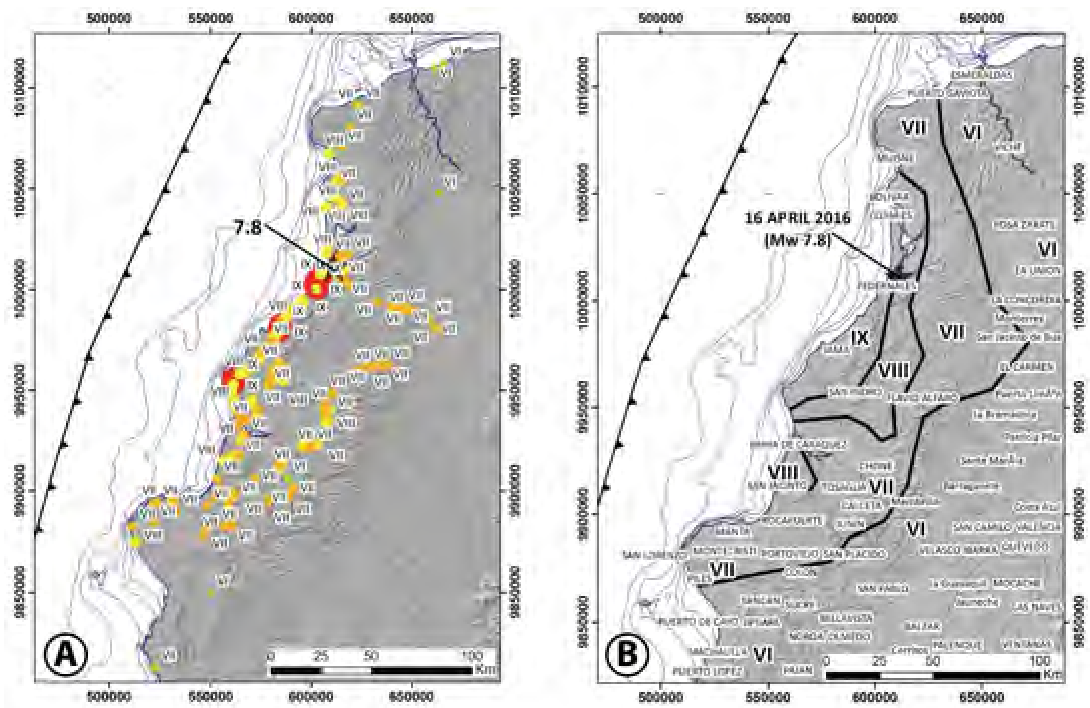

Fig. 31: (a) Seismic intensities of the main M_w7.8 earthquake according to the scale ESI-2007; and (b) Zoning of intensity degrees of VI to IX (Chunga et al., 2016).

6. EVALUATION OF COLLATERAL TSUNAMI

Worldwide, active continetal rims are capable to trigger massive submarine landlsides or slope failures, which in turn may generate devastating tsunamis (Heezen and Ewing, 1952; Hampton et al., 1996; Driscoll et al., 2000; Ward, 2001; Tappin et al., 2001; 2002; McAdoo and Watts, 2004; Fine et al., 2005; Masson et al., 2006). In such cases, the epicenter does not need to be in the seaside, but can rather be on the (dry) continental zone.

There is not certainty if the April 16th tsunami was triggered by a massive submarine landslide or seafloor coseimic deformation. According to Oceanographic Institute of the Navy, INOCAR, the crest of the tsunami wave arrived to the city of Esmeraldas 6 minutes after the earthquake. This is a very short time for the tsunami travel time from the tsunami landslides scars proposed by Ratzov et al, 2007, and also for the fault plane for the similar 1942 earthquake, as it is demonstrated in Ioualalen et al, 2011. Using both numerical simulation, the tsunami would have arrived more thar 20 minutes from its generation zones. For the case of seismically-induced tsunami, we would need to update the numerical simulation when the focal mechanism is well defined.

Nevertheless, the earthquake of the 16th of April 2016 in Ecuador triggered a tsunami, registered by 32411 and buoys from NOAA located at Panama and Peru basins, respectively. These were registered 2 and 3 hours after the earthquake when the waves passed over their positions. Furthermore, the seismic waves propagated over the seabed, affecting the register at the pressure sensor of these buoys until an hour after the earthquake (Fig. 32). Roughly, we were able to observe that the period of the tsunamis has been about 40 minutes with amplitude close to 1 cm.

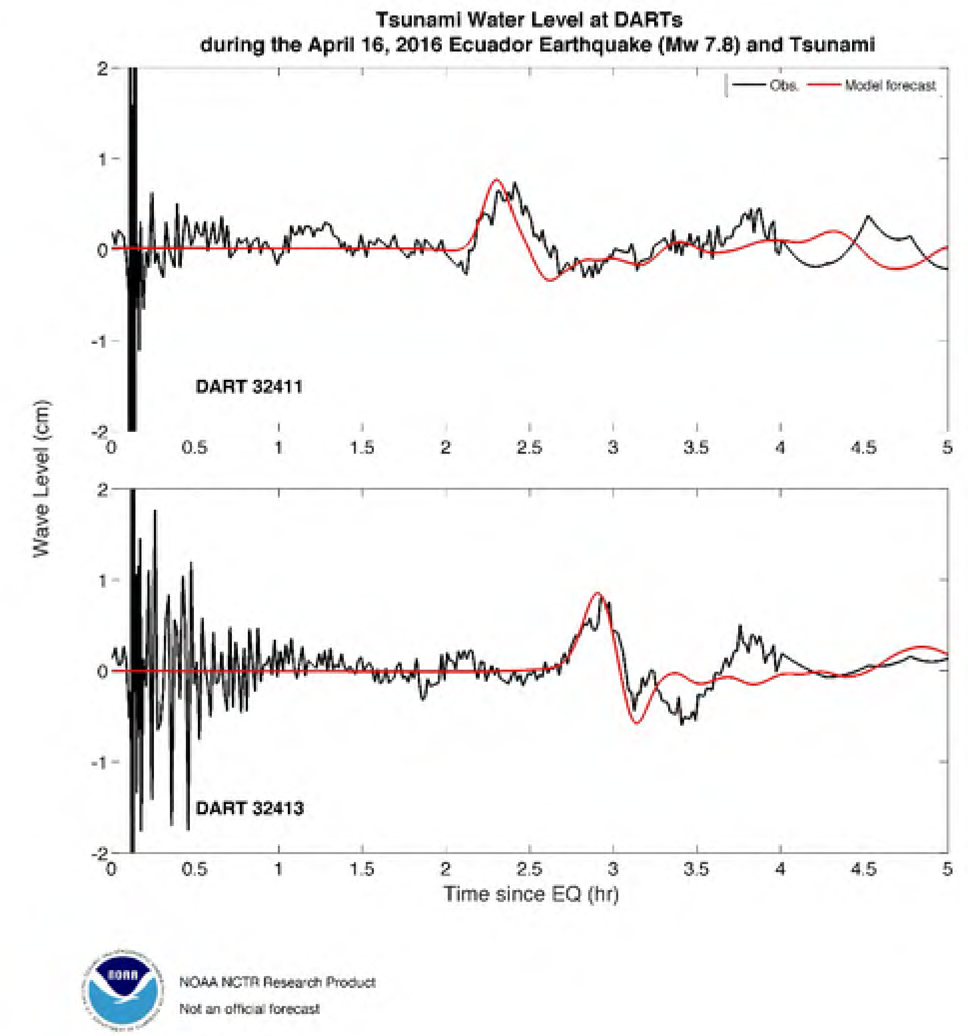

32413 DART

Fig. 32: Register of oceanic propagation of the tsunami at DART Buoy position. SOURCE: NOAA

Locally, the tsunami was registered by the INOCAR-DART buoy, which is close to the epicenter, immediately after the earthquake. It has been difficult to differentiate the tsunami signal from the noise produced by the earthquake, however it is notable that the perturbation exist after the earthquake time, changing the initial conditions in the calm water level (Fig. 33).

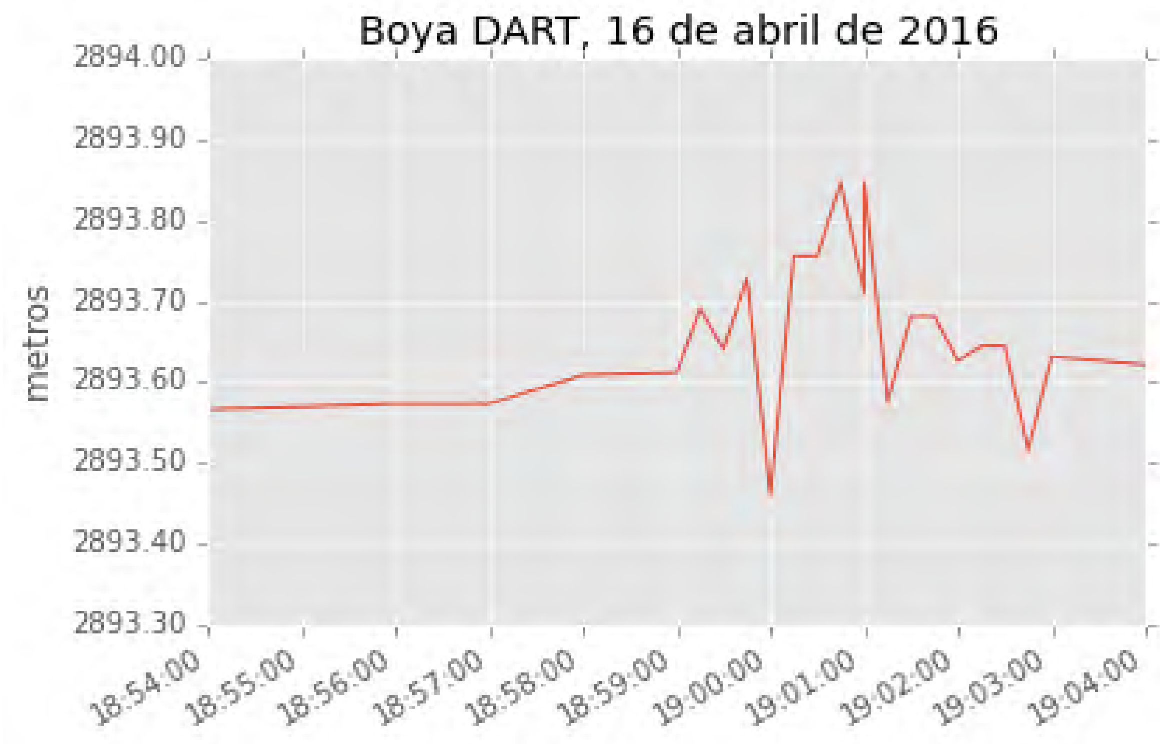

Figure 33 Tsunami sea level perturbations. Source: INOCAR.

INOCAR issued a Tsunami Warning over the entire Ecuadorian coast based on the data from the INOCAR-DATA buoy with remained in effect 4 hours after the event, considering the potential threat to the shores of the nearby Galapagos Islands.

Several people at the coastal communities reported remarkable changes in the seawater level and also strong rift currents, although the amplitude of the tsunami did not reach any high water level. Fortunately for these coastal communities, the tsunami impact occurred at low tide. This important fact appears to be the reason that no inundation occurred and considerable physical effects at the coastalines have been absent. However, this case could have been catastrophic under different tide conditions. It should be noted that some of the authorities were not alerted for a tsunami hazard due to the false perception that a tsunami would not be possible because the epicenter in the continental and not on the marine side.

The Esmeraldas Port registered the arrival of tsunami with the receiding of the water, which started at 19:00. From 19:06 to 19:09, the tide gauge registered the arrival of the tsunami crest which meant a rate of change in water level of ~50 cm/min. (Fig. 34)

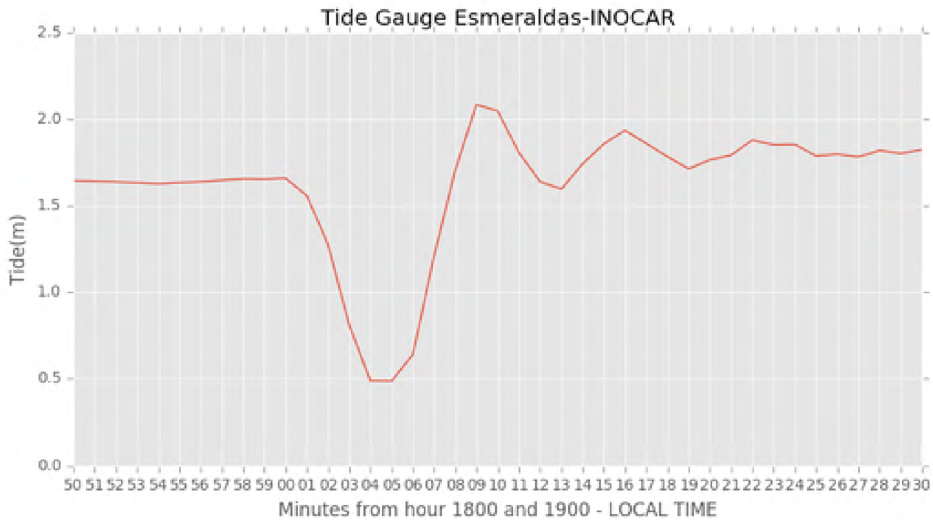

Fig. 34: Mareogram from Esmeraldas Tide Gauge. Note that tsunami crest wave arrived 6 minutes after the event. Source: INOCAR

Even with the arrival tsunami at low tide, the Esmeraldas Port was exposed to strong residual currents. Some small boats and buoys were moved from these anchorage sites due the strong currents (Fig. 35).

Fig. 35: Fishing Port Esmeraldas. At the time of tsunami arrival, a small boat and buoys set were moved from their anchorage. Source: ECU911

7. ECONOMIC DAMAGE

Natural disasters become an obstacle to economic development, particularly in small, less developed countries (Ferris and Petz, 2012; Kahn, 2005). A recent report by the United Nations (UNISDR, 2016) concludes that natural disasters in the Latin-American region have increased as have the losses in human life and economy that can reach a significant portion of the nation's Gross Domestic Product (GDP). In comparison to countries with social expenditures, it could reach between 30 up to 50% of social expenditures (UNISDR/Corporación OSSO, 2016).

According to the Ecuadorian government, the estimated total loss was a little over 3.3 billionUS$ being equivalent to 3.3% of the Ecuadorian GDP (SNGR, 2016; El Universo, 2016). A total of 29,672 properties, including family houses were affected and so far at least 5,000 have been demolished (El Universo, 2016). Insurance companies paid some 134 US$ million in disaster coverage (El Universo, 2016) three months after the earthquake. Regarding infrastructure, such as the Ecuadorean Pacific Highway, 70 km have been affected in the Province of Manabi alone and its reconstruction cost is estimated at 35 million US$ (El Universo, 2016). In addition to losses in infrastructure and properties, over 28,000 jobs were lost and about 300 million US$ in trade and businesses. Over 7,000 businesseds were directly affected, some of which may have to declare bankruptcy. From the people affected, 97% did not have savings and 23% did not have property rights or any way to prove ownership of their homes (El Universo, 2016).

The recent earthquake has been one of the most devastating natural disasters in recent decades in Ecuador as shown on Table 1 that compares it to other historic earthquakes. The 2016 event claimed the second largest ever loss of life, but the highest amount of injured, while it ranks 5th in home losses. However, this earthquake has been the most devastating in terms of economic damage. The cost estimated do not include cost of recovery teams, firefighters and volunteers, who have been successful and efficient not only in terms of efforts and time, but also the impact these people have had in the local population (El Universo, 2016).

Table 1. Comparison of historic earthquake effects. Source: EM-DATA, CRED/IRSS 2016

Year	Disasters	Killed	Injured	Affected	Homeless	Total affected	Total dam x million
1970	1	29	120	60000	27992	88112	4,00
1976	2	20	-	-	20000	20000	4,00
1980	1	8	40	-	-	40	-
1987	2	5002	6	4500	15000	19506	1500,00
1990	1	4	10	6500	-	6510	-
1995	2	3	90	200	600	890	-
1996	1	27	180	15000	15525	30705	7,00
1998	1	3	40	1250	750	2040	-
2014	1	3	18	-	-	18	-
2016	1	671	4859	70000	11400	81400	3344,00

The second decade of this millennium has been particularly active in terms of earthquakes and tsunamis along the Pacific "Ring of Fire." The mega-earthquake and associated tsunami of Chile on February 27th, 2010 claimed 525 lifes and generated an economic loss of 24 billion US$, representing about 12% of country's GDP (Insurance Information Institute, 2016; Biblioteca del Congreso Nacional de Chile, 2010). About a year later, on March 11th, 2011, Japan was hit by a mega-earthquake and tsunami with death toll of 15,854 people and an economic loss reaching 309 billion US$ (6% of Japan's GDP), destroying about 650 businesses (Insurance Information Institute, 2016). New Zealand was hit by a sequence of earthquakes with main events on February 21st and June 13th 2011, leaving economic losses of about 40 billion US$, representing 28% of the country's GDP, in addition to killing 185 persons (Insurance Information Institute. 2016). Based on the International Disaster Database EM-DAT, Figure 36 demonstrates the increase in earthquake-induced economic losses around the Pacific Ocean´s countries since 1951 (CRED, 2016).

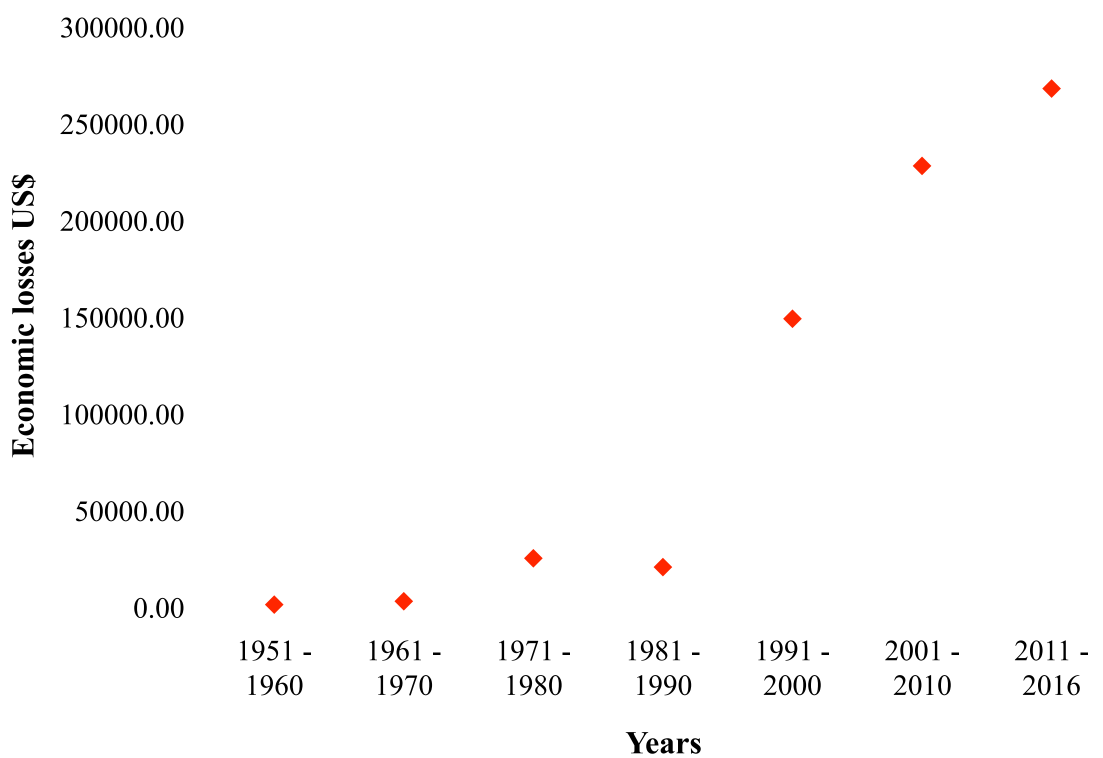

Fig. 36: Earthquake-induced economic losses around the Pacific Ocean´s countries since 1951 (CRED, 2016).

Table 2 presents economic losses in US$ in countries in the Pacific Ring of Fire as function of the decade since 1951. China, Chile and Japan are the most affected countries since 1951 in economic damages (Insurance Information Institute. 2016). However, China had several earthquakes in the last few decades, but only one caused an enormous economic impact on its GDP. The 2008 earthquake induced economic losses of 4% of China's GDP (Insurance Information Institute. 2016). Meanwhile, Chile and Japan have had at least one major earthquake and/or tsunami each decade since 1961. New Zealand's economy has also been critically affected by repeateative earthquakes with the 2011 sequence affecting international trade totaling 28% of its GDP in economic losses (Insurance Information Institute. 2016).

Ecuador, as well as Mexico have been hit by earthquakes and tsunamis almost once in each decade and the destruction has been severe with economic losses exceeding 4.8 billion US$ since 1951 (Insurance Information Institute. 2016).

Table 2: Economic effects per decade by natural disasters of some selected countries. Source: EM-DATA, CRED/IRSS 2016; INSURANCE INFORMATION INSTITUTE 2016

COUNTRY	1951 - 1960	1961 - 1970	1971 - 1980	1981 - 1990	1991 - 2000	2001 - 2010	2011 - 2016	TOTAL COUNTRY
Chile	550,0	360,4	236,4	1501,0	49,7	30105,0	24000,0	56802,5
China			22900,0			137500,0	5025,0	165425,0
Colombia	0	1,0	28,0	410,9	1859,8	10,0	4,0	2313,7
Costa Rica	0	0,0	0,2	20,5	100,0	200,0	45,0	365,7
Ecuador	0	4,0	4,0	1500,0	7,0	0,0	3344,0	4859,0
El Salvador	0	35,0	0	1500,0	0	1848,5	0	3383,5
Honduras	0	0	0	0	0	100,0	0	100,00
Japan	140,0	931,0	865,0	459,0	102028,4	43534,0	210000,0	357957,4
Mexico	0	3,0	30,0	4104,0	412,7	1266,3	320,0	6136,0
New Zealand	0	0	0	210	0	10000,0	24000,0	34210,0
Peru	0	552,1	30,0	23,0	0,0	900,1	0,0	1505,2
United States	0	540,0	550,0	10360,0	44000,0	2000,0	700,0	58150,0
TOTAL	690,00	2426,5	24643,6	20088,4	148457,5	227463,9	267438,0	691207,9

The 2016 earthquake in Ecuador had the most severe economic effect in this country as demonstrated in Table 2, in addition to being the second deadliest event since 1949 (Secretaria Nacional de Riesgo, 2016). During the recovery process, Ecuador received loans from multilateral organizations such as Inter-American Development Bank (BID), International Monetary Fund (IMF), World Bank (WB), and Latin-American Development Bank among others, totaling about 914 million $US. Ecuador received also a little over 180 million $ US from the International Cooperation and Disaster relief and from several governments, as well as international organizations including the UNO with 73 million $US 2 million $US from China, 100 million $US from Spain, 5.5 million $US from the United States of America and some 1,1 million $US from the European Union (El Universo, 2016).

All these funds and loans will cover approximately 37% of the total damage and reconstruction costs. Another third of the total cost will be covered by the increase in taxes such Added Value Tax, which has increased from 12% to up to 14% (Martínez and EL Comercio-DATA, 2016). Due to the absent international monetary reserves, weak financial institutions and low prices of commodities such as oil and minerals, the recovery process will take some time (World Bank, 2016). These fragile economic predictions are supported by the reduced growth estimates of Ecuador which, for 2016, was -4.5% as reported by the IMF. Under these conditions, the reconstruction total costs may reach between 15 to up to 30 billion US$, based on estimates from economic losses from Chile and Haiti earthquakes (Biblioteca del Congreso Nacional de Chile, 2010; Cavallo et al., 2010; UNISDR/Corporación OSSO, 2016).

The April 16th, 2016 earthquake in Pacific coast of Ecuador took place in moments of a contraction of Ecuadorean economy, due to external effects such as oil prices plunge in 2015. According to IMF, the economic impact of 3.344 billion US$ GDP reduced its growth in 4.5% (0.5% of the 2.25% of the contraction expected), so it will take years to come back to previous economic conditions. From the economic point of view, a trust fund or other type of financial instrument would reduce such economical impact in terms of speeding up nation's recovery. Nonetheless, an overall conclusion based on the observations and estimated effects of this natural disaster, is that a radical changes in several directions are necessary to rebuild the country targeting effective resillence goals: (1) an improvement in the national seismic monitoring means with automated and verified information to be rapidly provided to scientists and stakeholders after an earthquake with verified epicenter location and magnitude estimate; (2) advanced planning for the response and decision-making chain; (3) implementation of a national research network for early warning in seismic hazards and a national earthquake center; (4) improvement of the national building code to include seismic risk assessment and management; (5) implementation of inspection quality control in the implementation of building normatives; (6) development of a clear awareness, preparation, and response plan for the public, including shake-out exercises (7) development and implementation of a dedicated national emergency unit with all necessary disciplines involved; (8) creation of long-plan resilience goals for infrastructure networks; and (9) evaluation of multi-hazard exposure of the country to other natural phenomena.

Finally, about the tsunami hazard in particular, more research is needed to clarify if the tsunami was triggered by a landslide or by the earthquake itself. This research should include bathymetric surveys and multitemporal analysis to identify the scars or the seafloor deformation. A better estimation of the focal mechanism of the main event is important in order to simulate a synthetic tsunami, to mimic the mareograms obtained at Esmeraldas Port. Moreover, the strong currents generated by the tsunami arrival must be considered by the Maritime Authority for the development of Contingency Plans, since these occurred even when the tsunami not caused an inundation in the coastal basin.

Acknowledgements

The authors acknowledge the collaboration and exchange of information with the US reconnaissance team of the Geotechnical Extreme Events Reconnaisance (GEER) Association, funded by the National Science Foundation (NSF), and the Applied Technology Council (ATC) are gratefully acknowledged. Fernando Mato also acknowledges support from the Prometeo Project of the National Secretariat of Higher Education, Science, Technology and Innovation (SENESCYT), Ecuador.

REFERENCES

Anbarci, N., Escaleras, M. and Register, C.A., 2005. Earthquake fatalities: the interaction of nature and political economy. Journal of Public Economics, 89(9): 1907-1933.

Baldock, J.W., 1982. Geology of Ecuador: explanatory bulletin of the national geological map of the Republic of Ecuador; 1: 1,000,000 scale. Ministerio de Recursos Naturales y Energéticos, Dirección General de Geología y Minas, Quito, Ecuador: 54pp

Bardet, J.P., Synolakis, C.E., Davies, H.L., Imamura, F. and Okal, E.A., 2003. Landslide tsunamis: Recent findings and research directions. Birkhäuser Basel: 1793-1809.

Beck, S.L. and Ruff, L.J., 1984: The rupture process of the great 1979 Colombia earthquake: evidence for the asperity model. J.Geophys. Res., 89: 9281–9291

Bender, B. (1983): Maximum likelihood estimation of b values for magnitude grouped data, Bull. Seismol. Soc. Am., 73: 831-851

Berninghausen, W.H., 1962. Tsunamis reported from the west coast of South America 1562-1960. Bull. of the Seismological Soc. of America, 52 (4): 915-921.

Biblioteca del Congreso Nacional de Chile. 2010. Efectos Económicos del Terremoto en Chile, por sectores y enel empleo: Una evaluación preliminar. BCN Informe, Santiago, Chile: 7pp.

Bristow, C.R. and Hoffstetter, R., 1977. Lexique Stratigraphique International; Ecuador. Second edition. Paris: Centre National de la Recherche Scientifique: 412p

Bryant, E., 2014. Tsunami: the underrated hazard. Springer: 222pp

Butler, R., Stewart, G.S. and Kanamori, H., 1979. The July 27, 1976 Tangshan, China earthquake—a complex sequence of intraplate events. Bulletin of the Seismological Society of America, 69(1): 207-220.

Cavallo, E.A., Powell A. and Becerra, O. 2010: Estimating the Direct Economic Damage of the Earthquake in Haiti.IDB Working Paper Series No.IDB-WP-163. The Inter American Development Bank; Department of Research and Chief Economist. Washington DC. 16 pp.

Chen, Y. ed., 1988. The great Tangshan earthquake of 1976: an anatomy of disaster. Pergamon: 162pp

Chunga, K., Besenzon, D., Mulas, M., Loayza, G. and Pindo JC., 2016: Areal distribution of Ground effects induced by the 2016 Mw 7.8 Pedernales earthquake (Ecuador). 88° Congresso della Societa' Geologica Italiana. S1. Earthquakes and Active Tectonics: a multidisciplinary approach. Napoli, 7/9 sept.

Chunga, K. and Toulkeridis, T. (2014). First evidence of paleo-tsunami deposits of a major historic event in Ecuador. J. Tsunami Soc. Int, 33: 55-69.

Collot, J.-Y., Michaud, F., Alvarado, A., Marcaillou, B., Sosson, M., Ratzov, G., Migeon, S., Calahorrano, A. and Pazmino, A., 2010. Vision general de la morfologa submarina del margen convergente de Ecuador-Sur de Colombia: implicaciones sobre la transferencia de masa y la edad de la subduccion de la Cordillera de Carnegie, in Sintesis de los Resultados de Investigacion Geologica y Geofisica Sobre el Margen Ecuatoriano, la Costa, la Cordillera Submarina de Carnegie, y de la Plataforma Volcanica de Galapagos, eds Collot, J.-Y., Sallares, V. & Pazmio, A., Publicacion CNDM-INOCAR-IRD, PSE001-09, Guayaquil, Ecuador: 47–74.

Collot, J.-Y., Michaud, F., Legonidec, Y., Calahorrano, A., Sage, F., Alvarado, A. & el personal

cientifico y tecnico del INOCAR, 2005. Mapas del margen continental centro y sur de Ecuador: Bathymetria, relieve, refllectividad acustica e interpretacion geologica, Publicacion IOA - CVM- 04 - POST.
Collot, J.Y., Marcaillou, B., Sage, F., Michaud, F., Agudelo, W., Charvis, P., Graindorge, D., Gutscher, M.A. and Spence, G., 2004. Are rupture zone limits of great subduction earthquakes controlled by upper plate structures? Evidence from multichannel seismic reflection data acquired across the northern Ecuador–southwest Colombia margin. Journal of Geophysical Research: Solid Earth, 109(B11).
CRED (Centre for Research on the Epidemiology of Disasters) 2016: http://www.cred.be/node/1516
Driscoll, N.W., Weissel, J.K. and Goff, J.A., 2000. Potential for large-scale submarine slope failure and tsunami generation along the US mid-Atlantic coast. Geology, 28(5), pp.407-410.
Egbue, O. and Kellogg, J., 2010: Pleistocene to Present North Andean "escape". Tectonophysics 489: 248-257.
El Telegrafo, 2016: http://www.eltelegrafo.com.ec/noticias/ecuador/3/manana-se-daran-a-conocer-cifras-oficiales-del-costo-del-terremoto
El Universo, 2016: http://www.eluniverso.com/noticias/2016/04/25/nota/5544318/multilaterales-paises-ong-envian-recursos-exterior
Feininger, T. 1980. La geología histórica del Cretácico y el Paleógeno de la Costa Ecuatoriana, Politécnica, Monograf. Geología, V, 2: 7-48.
Ferris E. and Petz D. 2012. The year shock the rich: A review of natural disasters in 2011. Project on Internal Displacement, The Brookings Institution-The London School of Economics. Washington DC. 142 pp.
Fine I.V, Rabinovich A.B, Bornhold B.D, Thomson R.E, Kulikov E.A 2005 The Grand Banks landslide-generated tsunami of November 18, 1929: preliminary analysis and numerical modelling. Mar. Geol. 215, 45–57
Gang, Q., 1989: The Great China Earthquake. Beijing: Foreign Languages Press. 354pp
GEER-ATC Report (GEER-049), Nikolaou, S., Vera-Grunauer, X., Gilsanz, R. eds., "2016 Ecuador GEER-ATC Report version 1". Published in geerassociation.org: http://www.geerassociation.org/component/geer_reports/?view=geerreports&id=77&layout=default
Ghobarah, A., Saatcioglu, M. and Nistor, I., 2006. The impact of the 26 December 2004 earthquake and tsunami on structures and infrastructure. Engineering structures, 28(2): 312-326.
Gupta, H.K., Rao, N.P., Rastogi, B.K. and Sarkar, D., 2001. The deadliest intraplate earthquake. Science, 291(5511): 2101-2102.
Gusiakov, V.K., 2005: Tsunami generation potential of different tsunamigenic regions in the Pacific. Marine Geology, 215, 1-2: 3-9.
Gutenberg, B., 1939. Tsunamis and earthquakes. Bulletin of the Seismological Society of America, 29(4): 517-526.
Gutscher, M.A., Malavieille, J.S.L. and Collot, J.-Y., 1999: Tectonic segmentation of the North Andean margin: impact of the Carnegie ridge collision. Earth Planet. Sci. Lett. 168: 255–270.

Hampton M.A, Lee H.J, Locat J 1996 Submarine landslides. Rev. Geophys. 34: 33–59.

Harpp, K. S. and White, W. M., 2001: Tracing a mantle plume: Isotopic and trace element variations of Galápagos seamounts. Geochemistry, Geophysics, Geosystems, 2(6).

Harpp, K. S., Fornari, D. J., Geist, D. J. and Kurz, M. D., 2003: Genovesa Submarine Ridge: A manifestation of plume‐ridge interaction in the northern Galápagos Islands. Geochemistry, Geophysics, Geosystems, 4(9).

Heezen B.C, Ewing M 1952 Turbidity currents and submarine slumps, and the 1929 Grand Banks Earthquake. Am. J. Sci. 250: 775–793.

Holden, J. C. and Dietz, R. S. (1972). Galapagos gore, NazCoPac triple junction and Carnegie/Cocos ridges. Nature, 235: 266-269.

Holzer, T.L. and Savage, J.C., 2013. Global earthquake fatalities and population. Earthquake Spectra, 29(1): 155-175.

Hou, J.J., Han, M.K., Chai, B.L. and Han, H.Y., 1998. Geomorphological observations of active faults in the epicentral region of the Huaxian large earthquake in 1556 in Shaanxi Province, China. Journal of structural geology, 20(5): 549-557.

Insurance Information Institute, 2016, Earthquakes and Tsunamis, Insurance Information Institute Insurance topics, from: http://www.iii.org/fact-statistic/earthquakes-and-tsunamis

International Monetary Fund. 2016. Ecuador and the IMF. Country Info August 8 2016. International Monetary Fund, Washington DC: https://www.imf.org/external/country/ECU/index.htm

IGEPN (Instituto Geofísico Escuela Politécnica Nacional), 2016a: Informe Sísmico Especial Nº 22, 2016. www.igepn.edu.ec/servicios/noticias/1341-informe-sismico-especial-n-22-2016

IGEPN (Instituto Geofísico Escuela Politécnica Nacional), 2016b: Earthquake Overview. www.igepn.edu.ec

Ioualalen, M., Ratzov, G., Collot, J.Y. and Sanclemente, E., 2011. The tsunami signature on a submerged promontory: the case study of the Atacames Promontory, Ecuador. Geophysical Journal International, 184(2): 680-688.

Kahn, M.E., 2005. The death toll from natural disasters: the role of income, geography, and institutions. Review of economics and statistics, 87(2): 271-284.

Kanamori, H. and McNally, K.C., 1982. Variable rupture mode of the subduction zone along the Ecuador-Colombia coast. Bulletin of the Seismological Society of America, 72(4): 1241-1253.

Kelleher, J.A., 1972: Ruptures zones of large South American earthquakes and some predictions. Journal of Geophysical Research, 77, 11: 2087-2103.

Kellogg, J.N. and Vega, V., 1995: Tectonic development of Panama, Costa Rica and the Colombian Andes: Constraints from Global Positioning System geodetic studies and gravity. Geol. Soc. Am. Special Paper 295: 75–90.

Lebrat, M., Megard, F., Dupuy, C and Dostal, J., 1987: Geochemistry and tectonic setting of pre-collision Cretaceous and Paleogene volcanic rocks of Ecuador. Bulletin of the geological society of America, 99: 569-578.

Marano, K.D., Wald, D.J. and Allen, T.I., 2010. Global earthquake casualties due to secondary effects: a quantitative analysis for improving rapid loss analyses. Natural hazards, 52(2): 319-328.

Martínez, S. and El Comercio DATA. 2016: Conozca 208 bienes y servicios que pagarán 14% de IVA en Ecuador. Sección El Comercio-DATA, Compañía Anómima El Comercio, Quito, Ecuador. http://www.elcomercio.com/datos/servicios-productos-aumento-iva-ecuador.html

Masson, D.G., Harbitz, C.B., Wynn, R.B., Pedersen, G. and Løvholt, F., 2006: Submarine landslides: processes, triggers and hazard prediction. Philosophical Transactions of the Royal Society of London A: Mathematical, Physical and Engineering Sciences, 364(1845): 2009-2039.

McAdoo, B.G. and Watts, P., 2004: Tsunami hazard from submarine landslides on the Oregon continental slope. Marine Geology, 203(3): 235-245.

McCaffrey, R., 2008. Global frequency of magnitude 9 earthquakes. Geology, 36(3): 263-266.

McGuire, R.K., 1995. Probabilistic seismic hazard analysis and design earthquakes: closing the loop. Bulletin of the Seismological Society of America, 85(5): 1275-1284.

Michetti A.M., Esposito E., Guerrieri L., Porfido S., Serva L., Tatevossian R., Vittori E., Audemard F., Azuma T., Clague J., Comerci V., Gürpinar A., McCalpin J., Mohammadioun B., Mörner N.A., Ota Y. and Rogozhin E., 2007:. Intensity Scale ESI 2007. La Scala di Intensità ESI 2007, ed. L. Guerrieri e E. Vittori (Memorie Descrittive della Carta Geologica d'Italia, vol.74, Servizio Geologico d'Italia – Dipartimento Difesa del Suolo, APAT), Roma, http://www.apat.gov.it/site/it-IT/Progetti/-INQUA_Scale/.

Papanikolaou, I.D., Foumelis, M., Parcharidis, I., Lekkas, E.L. and Fountoulis, I.G., 2010: Deformation pattern of the 6 and 7 April 2009, MW= 6.3 and MW= 5.6 earthquakes in L'Aquila (Central Italy) revealed by ground and space based observations. Nat. Hazards Earth Syst. Sci, 10(1): 73-87.

Pararas-Carayannis, G. 1980: The Earthquake and Tsunami of December 12, 1979, in Colombia. Intern. Tsunami Information Center Report, Abstracted article in Tsunami Newsletter, Vol. XIII, No. 1.

Pararas-Carayannis, G., 1967: A study of the source mechanism of the Alaska earthquake and tsunami of March 27, 1964: Part I, Water waves. Pacific Science, 21: 301-310.

Pararas-Carayannis, G., 2006: The potential of tsunami generation along the Makran Subduction Zone in the northern Arabian Sea: Case study: The earthquake and tsunami of November 28, 1945. Science of Tsunami Hazards, 24(5): 358-384.

Pararas-Carayannis, G., 2010: The earthquake and tsunami of 27 February 2010 in Chile–Evaluation of source mechanism and of near and far-field tsunami effects. Science of Tsunami Hazards, 29, 2: 96-126.

Pararas-Carayannis, G., 2012: Potential of tsunami generation along the Colombia/Ecuador subduction margin and the Dolores-Guayaquil Mega-Thrust. Science of Tsunami Hazards, 31, 3: 209-230.

Pararas-Carayannis, G., 2014. The Great Tohoku-Oki earthquake and tsunami of March 11, 2011 in Japan: A critical review and evaluation of the tsunami source mechanism. Pure and applied geophysics, 171(12): 3257-3278.

Parra, H; Benito, B, Gaspar-Escribano, J. (2016). Seismic Hazard Assessment in Continental Ecuador. Bull Earthquake Eng., 1-31. DOI 10.1007/s10518-016-9906-7

Pilger, R. H., 1983. Kinematics of the South American subduction zone from global plate reconstructions. Geodynamics of the eastern Pacific region, Caribbean and Scotia arcs: 113-125.

Pontoise, B. and Monfret, T. (2004). Shallow seismogenic zone detected from an offshore-onshore temporary seismic network in the Esmeraldas area (northern Ecuador). Geochemistry, Geophysics, Geosystems, 5(2).

Raschky, P.A. 2008. Institutions and the losses from natural disasters. Natural Hazards and Earth System Science 8: 627-634.

Ratzov, G., Collot, J. Y., Sosson, M. and Migeon, S. (2010). Mass-transport deposits in the northern Ecuador subduction trench: Result of frontal erosion over multiple seismic cycles. Earth and Planetary Science Letters, 296(1): 89-102.

Ratzov, G., Sosson, M., Collot, J. Y., Migeon, S., Michaud, F., Lopez, E. and Le Gonidec, Y. (2007). Submarine landslides along the North Ecuador–South Colombia convergent margin: possible tectonic control. In Submarine Mass Movements and Their Consequences. Springer Netherlands: 47-55

Reyes, P & Michaud, F, 2012 "Mapa Geológico de la Margen Costera Ecuatoriana", 1:500.000. Petroecuador – EP – IRD (Eds). Quito Ecuador.

Reynaud, C., Jaillard, É., Lapierre, H., Mamberti, M. and Mascle, G. H. (1999). Oceanic plateau and island arcs of southwestern Ecuador: their place in the geodynamic evolution of northwestern South America. Tectonophysics, 307(3): 235-254.

Rodriguez, F., DHowitt, M.C., Toulkeridis, T., Salazar, R., Romero, G.E.R., Moya, V.A.R. and Padilla, O., 2016. The economic evaluation and significance of an early relocation versus complete destruction by a potential tsunami of a coastal city in Ecuador. Journal of Tsunami Society International, 35(1). 18-35

Rudolph E. and Szirtes S., 1911: Das kolumbianische Erdbeben am 31 Januar 1906, Gerlands Beitr. z. Geophysik , 2: 132- 275.

Ruff, L.J., and Kanamori, H., 1980, Seismicity and the subduction process: Physics of the Earth and Planetary Interiors, v. 23: 240–252, doi: 10.1016/0031–9201(80)90117-X.

Sato, H., Fehler, M.C. and Maeda, T., 2012. Seismic wave propagation and scattering in the heterogeneous earth, Berlin: Springer. 496pp

Secretaria Nacional de Gestión de Riesgos-SNGR. 2016. Informe de Siatuación No. 71. Equipo Técnico de la Secretaría de Gestión de Riesgos, SNGR. 15 pp. http://www.gestionderiesgos.gob.ec/wp-content/uploads/downloads/2016/05/INFORME-n71-SISMO-78-20302.pdf

Senplades. 2016. Evaluación de los Costos de Reconstrucción Sismo en Ecuador, abril 2016.Secretaría Nacional de Planificación y Desarrollo - Senplades, Quito, Ecuador. 20 pp.

Shepperd, G.L. and Moberly, R., 1981: Coastal structure of the continental margin, northwest Peru and southwest Ecuador. Geological Society of America Memoirs, 154: 351-392,

Shome, N., Cornell, C.A., Bazzurro, P. and Carballo, J.E., 1998. Earthquakes, records, and nonlinear responses. Earthquake Spectra, 14(3): 469-500.

Sieh K 2005 Aceh-Andaman earthquake: What happened and what's next?. Nature. 434: 573–574

Stainforth, R.M. 1948. Applied micropaleontology in Coastal Ecuador, Jour. Paleontology, 22, 142-146.

Swenson, J.L. and Beck, S.L., 1996: Historical 1942 Ecuador and 1942 Peru subduction earthquakes, and earthquake cycles along Colombia–Ecuador and Peru subduction segments. Pure Appl. Geophys.146 (1): 67–101.

Synolakis, C.E., Bardet, J.P., Borrero, J.C., Davies, H.L., Okal, E.A., Silver, E.A., Sweet, S. and Tappin, D.R., 2002, April. The slump origin of the 1998 Papua New Guinea tsunami. In Proceedings of the Royal Society of London A: Mathematical, Physical and Engineering Sciences, Vol. 458, No. 2020: 763-789.

Tappin, D.R., Watts, P., McMurtry, G.M., Lafoy, Y., Matsumoto, T., 2001. The Sissano Papua New Guinea tsunami of July 1998 - ofshore evidence on the source mechanism. Mar. Geol. 175, 1-23; Nature 379(18): 246-249.

Tappin, D.R., Watts, P., McMurtry, G.M., Lafoy, Y., Matsumoto, T., 2002. Prediction of slump generated tsunamis: The July 17, 1998 Papua New Guinea event. Sci. Tsunami Hazards 20: 222-238.

The World Bank. 2016. Ecuador Overview. World Bank – Ecuador home. Washington DC: http://www.worldbank.org/en/country/ecuador/overview

Tierra, A., Toulkeridis, T., Sani, J., Padilla Almeida, O. and Parra, H., 2017: Evaluation of horizontal and vertical positions obtained from an unmanned aircraft vehicle applied to large scale cartography of Infrastructure loss due to the Earthquake of April 2016 in Ecuador. Journal of Disaster Research, in press

Tinti, S., Armigliato, A., Pagnoni, G. and Zaniboni, F., 2005. Scenarios of giant tsunamis of tectonic origin in the Mediterranean. ISET Journal of Earthquake Technology, 42(4): 171-188.

Toulkeridis et al., 2017b; Real-Time Radioactive Precursor of the April 16, 2016 Mw 7.8 Earthquake in Ecuador. Submitted

Toulkeridis, T., Parra, H., Mato, F., Cruz D´Howitt, M., Sandoval, W., Padilla Almeida, O., Rentería, W., Rodríguez Espinosa, F., Salazar martinez, R., Cueva Girón, J., Taipe Quispe, A. and Bernaza Quiñonez, L., 2017a: Contrasting results of potential tsunami hazards in Muisne, central coast of Ecuador. J. Tsunami Soc. Int, 36: 13-40.

Toulkeridis, 2011: Volcanic Galápagos Volcánico. Ediecuatorial, Quito, Ecuador: 364 pp

Tschopp, H.J. 1953. Oil exploration in the Oriente of Ecuador. Bull.AAPG, 37: 2303-2347.

UNISDR, Corporación OSSO, 2016: Impacto de los desastres en América latina y el Caribe 1990-2013: Tendencias y estadísticas para 22 países. Oficina de las Naciones Unidas para la Reducción del Riesgo de Desastres-INISDR, Agencia Española de Cooperación Internacional para el Desarrollo-aecid, Corporación OSSO: 70 pp.

USGS (United States Geological Service), 2016a: Historic Earthquakes, 1906 January 31st. (http://earthquake.usgs.gov/earthquakes/world/events/1906_01_31.php)

USGS (United States Geological Service), 2016b: M7.8 - 29km SSE of Muisne, Ecuador.http://earthquake.usgs.gov/earthquakes/eventpage/us20005j32#general

USGS (United States Geological Service), 2016c: Earthquake Glossary - aftershocks.https://earthquake.usgs.gov/learn/glossary/?term=aftershocks

USGS (United States Geological Service), 2016d: Earthquake Catalog Search.https://earthquake.usgs.gov/earthquakes/search/

Ward S.N 2001 Landslide tsunami. J. Geophys. Res. 106, 11201–11215.
Baldock, J.W., 1982. Geology of Ecuador: explanatory bulletin of the national geological map of the Republic of Ecuador; 1: 1,000,000 scale. Ministerio de Recursos Naturales y Energéticos, Dirección General de Geología y Minas, Quito, Ecuador: 54pp
Bardet, J.P., Synolakis, C.E., Davies, H.L., Imamura, F. and Okal, E.A., 2003. Landslide tsunamis: Recent findings and research directions. Birkhäuser Basel: 1793-1809.
Beck, S.L. and Ruff, L.J., 1984: The rupture process of the great 1979 Colombia earthquake: evidence for the asperity model. J.Geophys. Res., 89: 9281–9291
Bender, B. (1983): Maximum likelihood estimation of b values for magnitude grouped data, Bull. Seismol. Soc. Am., 73: 831-851
Berninghausen, W.H., 1962. Tsunamis reported from the west coast of South America 1562-1960. Bull. of the Seismological Soc. of America, 52 (4): 915-921.
Biblioteca del Congreso Nacional de Chile. 2010. Efectos Económicos del Terremoto en Chile, por sectores y enel empleo: Una evaluación preliminar. BCN Informe, Santiago, Chile: 7pp.
Bristow, C.R. and Hoffstetter, R., 1977. Lexique Stratigraphique International; Ecuador. Second edition. Paris: Centre National de la Recherche Scientifique: 412p
Bryant, E., 2014. Tsunami: the underrated hazard. Springer: 222pp
Butler, R., Stewart, G.S. and Kanamori, H., 1979. The July 27, 1976 Tangshan, China earthquake—a complex sequence of intraplate events. Bulletin of the Seismological Society of America, 69(1): 207-220.
Cavallo, E.A., Powell A. and Becerra, O. 2010: Estimating the Direct Economic Damage of the Earthquake in Haiti.IDB Working Paper Series No.IDB-WP-163. The Inter American Development Bank; Department of Research and Chief Economist. Washington DC. 16 pp.
Chen, Y. ed., 1988. The great Tangshan earthquake of 1976: an anatomy of disaster. Pergamon: 162pp
Chunga, K., Besenzon, D., Mulas, M., Loayza, G. and Pindo JC., 2016: Areal distribution of Ground effects induced by the 2016 Mw 7.8 Pedernales earthquake (Ecuador). 88° Congresso della Societa' Geologica Italiana. S1. Earthquakes and Active Tectonics: a multidisciplinary approach. Napoli, 7/9 sept.
Chunga, K. and Toulkeridis, T. (2014). First evidence of paleo-tsunami deposits of a major historic event in Ecuador. J. Tsunami Soc. Int, 33: 55-69.
Collot, J.-Y., Michaud, F., Alvarado, A., Marcaillou, B., Sosson, M., Ratzov, G., Migeon, S., Calahorrano, A. and Pazmino, A., 2010. Vision general de la morfologa submarina del margen convergente de Ecuador-Sur de Colombia: implicaciones sobre la transferencia de masa y la edad de la subduccion de la Cordillera de Carnegie, in Sintesis de los Resultados de Investigacion Geologica y Geofisica Sobre el Margen Ecuatoriano, la Costa, la Cordillera Submarina de Carnegie, y de la Plataforma Volcanica de Galapagos, eds Collot, J.-Y., Sallares, V. & Pazmio, A., Publicacion CNDM-INOCAR-IRD, PSE001-09, Guayaquil, Ecuador: 47–74.
Collot, J.-Y., Michaud, F., Legonidec, Y., Calahorrano, A., Sage, F., Alvarado, A. & el personal cientifico y tecnico del INOCAR, 2005. Mapas del margen continental centro y sur de Ecuador: Bathymetria, relieve, refllectividad acustica e interpretacion geologica, Publicacion IOA - CVM- 04 - POST.

Collot, J.Y., Marcaillou, B., Sage, F., Michaud, F., Agudelo, W., Charvis, P., Graindorge, D., Gutscher, M.A. and Spence, G., 2004. Are rupture zone limits of great subduction earthquakes controlled by upper plate structures? Evidence from multichannel seismic reflection data acquired across the northern Ecuador–southwest Colombia margin. Journal of Geophysical Research: Solid Earth, 109(B11).
CRED (Centre for Research on the Epidemiology of Disasters) 2016: http://www.cred.be/node/1516
Driscoll, N.W., Weissel, J.K. and Goff, J.A., 2000. Potential for large-scale submarine slope failure and tsunami generation along the US mid-Atlantic coast. Geology, 28(5), pp.407-410.
Egbue, O. and Kellogg, J., 2010: Pleistocene to Present North Andean "escape". Tectonophysics 489: 248-257.
El Telegrafo, 2016: http://www.eltelegrafo.com.ec/noticias/ecuador/3/manana-se-daran-a-conocer-cifras-oficiales-del-costo-del-terremoto
El Universo, 2016: http://www.eluniverso.com/noticias/2016/04/25/nota/5544318/multilaterales-paises-ong-envian-recursos-exterior
Feininger, T. 1980. La geología histórica del Cretácico y el Paleógeno de la Costa Ecuatoriana, Politécnica, Monograf. Geología, V, 2: 7-48.
Ferris E. and Petz D. 2012. The year shock the rich: A review of natural disasters in 2011. Project on Internal Displacement, The Brookings Institution-The London School of Economics. Washington DC. 142 pp.
Fine I.V, Rabinovich A.B, Bornhold B.D, Thomson R.E, Kulikov E.A 2005 The Grand Banks landslide-generated tsunami of November 18, 1929: preliminary analysis and numerical modelling. Mar. Geol. 215, 45–57
Gang, Q., 1989: The Great China Earthquake. Beijing: Foreign Languages Press. 354pp
GEER-ATC Report (GEER-049), Nikolaou, S., Vera-Grunauer, X., Gilsanz, R. eds., "2016 Ecuador GEER-ATC Report version 1". Published in geerassociation.org: http://www.geerassociation.org/component/geer_reports/?view=geerreports&id=77&layout=default
Ghobarah, A., Saatcioglu, M. and Nistor, I., 2006. The impact of the 26 December 2004 earthquake and tsunami on structures and infrastructure. Engineering structures, 28(2): 312-326.
Gupta, H.K., Rao, N.P., Rastogi, B.K. and Sarkar, D., 2001. The deadliest intraplate earthquake. Science, 291(5511): 2101-2102.
Gusiakov, V.K., 2005: Tsunami generation potential of different tsunamigenic regions in the Pacific. Marine Geology, 215, 1-2: 3-9.
Gutenberg, B., 1939. Tsunamis and earthquakes. Bulletin of the Seismological Society of America, 29(4): 517-526.
Gutscher, M.A., Malavieille, J.S.L. and Collot, J.-Y., 1999: Tectonic segmentation of the North Andean margin: impact of the Carnegie ridge collision. Earth Planet. Sci. Lett. 168: 255–270.
Hampton M.A, Lee H.J, Locat J 1996 Submarine landslides. Rev. Geophys. 34: 33–59.
Harpp, K. S. and White, W. M., 2001: Tracing a mantle plume: Isotopic and trace element variations of Galápagos seamounts. Geochemistry, Geophysics, Geosystems, 2(6).

Harpp, K. S., Fornari, D. J., Geist, D. J. and Kurz, M. D., 2003: Genovesa Submarine Ridge: A manifestation of plume‐ridge interaction in the northern Galápagos Islands. Geochemistry, Geophysics, Geosystems, 4(9).

Heezen B.C, Ewing M 1952 Turbidity currents and submarine slumps, and the 1929 Grand Banks Earthquake. Am. J. Sci. 250: 775–793.

Holden, J. C. and Dietz, R. S. (1972). Galapagos gore, NazCoPac triple junction and Carnegie/Cocos ridges. Nature, 235: 266-269.

Holzer, T.L. and Savage, J.C., 2013. Global earthquake fatalities and population. Earthquake Spectra, 29(1): 155-175.

Hou, J.J., Han, M.K., Chai, B.L. and Han, H.Y., 1998. Geomorphological observations of active faults in the epicentral region of the Huaxian large earthquake in 1556 in Shaanxi Province, China. Journal of structural geology, 20(5): 549-557.

Insurance Information Institute, 2016, Earthquakes and Tsunamis, Insurance Information Institute Insurance topics, from: http://www.iii.org/fact-statistic/earthquakes-and-tsunamis

International Monetary Fund. 2016. Ecuador and the IMF. Country Info August 8 2016. International Monetary Fund, Washington DC: https://www.imf.org/external/country/ECU/index.htm

IGEPN (Instituto Geofísico Escuela Politécnica Nacional), 2016a: Informe Sísmico Especial Nº 22, 2016. www.igepn.edu.ec/servicios/noticias/1341-informe-sismico-especial-n-22-2016

IGEPN (Instituto Geofísico Escuela Politécnica Nacional), 2016b: Earthquake Overview. www.igepn.edu.ec

Ioualalen, M., Ratzov, G., Collot, J.Y. and Sanclemente, E., 2011. The tsunami signature on a submerged promontory: the case study of the Atacames Promontory, Ecuador. Geophysical Journal International, 184(2): 680-688.

Kahn, M.E., 2005. The death toll from natural disasters: the role of income, geography, and institutions. Review of economics and statistics, 87(2): 271-284.

Kanamori, H. and McNally, K.C., 1982. Variable rupture mode of the subduction zone along the Ecuador-Colombia coast. Bulletin of the Seismological Society of America, 72(4): 1241-1253.

Kelleher, J.A., 1972: Ruptures zones of large South American earthquakes and some predictions. Journal of Geophysical Research, 77, 11: 2087-2103.

Kellogg, J.N. and Vega, V., 1995: Tectonic development of Panama, Costa Rica and the Colombian Andes: Constraints from Global Positioning System geodetic studies and gravity. Geol. Soc. Am. Special Paper 295: 75–90.

Lebrat, M., Megard, F., Dupuy, C and Dostal, J., 1987: Geochemistry and tectonic setting of pre-collision Cretaceous and Paleogene volcanic rocks of Ecuador. Bulletin of the geological society of America, 99: 569-578.

Marano, K.D., Wald, D.J. and Allen, T.I., 2010. Global earthquake casualties due to secondary effects: a quantitative analysis for improving rapid loss analyses. Natural hazards, 52(2): 319-328.

Martínez, S. and El Comercio DATA. 2016: Conozca 208 bienes y servicios que pagarán 14% de IVA en Ecuador. Sección El Comercio-DATA, Compañía Anómima El Comercio, Quito, Ecuador. http://www.elcomercio.com/datos/servicios-productos-aumento-iva-ecuador.html

Masson, D.G., Harbitz, C.B., Wynn, R.B., Pedersen, G. and Løvholt, F., 2006: Submarine landslides: processes, triggers and hazard prediction. Philosophical Transactions of the Royal Society of London A: Mathematical, Physical and Engineering Sciences, 364(1845): 2009-2039.

McAdoo, B.G. and Watts, P., 2004: Tsunami hazard from submarine landslides on the Oregon continental slope. Marine Geology, 203(3): 235-245.

McCaffrey, R., 2008. Global frequency of magnitude 9 earthquakes. Geology, 36(3): 263-266.

McGuire, R.K., 1995. Probabilistic seismic hazard analysis and design earthquakes: closing the loop. Bulletin of the Seismological Society of America, 85(5): 1275-1284.

Michetti A.M., Esposito E., Guerrieri L., Porfido S., Serva L., Tatevossian R., Vittori E., Audemard F., Azuma T., Clague J., Comerci V., Gürpinar A., McCalpin J., Mohammadioun B., Mörner N.A., Ota Y. and Rogozhin E., 2007:. Intensity Scale ESI 2007. La Scala di Intensità ESI 2007, ed. L. Guerrieri e E. Vittori (Memorie Descrittive della Carta Geologica d'Italia, vol.74, Servizio Geologico d'Italia – Dipartimento Difesa del Suolo, APAT), Roma, http://www.apat.gov.it/site/it-IT/Progetti/-INQUA_Scale/.

Papanikolaou, I.D., Foumelis, M., Parcharidis, I., Lekkas, E.L. and Fountoulis, I.G., 2010: Deformation pattern of the 6 and 7 April 2009, MW= 6.3 and MW= 5.6 earthquakes in L'Aquila (Central Italy) revealed by ground and space based observations. Nat. Hazards Earth Syst. Sci, 10(1): 73-87.

Pararas-Carayannis, G. 1980: The Earthquake and Tsunami of December 12, 1979, in Colombia. Intern. Tsunami Information Center Report, Abstracted article in Tsunami Newsletter, Vol. XIII, No. 1.

Pararas-Carayannis, G., 1967: A study of the source mechanism of the Alaska earthquake and tsunami of March 27, 1964: Part I, Water waves. Pacific Science, 21: 301-310.

Pararas-Carayannis, G., 2006: The potential of tsunami generation along the Makran Subduction Zone in the northern Arabian Sea: Case study: The earthquake and tsunami of November 28, 1945. Science of Tsunami Hazards, 24(5): 358-384.

Pararas-Carayannis, G., 2010: The earthquake and tsunami of 27 February 2010 in Chile–Evaluation of source mechanism and of near and far-field tsunami effects. Science of Tsunami Hazards, 29, 2: 96-126.

Pararas-Carayannis, G., 2012: Potential of tsunami generation along the Colombia/Ecuador subduction margin and the Dolores-Guayaquil Mega-Thrust. Science of Tsunami Hazards, 31, 3: 209-230.

Pararas-Carayannis, G., 2014. The Great Tohoku-Oki earthquake and tsunami of March 11, 2011 in Japan: A critical review and evaluation of the tsunami source mechanism. Pure and applied geophysics, 171(12): 3257-3278.

Parra, H; Benito, B, Gaspar-Escribano, J. (2016). Seismic Hazard Assessment in Continental Ecuador. Bull Earthquake Eng., 1-31. DOI 10.1007/s10518-016-9906-7

Pilger, R. H., 1983. Kinematics of the South American subduction zone from global plate reconstructions. Geodynamics of the eastern Pacific region, Caribbean and Scotia arcs: 113-125.

Pontoise, B. and Monfret, T. (2004). Shallow seismogenic zone detected from an offshore‐onshore temporary seismic network in the Esmeraldas area (northern Ecuador). Geochemistry, Geophysics, Geosystems, 5(2).

Raschky, P.A. 2008. Institutions and the losses from natural disasters. Natural Hazards and Earth System Science 8: 627-634.
Ratzov, G., Collot, J. Y., Sosson, M. and Migeon, S. (2010). Mass-transport deposits in the northern Ecuador subduction trench: Result of frontal erosion over multiple seismic cycles. Earth and Planetary Science Letters, 296(1): 89-102.
Ratzov, G., Sosson, M., Collot, J. Y., Migeon, S., Michaud, F., Lopez, E. and Le Gonidec, Y. (2007). Submarine landslides along the North Ecuador–South Colombia convergent margin: possible tectonic control. In Submarine Mass Movements and Their Consequences. Springer Netherlands: 47-55
Reyes, P & Michaud, F, 2012 "Mapa Geológico de la Margen Costera Ecuatoriana", 1:500.000. Petroecuador – EP – IRD (Eds). Quito Ecuador.
Reynaud, C., Jaillard, É., Lapierre, H., Mamberti, M. and Mascle, G. H. (1999). Oceanic plateau and island arcs of southwestern Ecuador: their place in the geodynamic evolution of northwestern South America. Tectonophysics, 307(3): 235-254.
Rodriguez, F., DHowitt, M.C., Toulkeridis, T., Salazar, R., Romero, G.E.R., Moya, V.A.R. and Padilla, O., 2016. The economic evaluation and significance of an early relocation versus complete destruction by a potential tsunami of a coastal city in Ecuador. Journal of Tsunami Society International, 35(1). 18-35
Rudolph E. and Szirtes S., 1911: Das kolumbianische Erdbeben am 31 Januar 1906, Gerlands Beitr. z. Geophysik , 2: 132- 275.
Ruff, L.J., and Kanamori, H., 1980, Seismicity and the subduction process: Physics of the Earth and Planetary Interiors, v. 23: 240–252, doi: 10.1016/0031–9201(80)90117-X.
Sato, H., Fehler, M.C. and Maeda, T., 2012. Seismic wave propagation and scattering in the heterogeneous earth, Berlin: Springer. 496pp
Secretaria Nacional de Gestión de Riesgos-SNGR. 2016. Informe de Siatuación No. 71. Equipo Técnico de la Secretaría de Gestión de Riesgos, SNGR. 15 pp. http://www.gestionderiesgos.gob.ec/wp-content/uploads/downloads/2016/05/INFORME-n71-SISMO-78-20302.pdf
Senplades. 2016. Evaluación de los Costos de Reconstrucción Sismo en Ecuador, abril 2016.Secretaría Nacional de Planificación y Desarrollo - Senplades, Quito, Ecuador. 20 pp.
Shepperd, G.L. and Moberly, R., 1981: Coastal structure of the continental margin, northwest Peru and southwest Ecuador. Geological Society of America Memoirs, 154: 351-392,
Shome, N., Cornell, C.A., Bazzurro, P. and Carballo, J.E., 1998. Earthquakes, records, and nonlinear responses. Earthquake Spectra, 14(3): 469-500.
Sieh K 2005 Aceh-Andaman earthquake: What happened and what's next?. Nature. 434: 573–574
Stainforth, R.M. 1948. Applied micropaleontology in Coastal Ecuador, Jour. Paleontology, 22, 142-146.
Swenson, J.L. and Beck, S.L., 1996: Historical 1942 Ecuador and 1942 Peru subduction earthquakes, and earthquake cycles along Colombia–Ecuador and Peru subduction segments. Pure Appl. Geophys.146 (1): 67–101.

Synolakis, C.E., Bardet, J.P., Borrero, J.C., Davies, H.L., Okal, E.A., Silver, E.A., Sweet, S. and Tappin, D.R., 2002, April. The slump origin of the 1998 Papua New Guinea tsunami. In Proceedings of the Royal Society of London A: Mathematical, Physical and Engineering Sciences, Vol. 458, No. 2020: 763-789.

Tappin, D.R., Watts, P., McMurtry, G.M., Lafoy, Y., Matsumoto, T., 2001. The Sissano Papua New Guinea tsunami of July 1998 - ofshore evidence on the source mechanism. Mar. Geol. 175, 1-23; Nature 379(18): 246-249.

Tappin, D.R., Watts, P., McMurtry, G.M., Lafoy, Y., Matsumoto, T., 2002. Prediction of slump generated tsunamis: The July 17, 1998 Papua New Guinea event. Sci. Tsunami Hazards 20: 222-238.

The World Bank. 2016. Ecuador Overview. World Bank – Ecuador home. Washington DC: http://www.worldbank.org/en/country/ecuador/overview

Tierra, A., Toulkeridis, T., Sani, J., Padilla Almeida, O. and Parra, H., 2017: Evaluation of horizontal and vertical positions obtained from an unmanned aircraft vehicle applied to large scale cartography of Infrastructure loss due to the Earthquake of April 2016 in Ecuador. Journal of Disaster Research, in press

Tinti, S., Armigliato, A., Pagnoni, G. and Zaniboni, F., 2005. Scenarios of giant tsunamis of tectonic origin in the Mediterranean. ISET Journal of Earthquake Technology, 42(4): 171-188.

Toulkeridis et al., 2017b; Real-Time Radioactive Precursor of the April 16, 2016 Mw 7.8 Earthquake in Ecuador. Submitted

Toulkeridis, T., Parra, H., Mato, F., Cruz D´Howitt, M., Sandoval, W., Padilla Almeida, O., Rentería, W., Rodríguez Espinosa, F., Salazar martinez, R., Cueva Girón, J., Taipe Quispe, A. and Bernaza Quiñonez, L., 2017a: Contrasting results of potential tsunami hazards in Muisne, central coast of Ecuador. J. Tsunami Soc. Int, 36: 13-40.

Toulkeridis, 2011: Volcanic Galápagos Volcánico. Ediecuatorial, Quito, Ecuador: 364 pp

Tschopp, H.J. 1953. Oil exploration in the Oriente of Ecuador. Bull.AAPG, 37: 2303-2347.

UNISDR, Corporación OSSO, 2016: Impacto de los desastres en América latina y el Caribe 1990-2013: Tendencias y estadísticas para 22 países. Oficina de las Naciones Unidas para la Reducción del Riesgo de Desastres-INISDR, Agencia Española de Cooperación Internacional para el Desarrollo-aecid, Corporación OSSO: 70 pp.

USGS (United States Geological Service), 2016a: Historic Earthquakes, 1906 January 31st. (http://earthquake.usgs.gov/earthquakes/world/events/1906_01_31.php)

USGS (United States Geological Service), 2016b: M7.8 - 29km SSE of Muisne, Ecuador.http://earthquake.usgs.gov/earthquakes/eventpage/us20005j32#general

USGS (United States Geological Service), 2016c: Earthquake Glossary - aftershocks.https://earthquake.usgs.gov/learn/glossary/?term=aftershocks

USGS (United States Geological Service), 2016d: Earthquake Catalog Search.https://earthquake.usgs.gov/earthquakes/search/

Ward S.N 2001 Landslide tsunami. J. Geophys. Res. 106, 11201–11215.

ISSN 8755-6839

SCIENCE OF TSUNAMI HAZARD

Journal of Tsunami Society International

Volume 36 Number 4 2017

SPECTRAL ANALYSIS OF ENERGY DISTRIBUTION AT TSUNAMI WAVE PROPAGATION IN OKHOTSK SEA BASIN

Alexandr RASSADIN[1], Artem TUGARYOV[1], Broneslav KISELMAN[1], Raissa MAZOVA[1] AND Leopold LOBKOVSKY[2]

[1] R.E.Alekseev Nizhny Novgorod State Technical University, 24 Minin str., Nizhny Novgorod 603695 Russia

[2]P.P.ShirshovInstitute of Oceanology, Russian Academy of Sciences, 36 Nakhimovsky ave., Moscow, 123456 Russia

E-mail address: science@arassadin.com, bkiselman@mail.ru, raissamazova@yandex.ru, llobkovsky@ocean.ru

ABSTRACT

The presence of residual subduction zone under Kuril island arc makes a region of Kuril ridge islands be potential seismic-danger since underwater earthquakes in subduction zone with magnitude $M > 6$ are usually tsunamigenic. Potential strong earthquakes near the Kuril-Kamchatka trench passes along Kuril island, and tsunami generated by them carry a greater risk while passing through Bussol and Krusenstern straits for all Okhotsk seashore including the Sakhalin coast where now taking place a rising of infrastructure development connected with development an oil and gas industry. In the history, a few occasions of tsunami generation near the Sakhalin coast, caused by earthquakes in Kuril ridge region had been recorded (see, e.g. [1]).

Such occasion taken place while strongest earthquake occurs recently near the Simushir island (15 November 2006). This earthquake and tsunami were predicted half of year before the event: while marine expedition clarified structure and size of possible undersea source in the area of seismic gap in Middle Kuril region. Then, the numerical

simulation of tsunami generation and propagation was performed using keyboard model of an earthquake. Since not all seismic gap area was activated, it's interesting to perform a numerical modeling of potential catastrophic earthquake and tsunami in residual seismic gap of Middle Kuril and compare results with similar scenario of earthquake and tsunami for hypothetical source placed in inactive part of seismic gap. In this paper, such modeling was performed based on keyboard model of tsunamigenic earthquakes [2]. Calculation was performed using nonlinear shallow water equations and considering bottom dissipation. Spectral analysis of tsunami wave field in this model gives new possibilities for determination of energy characteristics of tsunami in the whole modeling area.

1. INTRODUCTION

Currently, there are several seismic gaps, where earthquake did not happen for a long time. These include Aleutian, and Shumagin seismic gaps, and residual seismic gap in the area of middle Kuriles. The seismic gap of the Middle Kuril Islands [3] until 30 September 2006 was one of these "zones of silence." The hypothetical earthquake source in this area was determined by two Russian expeditions of the Shirshov Institute of Oceanology of the Russian Academy of Sciences, conducted in 2005 and 2006. This center was schematically represented as 8-keyboard blocks [4]. After the earthquake of September 30, 2006 and tsunamigenic earthquake November 15, 2006, seismic gap has been in fact halved. It is now possible to talk about a potential earthquake with a source, localized in the Pacific against the Kruzenshtern Strait, which is now presented by the remaining four blocks. Preliminary calculation performed before the events of 30 September and 15 November 2006 [4.5] for a full 8-block area of source in the middle Kuriles, has shown that the strong earthquake with a magnitude of more than 7.5 - 8 catastrophic tsunami on the coasts of the settlement area are possible. The occurred six months after these preliminary calculations of earthquake simulation in the area of the Kuril chain in September 30, 2017 with a magnitude of M = 7.1, does not cause catastrophic consequences, while earthquake 15 November.2006 with magnitude M = 8.3 caused a tsunami that confirm the preliminary calculation [4]. As known, on Sakhalin Island, there are numerous mining and processing of oil, and there are numerous settlements. For any significant earthquake and subsequent tsunami attacking the Sakhalin coast an enormous damage, both human and material is possible. In this regard, we now discuss in detail the wave energy distribution in the Sea of Okhotsk in different variants of its arrival in the Pacific Ocean. To analyze the process of generation and propagation of tsunami waves before and after the passage of the Bussole and Kruzenshtern straits in the water area synthetic tide gauges at given points were placed. At the propagation of tsunami waves both the amplitude characteristics of the wave field and distribution of energy over the frequencies are determined not only by bathymetry basin, depending not only on the direction of propagation, but also on a form of tsunami source and its evolution during the formation tsunami. Numerical modeling of tsunami generation and thus the formation of his

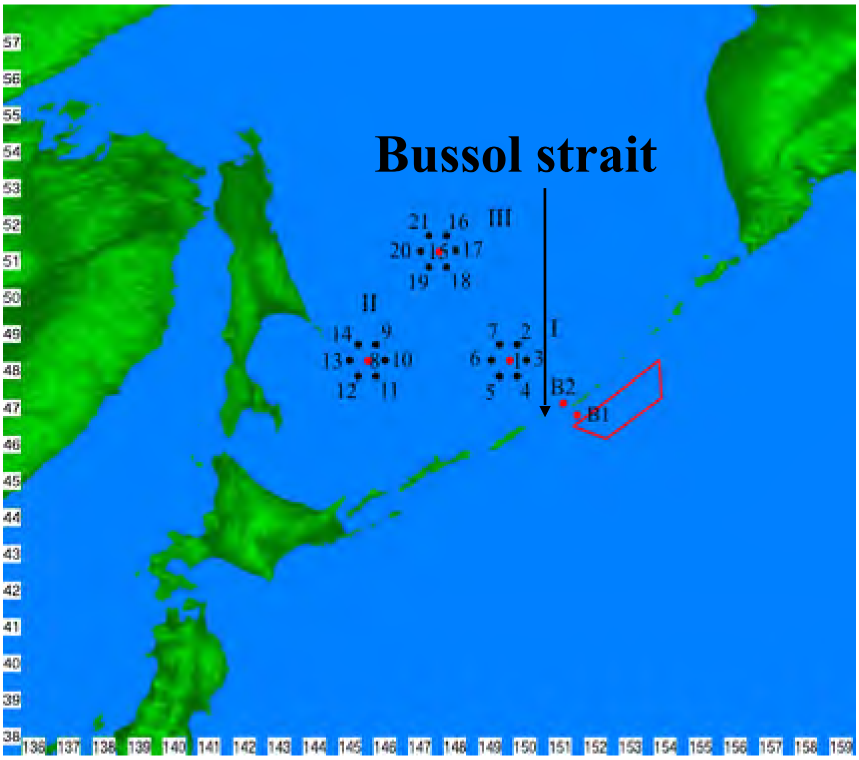

Fig. 1. Location of virtual tide gauges calculated: points B1, B2 correspond to input and output of wave flow through Bussole strait; points 1,8,15 correspond to centers of considered regions of the basin; points 2-7, 9-14, 16-21 indicate location of computed (synthetic) tide gauges.

source using the proposed keyboard block model of underwater seismic source [4-6] allows one to calculate the structure of the wave field in coastal area in more detail, which is important for practical applications [7].

2. STATEMENT OF THE PROBLEM

To simulate potential catastrophic earthquakes with a magnitude of 8.2, two hypothetical earthquake sources were selected, about 230 km long and 100 km wide, located in front of the Bussole strait (SCENARIO 1) (Fig. 1) and the Kruzenshtern strait (SCENARIO 2) (Fig. 2). To estimate the wave energy directivity of the given seismic sources the synthetic tide gauges have been placed at the inlet and outlet passages, and in the Sea of Okhotsk, where they are grouped into six "point clouds". Such an arrangement of synthetic tide gauges allows us to keep track of what part of the wave energy is transferred from the Pacific Ocean to the Okhotsk Sea through the Bussole and the Kruzenshtern straits, respectively, and how, for both scenarios, wave energy are distributed on the Sea of Okhotsk. Data from these gauges are analyzed using time-frequency analysis [8-12].

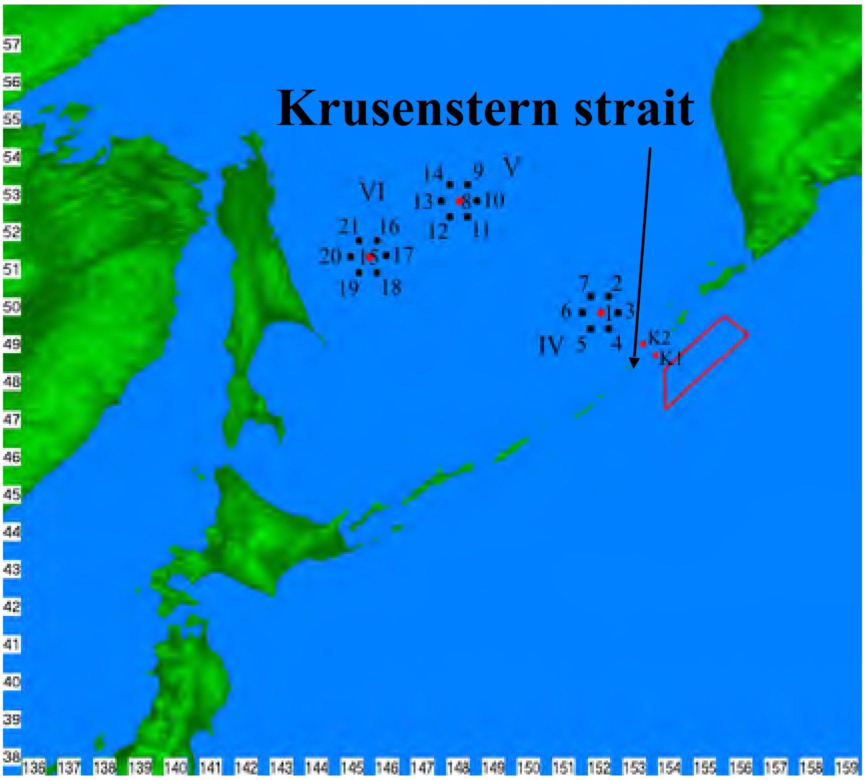

Fig.2. Location of virtual tide gauges: points K1,K2 correspond to input and output of wave flow through Kruzenshtern strait; points1,8,15 correspond to centers of considered regions of the basin; points 2-7, 9-14, 16-21 indicate location of computation synthetic tide gauges.

3. MATHEMATICAL MODEL USED FOR COMPUTATION

Simulation of the process of generation and propagation of tsunami wave was carried out in the framework of nonlinear shallow water equations (see, e.g. [3,4,13,14]

$$\begin{cases} \vec{U}_t + \vec{U} \cdot grad\ \vec{U} + g \cdot grad\,\eta = \vec{F} \\ \eta_t + div\left((H + \eta - B)\vec{U}\right) = B_t \end{cases} \tag{1}$$

where x and y are the spatial coordinates; t is the time, $\vec{U}(u,v)$ is the velocity of the particle; $u\ (x,\ y,\ t), v\ (x,\ y,\ t)$ are the velocity components; η is the water surface disturbance with respect to its initial level; H is the depth of the basin, $B(x,y,t)$ is the change in the seabed (considering the dynamic characteristics of the seismic source); g is the gravitational acceleration. Here,

4

$\vec{F} = \begin{pmatrix} f_1 \\ f_2 \end{pmatrix}$; where $f_1 = \frac{-C_h}{H+\eta} u\sqrt{u^2+v^2}$, $f_2 = \frac{-C_h}{H+\eta} v\sqrt{u^2+v^2}$ determine the bottom friction, and $Ch = \frac{(H+\eta-B)^{0.4}}{sh}$ - Shezy coefficient, and *sh* is the roughness coefficient function, $B(x,y,t)$ describes the variation of the sea bottom in the area of the seismic source. The computational domain is shown in Fig.1 and Fig.2.

Of the variety of difference schemes approximating equations (1), we chose the scheme proposed in [15] because of its high algorithmic versatility. The scheme is based on a divided difference and, in conjunction with the central difference approximation of spatial derivatives, simplifies the numerical implementation of boundary conditions.

For the numerical calculations it was used bathymetric map, compiled by Svarichevsky (see, e.g. [16]) with section isobaths from 100 to 250 m. When knowing step by coordinates, the best time step for the whole area was found. The distance between adjacent nodes on the parallel in meters calculated from the ratio $\Delta y_{p\,j} = \frac{\Delta x_p \cdot \pi \cdot \cos(y_n + j \cdot \Delta y)}{180}$, step at a time, in seconds, was obtained it turns out, on the basis of the conditions of stability of the difference scheme $\Delta t_j = \frac{\Delta x_p \cdot \Delta y_{p\,j} \cdot M}{\sqrt{g \cdot H_{max} \cdot (\Delta x_p{}^2 + \Delta y_{p\,j}{}^2)}}$, where H_{max} is the absolute value of the maximum depth of the water area under consideration $M^2 = \frac{1+\sqrt{f^2+1}}{2}$.

4. RESULTS OF THE NUMERICAL SIMULATION

In Figs.3,4, examples of realization of generation and propagation of tsunami waves for the two scenarios are presented. It is clearly seen that the ridge Vityaz and the Kuril Islands hinder the passage of the wave in the direction of the Sea of Okhotsk. In this part, the wave energy is reflected from the islands to the ocean, but the main part of the wave passes through the deep of Krusenstern and Bussole straits, which act as natural waveguides. After passing the Kurile chain these straits serve as two point sources being primary sources reradiating energy of waves. Wave fronts are generated as a function of time, speed and vertical position of moving keyboard blocks on the bottom.

In Fig.3, results of numerical simulation of generation and propagation of tsunami waves, when the seismic source is located in front of the Bussole strait (Scenario 1) are presented. The figure shows the position of the wave fronts for the 9 time points of wave propagation through the Bussole strait and propagation of tsunami waves across the Sea of Okhotsk. On the top left panel, t = 16 min wave passes through the strait. It is clearly seen that the wave front has a rounded shape, which is then slightly elongated toward the Deriugina Trough and is directed along the Kurile basin toward Sakhalin Island and

Hokkaido (Japan). It should be noted that the wave propagates at a relatively high speed (600 km / h), due to considerable depth (3300 m) of the basin. Intensely moving to the south-east of Sakhalin Island, the wave front for almost 3 hours evenly spread in the waters to the north, in the direction of the mainland (middle panel). It is only when reaching the middle of Sakhalin, the wave becomes pronounced acute form (third panel). This type of directional pattern is associated with the consideration of the work of one source (one Strait). In the case where the length of the seismic source, located in the middle part of Kuriles, is considerably more, so that the wave passes through both straits simultaneously, the radiation pattern is close to isotropic. Further, it is clearly seen that the wave front becomes almost flat.

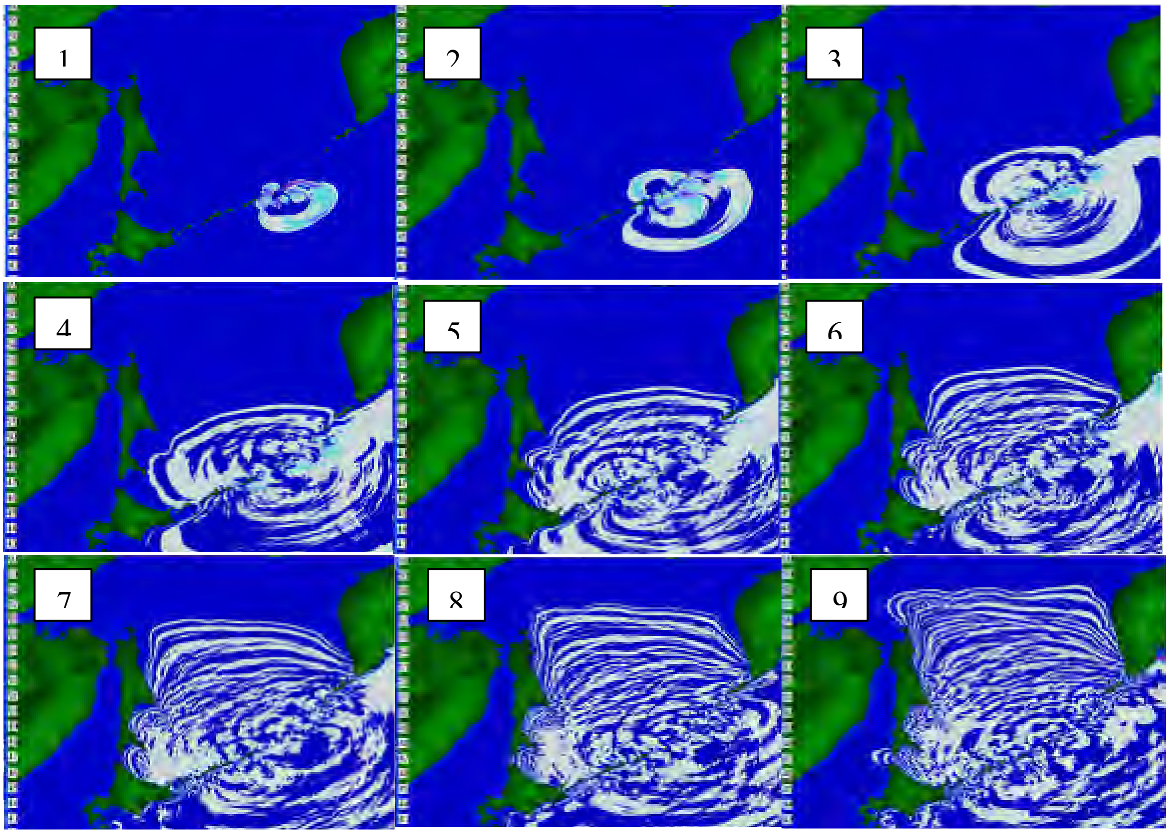

Fig.3. Position of wave fronts for 9 time moments for scenario 1.

Fig.4 shows results of simulation of the Scenario 2, when the seismic source is located in front of the of Kruzenshtern strait. The figure shows the position of the fronts of waves during the passage of the Kruzenshtern strait (upper panel) and return to the Sea of Okhotsk to 9 points in time. On the top left panel, t = 22 min wave passes through the strait, and the wave front passing through the Kruzenshtern strait has a distinctive acute form, and only 60 minutes to get a flat (middle panel).

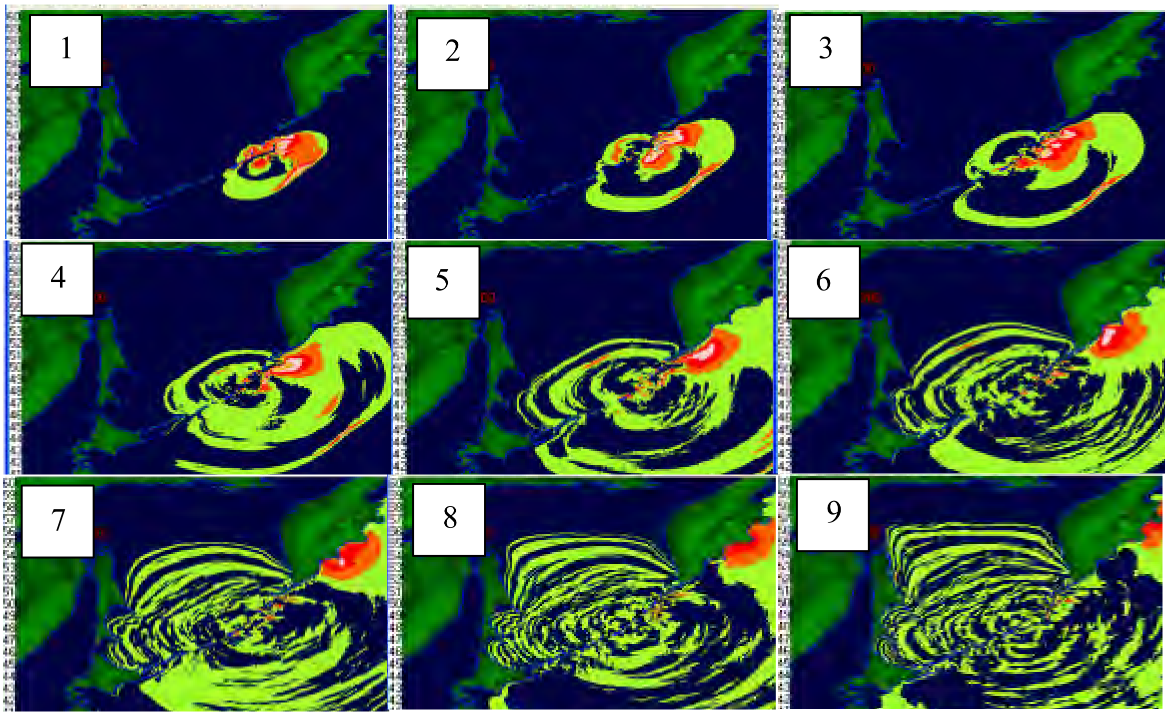

Fig.4. Position of wave fronts for 9 time moments for scenario 2.

5. SPECTRAL ANALYSIS

Using the above results of simulation of the generation and propagation of tsunami waves in the basin it was carried out the one-dimensional and two-dimensional (wavelet) spectral analysis and obtained spectral characteristics of tsunami waves in the Sea of Okhotsk for the potential strong underwater earthquakes with sources located in the seismic gap of middle Kuriles before Bussol and Kruzenshtern straits.

To analyze the energy distribution in the Sea of Okhotsk, two approaches were used: amplitude logarithmic transfer functions and amplitude wavelet-spectrogram. From each tide gauge records there were sampled segments of a length of N = 35,000 counts (about 5 RTC) [11-13]. The transfer functions of the amplitude spectra demonstrate the correlation between the absolute values of energies (the energy in our case is a quantity proportional to the square of the amplitude of the wave) in the two points of observation. For each set of tide-gauge data it was calculated spectral density of signal power received by the periodogram method

$$W(\omega) = \frac{1}{MN|w|^2} \sum_{m=1}^{M} \left| \sum_{n=l*(m-1)}^{n=l*m-1} x_n w_n exp(-i\omega nT) \right|^2 \tag{2}$$

$$l := \frac{N}{M}, T := \frac{t_{max}-t_0}{N},$$

as well as the value

$$L(\omega) = 10\lg|W(\omega)| \tag{3}$$

where T is the tide gauge record sampling interval, $x(t)$ is the signal received from a synthetic tide gauge, M is the number of spectral estimation segments, l is the number of samples in the segment , t_0 is the start time of observation, t_{max} is the end time of observation, $w(t)$ is the weighting function.

The transfer functions for the points with numbers m and n are as the ratio of the spectral density of the signal modules in the corresponding points [12]:

$$L_{m\to n} = L(\omega)_n - L(\omega)_m = 10\lg\left(\frac{|W(\omega)_n|}{|W(\omega)_m|}\right) \tag{4}$$

Spectrogram is the most obvious way to understand how to change over time, the frequency distribution of wave energy. Amplitude spectra were calculated using a filter set based on a Gaussian function for different σ

$$f_k(t) = \frac{1}{\sqrt{2\pi}} exp\left(-\frac{t^2}{2\sigma^2}\right) exp\ (i\omega kT)$$

$$f_j(t) = \frac{1}{\sqrt{2\pi}} exp\left(-\frac{{\omega_j}^2 t^2}{\sigma_j}\right) exp(i\omega_j t)$$

$\omega_j \in [\omega_{min}, \omega_{max}]$, for different σ. (5)

200 filters were used with same Q-factor and central frequency, linearly distributed from 0.1 to 8 cph.

6. IMPLEMENTATION OF SCENARIOS I AND II

6.1 Analysis of the implementation scenario I.

Fig.5 shows the wave and power characteristics for the tsunami wave that came from the Pacific Ocean to the Bussole strait (see Fig.1, B1). Fig.5.1 shows the calculated tide gauge record with synthetic tide gauge located at the entrance to the strait. Built to it, using the formulas (2) - (5) wavelet-spectrogram is shown in Fig.5.3. The figure which clearly shows that the main wave energy to an entry point in the Strait is concentrated in the area of almost triangular in shape for the interval from 20 to 70 minutes, and the frequency in the range of 1-4 cph, which corresponds to T ~ 15-60 min waves. The intensity is of about 50 dB. This is reflected on the energy curve (Fig.5.4) as a peak at a given interval. It can be seen that the maximum concentration of energy is typical for the time range of 20-70 min (Fig.5.2). Energy for the exit of the Strait (Fig.6.3) is distributed more evenly over the entire range of observation, that can be well seen in the graph of wavelet-spectrogram. The highest intensity of the wave to 45 dB in the frequency range of 3.1 cph is observed in the range of 30 to 80

min. In the interval of 110 to 170 min in the same frequency range 3.1 cph, less intensity of up to 35 dB is obtained (Fig.6.3). At the energy curve (Fig.6.4) this range corresponds to a region of increasing functions. One can also see that the maximum concentration of energy is typical for the time range T ~ 30-80 min (Fig.6.2). The peak on the energy curve (Fig.6.2) is in the time interval T ~ 20-50 min. Comparing the peaks of the input points in the Strait of (B1) (Fig.5.4) and exit the Strait (B2) (Fig.6.4) in the plot of the instantaneous power, it can be concluded about the time of the passage of a wave of strait T ~ 20-30 min. Relevant frequency range for point B2 (out of the Strait) is wider than B1 (the entrance to the Strait) is 1.5 times that can be clearly seen from the graphs of the frequency distribution of energy (Fig.5.4, Fig.6.4).

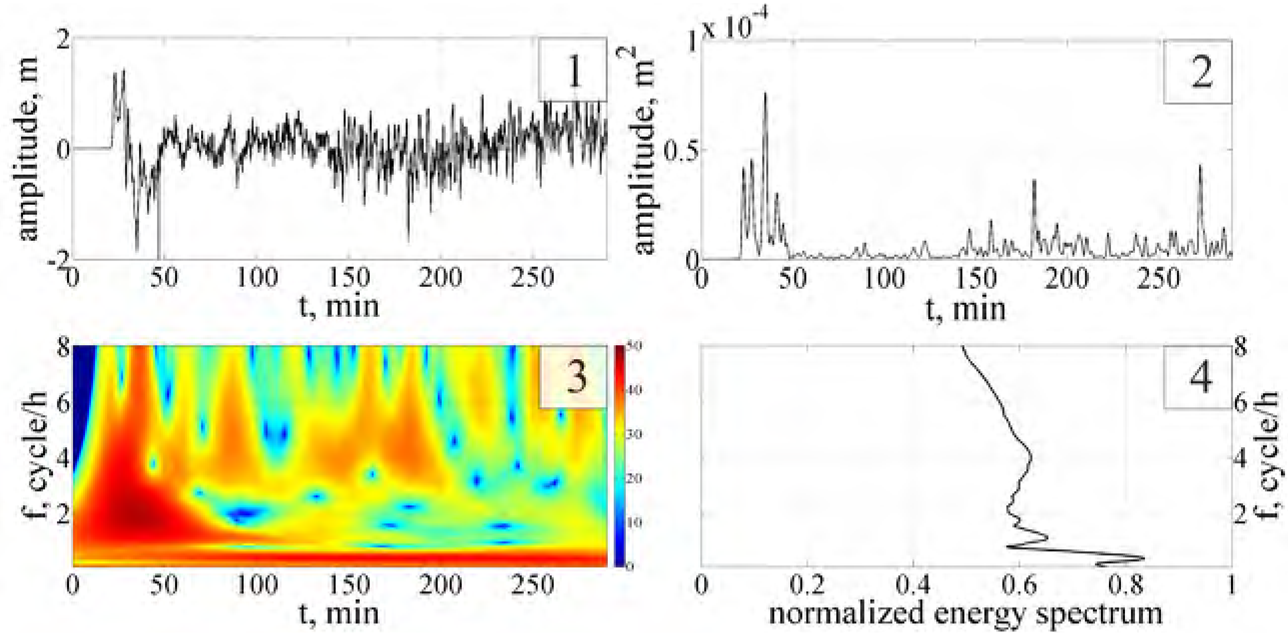

Fig.5. Wave and energy characteristics of tsunami before enter to Bussol strait: (1)- tide gauge record, (2)- short time power for wave front, (3)- wavelet-spectrogram, (4) - estimation of spectrum of energy.

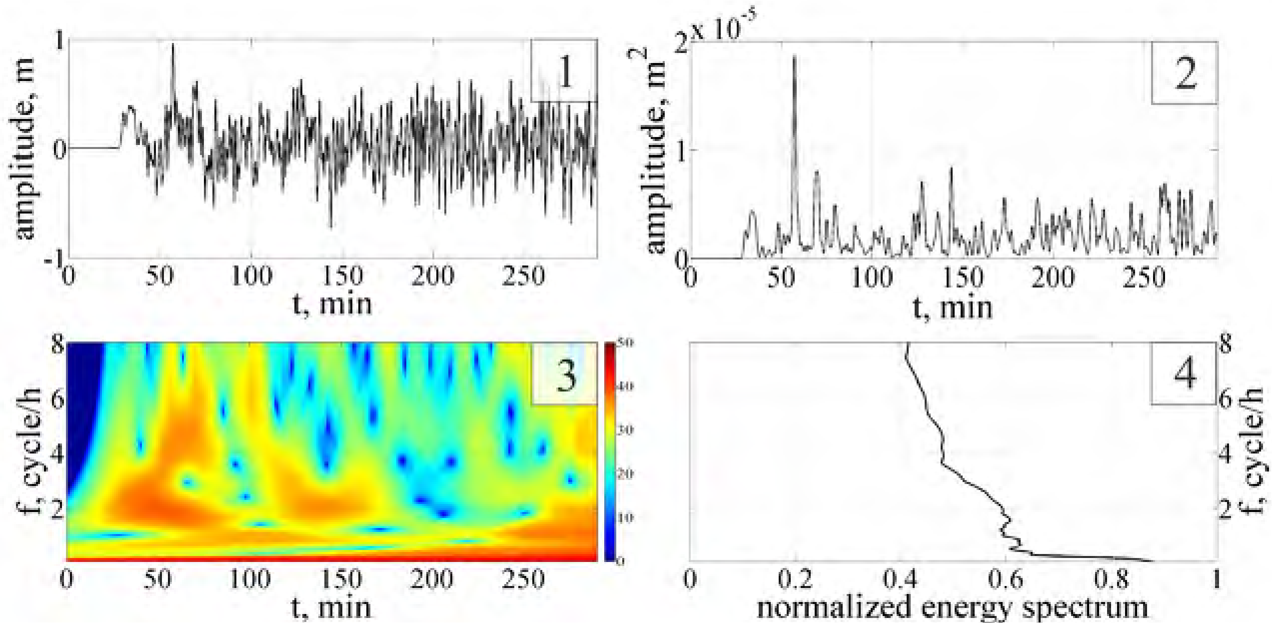

Fig.6. Wave and energy characteristics of tsunami at output from the Bussol strait: 1) tide gauge record, (2)- short time for wave front, (3)- wavelet spectrogram, (4) - estimation of spectrum of energy.

Speaking about the transfer of energy through the strait, it should be noted that the wave loses its energy much with the greatest loss was for long waves (up to 20 dB and a maximum of 7 dB on average) (see Fig.7). The attenuation for frequencies are 0.6, 2.5, 4.2, 7.5 cph i.e., for periods of T = 100 min, 25 min, 14 min, 8 min, most intense observed attenuation, although local maxima at the frequencies f = 1.5, 3.5, 6.5 cph (T = 40 min, 17 min, 6 min) are visible.

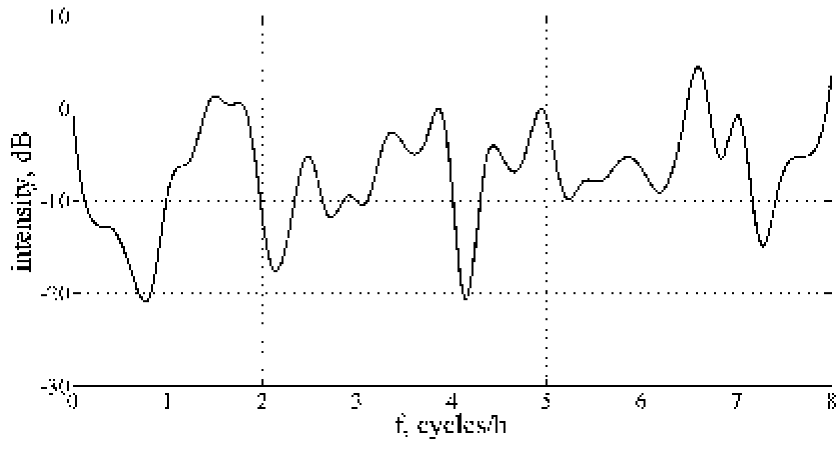

Fig.7. Logarithmic transfer function input-output for Bussol strait.

6.2 **Analysis of the implementation of the II scenario.**

Fig.8 and Fig.9 show the energy wave characteristics, at the entrance to the Strait of Kruzenshtern and after outcome the wave of the Strait. Fig.8.3 clearly shows that the spectrum contains three areas of signal amplification corresponding to the frequencies $f \approx$

1-3,5 cph (period T = 17-60 min). Analysis of the data shows that the amplification exists in range of T ~ 20-50 min, 125-175 min and 200-280 min with the greatest intensity to 45 dB. For the time range at the instantaneous power plot (Fig.8.2) the uniform energy distribution is characteristic with a peak at around 18 min.

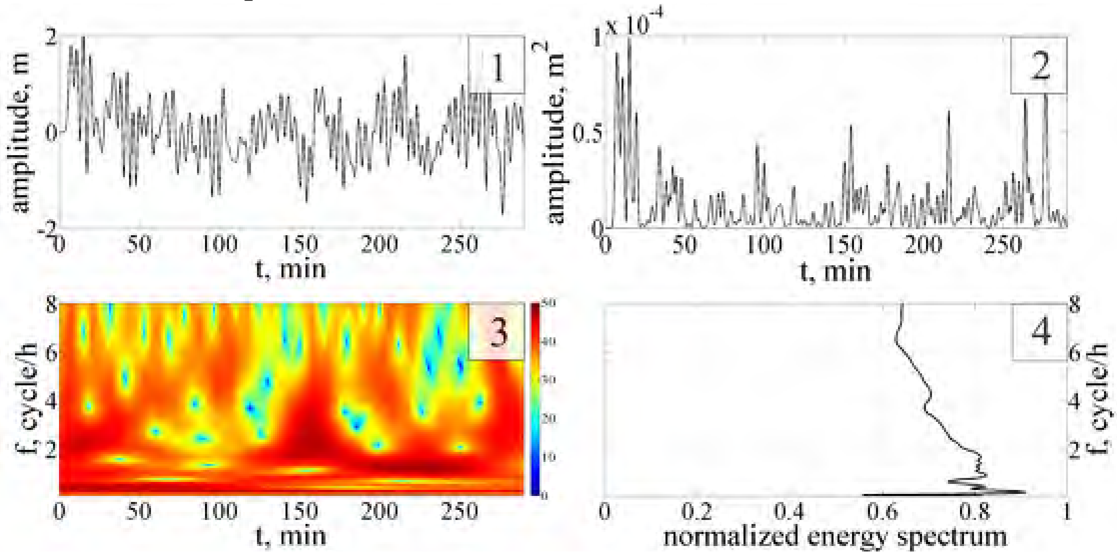

Fig.8. Wave and energy characteristics of tsunami before enter to Kruzenshtern strait: 1) tide gauge record, 2) instant power for wave front, 3) wavelet-spectrogram, 4) frequency characteristics of wave energy.

In Fig.9.3 it can be clearly seen that in spectrum it is present almost permanent component with a frequency of f ~ 1-2 cph (during 30-60min) with an intensity of > 50 dB. As follows from the instantaneous power plot (Fig.9.2), under the passage of the waves through the Strait Kruzenshtern part of the wave energy (up 2.5 times) is also lost. In the wave train at outcome from the Kruzenshtern Strait the long-wavelength component prevails what is reflected in the characteristic form of a graph of the frequency distribution (Fig.9.4).

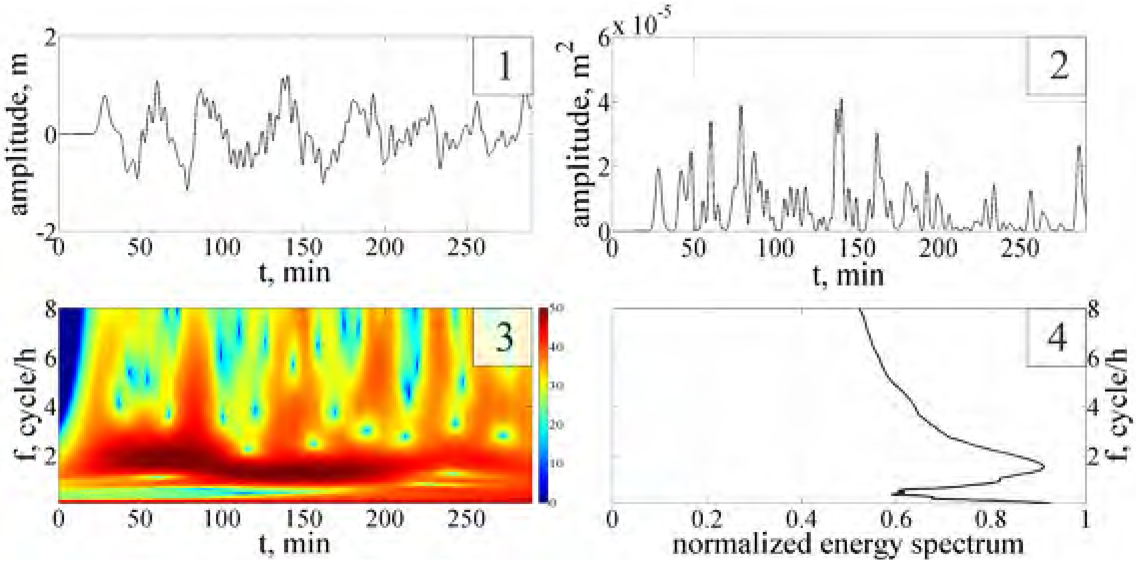

Fig.9. Wave and energy characteristics of tsunami after passing to Kruzenshtern strait: (1)- tide gauge record, (2)- short time power for wave front, (3)- wavelet-spectrogram, (4) -estimation of spectrum of energy

For Kruzenshtern Strait (Fig.10) it is clearly seen the amplification of the signal at the output for the low frequency range in the interval 1.5 4 cph. The transfer function quite changeable – in the plot there are present in the average much pronounced resonance regions, the most intense gain up to 15 dB is observed for frequencies of 1.5, 2.0, 4.0 cph, i.e. for periods T = 40 min, 30 min, 15 min, although there is a local minimum at a frequency f = 0,5 cph.

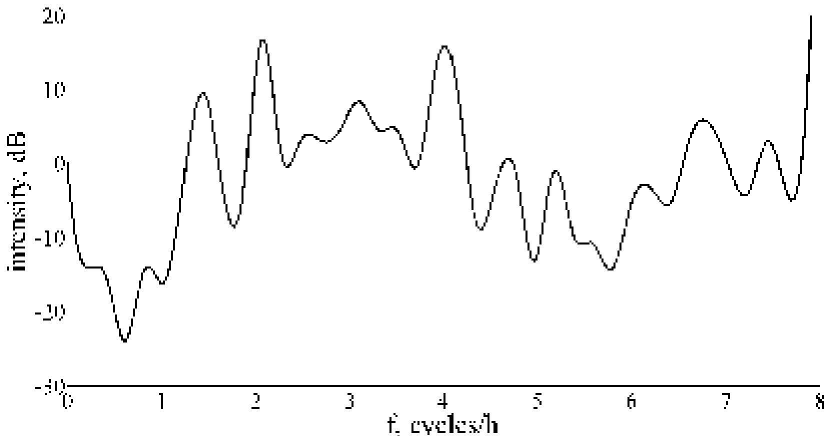

Fig.10. Logarithmic transfer function input-output for Kruzenshtern strait.

Consider now the propagation of wave energy in the Sea of Okhotsk and make analysis of the direction of its gain for Scenario 1. It can be seen that in comparison with the output of the Bussole strait (p.B2) component of the low-frequency waves, which came into the center of the "cloud 1" p.1 almost retains its energy (Fig.11.2). For the center of the "cloud II» (p.8) part of the low-frequency energy is transferred into the high-frequency range, while the center of the "cloud III» p.15, the low-frequency component prevails again.

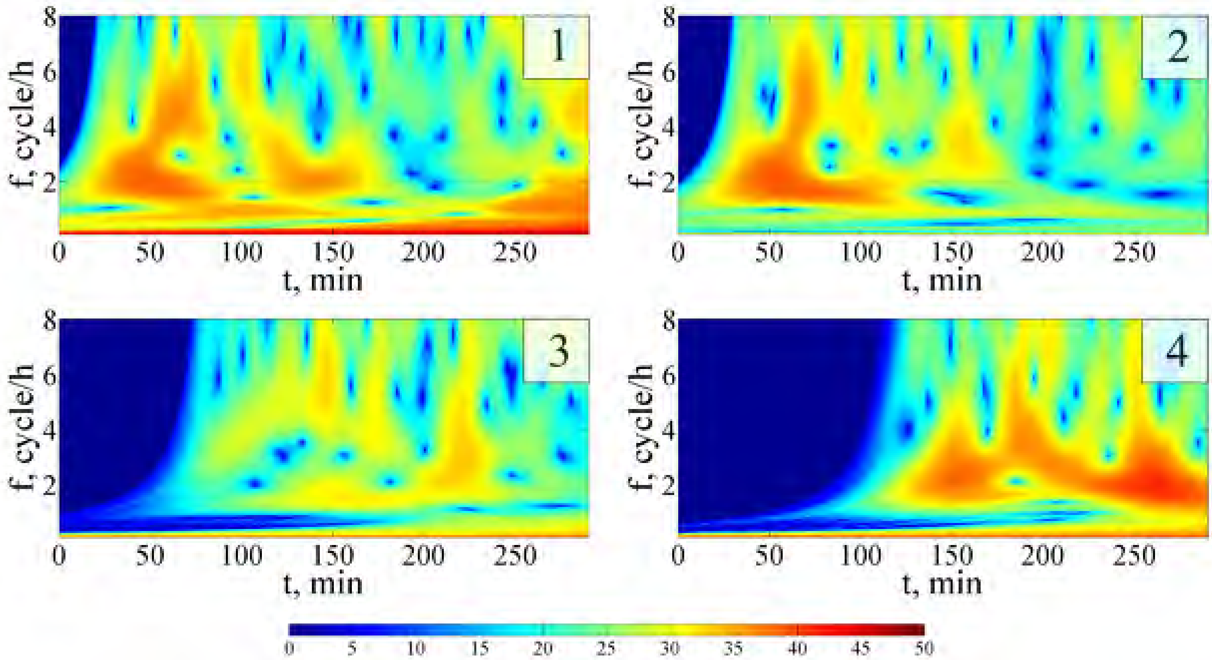

Fig. 11. Wavelet-spectrograms for scenario I : 1) p. B2; 2) p. 1; 3) p. 8: 4) p. 15 (see Fig. 1).

For a more detailed analysis of the propagation of wave energy on the Sea of Okhotsk, there were built transfer functions, with the smoothed cubic spline (Fig.12). Thus, Fig.12.1 shows the transfer functions for the points described in the wavelet-spectrograms in Fig.11. It is clearly seen that the attenuation of the wave energy is characteristic for the entire frequency range and in all directions. The lowest energy loss is for the low-frequency range up to 3.5 cph for a direction from p.B2 to p.1 (see Fig.1). For higher frequency bands 5-6 and 6.8-7.5 cph, i.e., duration of 10-12 min and 8-9 min, the waves with the least loss of energy, will be the direction of the exit of the Strait Bussol to points 8 and 15, respectively. In Figs. 12.2-12.4 there are presented transfer functions of the localization centers "point clouds" - gauges 1,8,15, to the points on the circle of the "cloud", where the synthetic gauges (see Fig. 1) were placed.

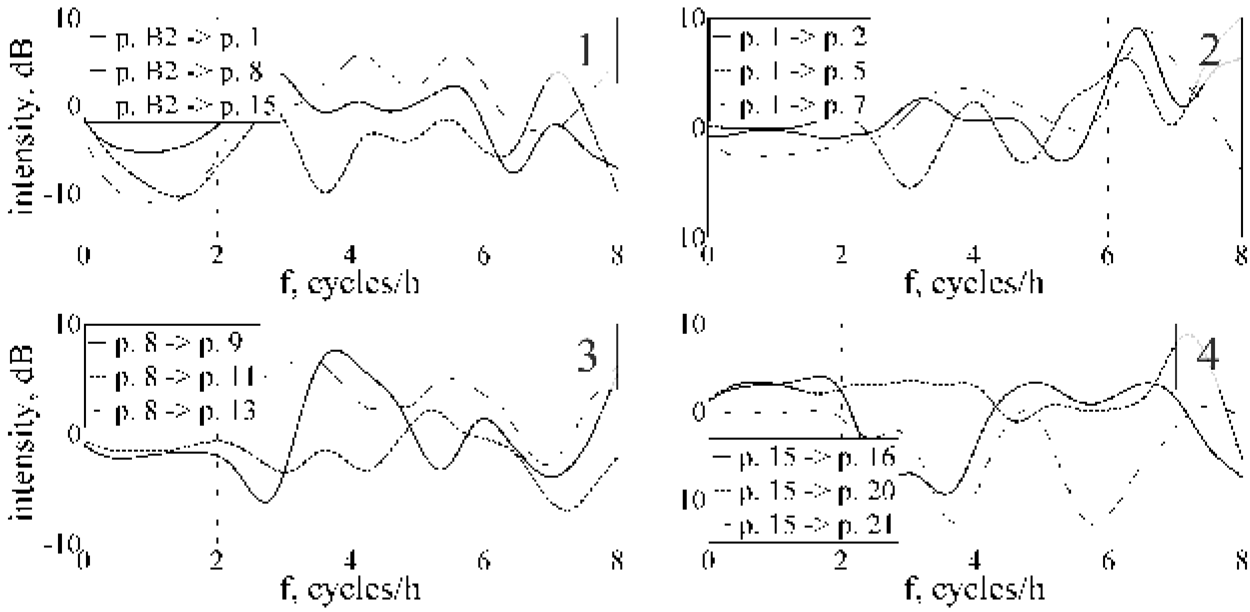

Fig.12. Logarithmic transfer functions: 1) for output from Bussol strait to centers of «clouds» of virtual tide gauges, 2)-4) from centers of «clouds» (pp.1,8,15) to points at the circle.

Choosing only three of the six areas, presented at the circles of "clouds" on Fig.1, connected with the preliminary analysis of the data of synthetic tide gauges, which allowed us to select the direction with the greatest intensity of wave energy. Fig.12.2 shows the transfer functions from the center of a "cloud I» to the pp.2,5,7; Fig.12.3 shows the transfer functions from the center of the "cloud II» (p.8) to pp.9,11,13 and Fig.12.4 shows the transfer functions from the center of the "cloud III» (p.15) to the pp.16,20,21 at the circles, in which the synthetic tide gauges are placed (the direction is indicated in the upper left corner of each block). For the "cloud I» it is characteristic a more uniform distribution of wave energy with a predominance in the direction of p.5 (direction to Sakhalin island). Considering the "cloud II», we come to the conclusion that a large part of the wave moves to the Terpeniya Gulf and a little less in the direction of "cloud III» (see Fig.1).

Consider now the propagation of wave energy in the Sea of Okhotsk for Scenario 2. As described above, when wave come from the output of the Kruzenshtern Strait, permanent component with a frequency of 1-2 cph, period (60-30 minutes) is present in its spectrum with an intensity of up to 50 dB. It is clearly seen that most of the wave energy is concentrated in the range of 30 to 200 min (Fig. 13.1).

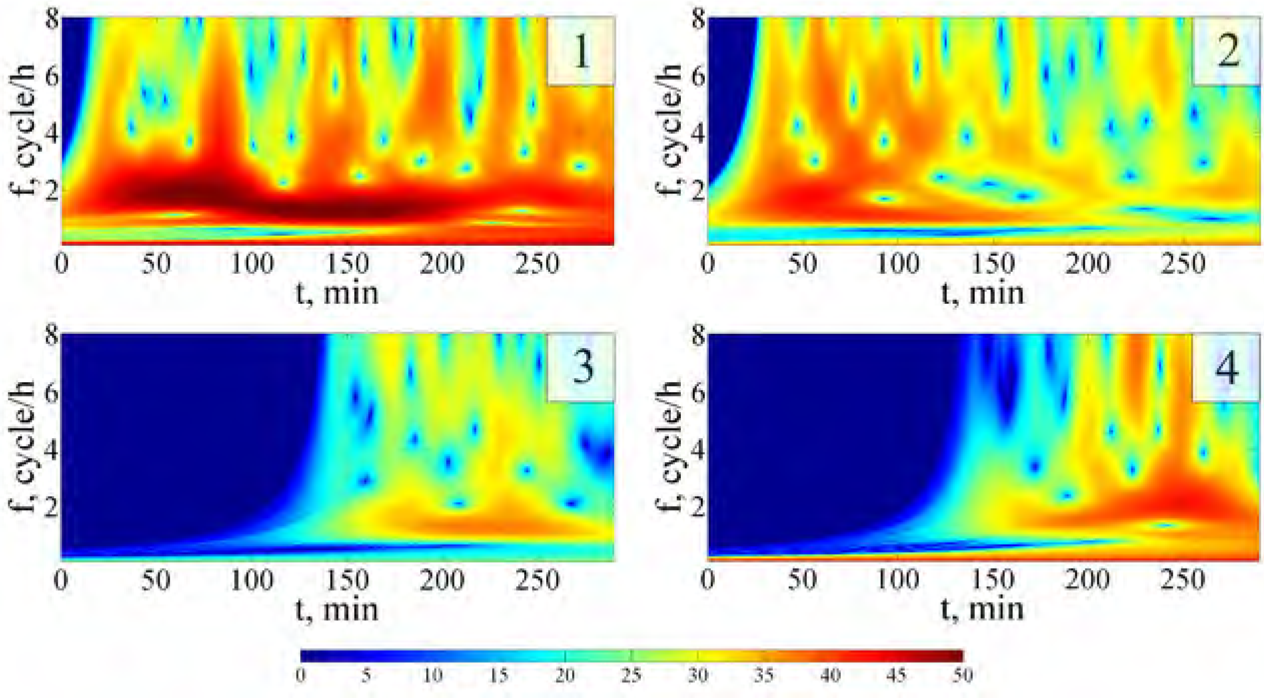

Fig. 13. Wavelet-spectrograms for scenario II : 1) p. K2; 2) p. 1; 3) p. 8; 4) p.5 (see Fig. 2).

It can be seen that in comparison with the outcome of the Strait (p.K2) low-frequency component of the wave, which came in p.1, is concentrated only in the range of ≈ 20-80 min, with low energy loss up to 35-40 dB (Fig. 13.2). It is clearly seen that for p.8 (Fig. 13.3) the low-frequency energy in the interval 170-300 min are considerably weakened, and for the third "cloud" center of p.15 (Fig.13.4), for the low-frequency component is a some amplification for frequencies of 1.5-3 cph, shifted in the time interval 200-300min.

For a more detailed analysis of the propagation of wave energy in the water area for Scenario II construct transfer functions, smoothed with cubic spline. Choosing only three of the six areas, presented on the circles of "clouds" on Fig.2, related to the preliminary analysis of the data of synthetic gauges, which allowed us to select the direction with the greatest intensity of wave energy. Fig.14.1 shows the transfer functions from the exit of the Kruzenshtern strait K1 in the "clouds" centers (IV, V, VI). It is clearly seen that the general weakening of the signal, with the exception of the direction to "cloud I» the center, and then the "cloud III». It is clearly seen that the wave intensity for the direction of the "cloud III», significantly less than in the first two directions.

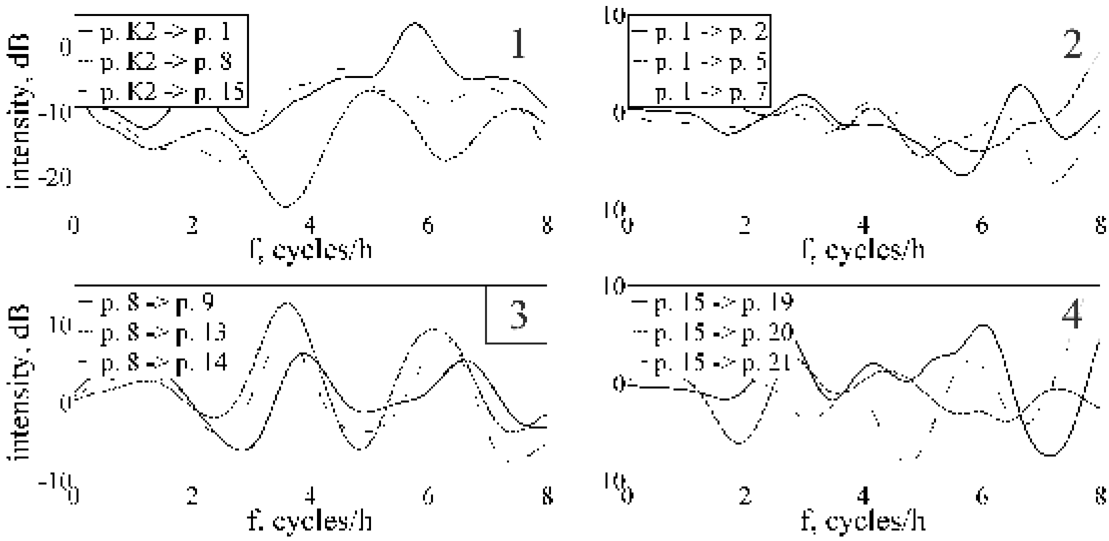

Fig.14. Logarithmic transfer functions: 1) for output from Kruzenshtern strait to centers of «clouds» of virtual tide gauges, 2)-4) from centers of «clouds» (pp.1,8,15) to points at the circle.

This leads to the conclusion that the main flow of the wave energy is turn to on Sakhalin. Fig.14.2 shows the transfer functions from the center of the "cloud IV» to the pp. 2,5,7; Fig.14.3 shows the transfer functions from the center of the "cloud V» to pp.9,13,14 and Fig.14.4 shows the transfer functions from the center of the "cloud VI» to pp.19,20,21 at the circles, at which synthetic tide gauges are placed (the directionis indicated in the upper left corner of each block). In Fig.14.2 we can see that in the "cloud IV» gauges (see Fig.2) is dominated by the energy in the direction of p.5 in the frequency range up to 2.3 cph, with a fairly sharp turn to the islands along the Deriugina Trough. One can see almost uniform energy distribution from 2.3 to 3,6 cph in all three directions (to the pp.2, 5 and 7, with a slight increase in the intensity to 2 (in the direction of Kamchatka).

For cloud V» (Fig.14.3) it is well seen practically uniform energy distribution with a predominance of direction to p.9, which is then in this direction, it decreases significantly. There are clearly seen energy peaks for frequencies of 3.5 cph and 6 cph (17 min and 10 min waves) for directions to pp.13 and 14 (north-east Sakhalin).

For the "cloud VI» (Fig.14.4) in the range of up to 2.2 cph (wavelength of 27 min) to the predominant direction of p.21 (northeast Sakhalin), a significant increase in energy towards the p.19 for the frequency 2 5 cph and 6 cph (24 min and 10 min wavelength) is observed. For a frequency of 1.8 cph (for 33 min waves) a significant decline in energy in the direction of p.20 (the middle of Sakhalin), then for frequencies 3-4,8 cph (20 to 12 min waves) uniform energy distribution for pp.19,20; for the frequency of 7.2 cph (8 min waves) a significant decline in energy.

7. DISCUSSION

Thus, the tsunami waves generation analysis of seismic sources located about Boussole Strait [7], as well as seismic sources other configurations (see, e.g, [17-21]), confirmed that an abnormally weak manifestations of tsunami waves 15 November 2006 in Sea of Okhotsk, the northern and southern parts of the Pacific coasts of the islands of the Kuril island arc and the Japanese islands, with a strong earthquake with a magnitude of 8.3, is not a random event, but a natural consequence of the "work" only of one - Boussole Strait, actively extinguishing energy suitable to the strait waves. It also shows that at a given location of the earthquake source, the greatest wave heights can be achieved only in the southern part of Sakhalin Island. In the middle of the Sakhalin gain achieved probably due to the effect of trapped waves (cf. [22,23]. At that time, in the case of the location of the seismic source near the Kruzenshtern Strait, signal amplification will be observed for all low-frequency range, and can lead to more serious consequences on the Okhotsk coast of our islands, especially in the north-eastern coast of Sakhalin Island and on the Pacific Coast of Kamchatka and the islands of Hokkaido and Honshu (Japan).

Fig. 15 compares the results of the presented calculations with the data of [24]. It is clearly seen that the direction of the energy flows from the Bussol Strait and the Krusenstern Strait coincides with the data of [24]. However, the direction of energy flows in more limited areas, where synthetic gauges are localized, differs somewhat from the data of the work [24]. For example, in Fig.15a, b, a turn of energy flows to Sakhalin Island is clearly seen, and when the wave passes through the Bussol Strait the flow goes to the middle part of Sakhalin, and when the wave passes through the Kruzenshtern Strait, the energy flow "attacks" the north-eastern part of Sakhalin Island.

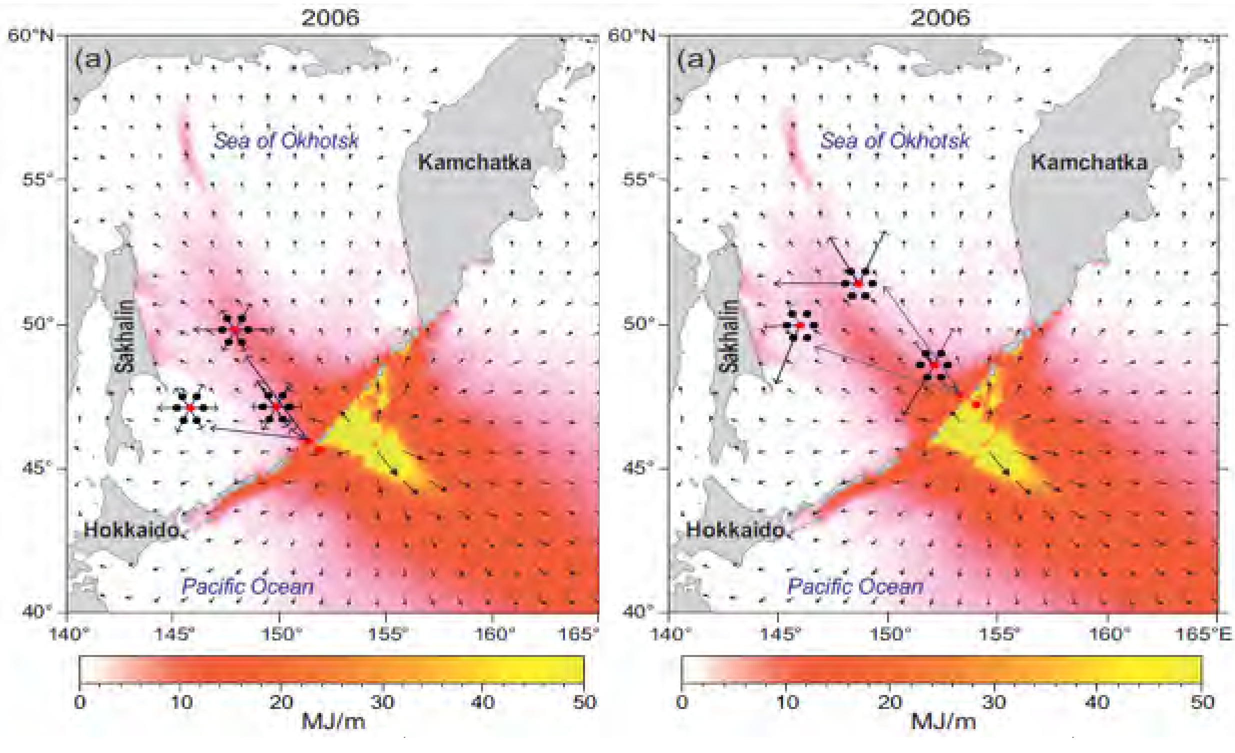

Fig. 15. Comparison of the synthetic energy fluxes for tsunami, generated by the November 2006 earthquake obtained in the present work with the data of the energy fluxes from the work of Rabinovich, et al. (2008) [24]. Red and black points indicate the location of virtual tide gauges of computed. The blue arrows show the direction of the propagation of energy flows from the Bussol Strait (a) and the Kruzenstern Strait (b).

8. CONCLUSION

Thus, from the analysis above, it follows that:

• Wave front, leaving the Boussole Strait in the Sea of Okhotsk, takes place on a broad front in the direction of the south-eastern tip of Sakhalin, as well as starting the movement to the northwest, is in the direction of the middle part of Sakhalin

• Bussol Strait actively dampens the energy of a suitable wavelength to the strait, in the first place, the low-frequency part of the spectrum;

• When comparing the graphs of transfer functions B1-B2 (input-output of the Bussole Strait) and K1-K2 (input-output of the Kruzenshtern Strait), the most intense attenuation for Boussole Strait is for frequencies of 0.6, 2.5, 4.2, 7.5 cph (signal attenuation interval); signal amplification intervals for Boussole Strait are slightly expressed, while as for Kruzenshtern Strait signal amplification was observed for all the low frequency band in the range of 10-18 cph;

• For Kruzenshtern Strait transfer functions are changeable enough - in the plots in the average a lot of distinct resonance regions is present; amplification of the signal is observed for all the low-frequency range;

• for waves coming from the Kruzenshtern Strait amplification of wave energy is significant in the areas of the middle and north-eastern regions of Sakhalin.

9. ACKNOWLEDGEMENTS

This work was supported by the Russian Science Foundation, project no. 14-50-00095.

REFERENCES

1. Shchetnikov N.A. The tsunami along the coast of Sakhalin and the Kuril Islands from tide-gauge data 1952-1968. *FEB USSR Academy of Sciences*, Vladivostok, 24, 1990

2. Lobkovsky L.I., Baranov B.V. Keyoard model of strong earthquakes in island arcs and active continental margins. *Doklady of the Academy of Sciences of the USSR*. V. 275. № 4. p. 843-847. 1984.

3. Lobkovsky L.I., Mazova R.Kh., Kataeva L.Y., Baranov B.V. Generation and distribution of the catastrophic tsunami in the Sea of Okhotsk. Possible scenarios. *Doklady AN* V. 410, pp 528-531, 2006a.

4. Lobkovsky LI Mazova AD Baranov BV Kataeva LY Simulation of a tsunami in the Sea of Okhotsk on the basis of the keyboard models of subduction zone. in the book .: *Fundamental research of seas and oceans* (Ed. Laverov NP), Moscow, Nauka Press, Part 1, p. 292- 303, 2006b.

5. Lobkovsky L.I., Baranov B.V., Mazova R.Kh., Kataeva L.Yu. Implications of the seismic source dynamics for the characteristics of a possible tsunami in a model problem of the seismic gap in the Central Kurile region, *Russ. J. Earth Sci.*, V.8,ES5002,doi:10.2205/2006ES000209, http://dx. doi. org/ 10.2205/2006ES000209, (2006c).

6. Lobkovsky L.I. Mazova R.H., Kiselman B.A. Morozova S.A. Numerical simulation and spectral analysis of the tsunami November 15, 2006 in the Kuril-Kamchatka region. *Oceanology* V.50. No. 4. p.1-10. 2010.
7. Gusiakov VK An estimate of the tsunami earthquake underwater spectral characteristics of Rayleigh waves // in: Proc : *Generation of tsunami waves and access to the beach*, Moscow, Radio and Communications, 1984, p.84-95.
8. Kulikov E.A., Poole S.L., Rabinovich A.B. The spectrum of long waves in the open ocean and the tides radiation // in Proc.: *Wave processes in the northwestern part of the Pacific Ocean*, Vladivostok: Far Eastern Scientific Center, Academy of Sciences of the USSR, 1980, p.28-38
9. Vetterli M., Kovacevic J., Goyal V. - *Foundation of Signal Processing*, Cambridge University Press (ISBN 110703860X), 2013, 707p.
10. Lyons R. *Digital Signal Processing* // Binom-Press, 2006.
11. Sergienko A.B. *Digital Signal Processing* // SPb .: Peter, 2002.
12. Mallat Stephane *A wavelet tour of signal processing* , Academic Press, 1999.
13. Pelinovsky E.N. Nonlinear dynamics of tsunami waves. *Preprint of Institute of Applied Physics Academy of Sciences of the USSR*, Gorky, 1982. - 226 p.
14. Voltsinger, N. E., Klevanny K. A., and Pelinovsky E. N., Long-wavelength dynamics of coastal zone (in Russian),., Hydrometeoizdat, Leningrad. 272 p (1989)
15. Marchuk, A. G., Chubarov L. B., and Shokin Yu. I., *Numerical Simulation of Tsunami Waves* (in Russian), 175 pp., Nauka Press, Novosibirsk. (1983).
16. Baranov B.V.,Pristavakina E.I., Dozorova K.A., Svarichevsky A.S The structure of the Okhotsk Sea and the development of its sedimentary basins, *Arctic and Russian Studies* II, Report 671, edited by R.Flecker, 997,Cambridge, 58p.
17. Soloviev S.L., Nekrasov A.V., Buhteev V.G. Pyaskovsky R.V. Pre-tsunami Kuril-Kamchatka coast, based on hydrodynamic calculations // in the book .: *Theoretical and experimental research on the tsunami.* Moscow, Nauka Press, 1977, p. 131-139.
18. Kurkin A.A. Pelinovsky E.N., Choi B.H., Lee D.S. Comparative evaluation of the coast tsunami Japonomorsky Russian numerical simulation. *Oceanology*.. T. 44. № 2. p. 179-188. 2004.
19. Horrillo J., Knight W., Kowalik Z. Kurile Islands tsunami of November 2006: 2. Impact at Crescent City by local enhancement. *J.Geophys.Res*. 2008. V.113. P.C01021 doi:10.1029/2007JC004404.
20.Kowalik Z., Horrillo J., Knight W., Logan T. Kurile Islands tsunami of November 2006: 1. Impact at Crescent City by distant scattering. *J.Geophys.Res*. 2008. V. 113. P.C01020. doi: 10.1029/2007JC004402
21. AI Zaitsev, DP Kovalev, Kurkin AA, Levin BV, Pelinovsky EN, Chernov AG, Yalchiner A. Nevelsk tsunami 2 August 2007: Tool data and numerical simulation // *Doklady of the Academy of Sciences*.. T. 421. № 2. p.249-252. 2008
22. Levin B.V., Chernov A.G., Shevchenko G.V., Kovalev P.D., Kovalev D.P., Kurkin A.A. Likhachev O.N., Shishkin A.A. First results registration wavelength range periods of tsunami Kuril ridge on network diversity stations // *Doklady of the Academy of Sciences*. V. 427. № 2. p. 239-244. 2009

23.Lobkovsky, L.I., Rabinovich, A.B., Kulikov, E.A., Ivashchenko, A.I., Fine, I.V., Thomson, R.E., Ivelskaya, T.N. and Bogdanov, G.S.,. The Kuril Earthquakes and tsunamis of November 15, 2006, and January 13, 2007: Observations, analysis, and numerical modeling. *Oceanology*, 49(2), pp.166-181. 2009

24.Rabinovich, A.B., Lobkovsky, L.I., Fine, I.V., Thomson, R.E., Ivelskaya, T.N. and Kulikov, E.A.,. Near-source observations and modeling of the Kuril Islands tsunamis of 15 November 2006 and 13 January 2007. *Advances in Geosciences*, 14, pp.105-116. 2008.

25.Mazova R.K., Kiselman B.A., Kolchina E.A.,. Numerical simulation of tsunami wave height distribution for Turkish Black Sea coast in nonlinear dynamic keyboard model of underwater seismic source. *Journal of Computational and Applied Mathematics*, 259, pp. 887-89. 2014.

ISSN 8755-6839

SCIENCE OF TSUNAMI HAZARDS

Journal of Tsunami Society International

Volume 36 Number 4 2017

INCIPIENT EVALUATION OF TEMPORAL EL NINO AND OTHER CLIMATIC ANOMALIES IN TRIGGERING EARTHQUAKES AND TSUNAMIS – Case Study: The Earthquake and Tsunami of 16th April 2016 in Ecuador.

George Pararas-Carayannis[1] & Peter Zoll[2]
[1]Tsunami Society International, [2]CIO I-MAG STS

ABSTRACT

The present study provides an incipient, cursory evaluation of the unusually strong 2015-2016 El Niño Southern Oscillation (ENSO) and of the quasi-periodic fluctuation and anomalies of sea surface temperature (SST) across the equatorial Pacific during that period, as being the cause for the prolonged rainfall and flooding of coastal valleys near Guayaquil and Esmeraldas in Ecuador in December 2015, as well as in late January and February 2016 – which proceeded the 16 April, 2016 tsunamigenic earthquake in Ecuador. Also examined is the seasonality of recent tsunamigenic and non-tsunamigenic earthquakes in Ecuador and elsewhere in South America, in relation to strong ENSO and documented SST Anomalies - as well as to the differently proposed mechanisms that may cause them in Ecuador and elsewhere, with climatic changes induced by the global impact of volcanic explosions and by other terrestrial and extraterrestrial influences, as to impacts they may have on the geostrophic circulation and surface water temperatures of oceanic currents, which perhaps are also associated with the cycles of Atlantic Multidecadal Oscillations (AMO's) of small water temperature differences which may result in clusters of hurricanes generated near the earth's oceanic equatorial zones.

Regarding the 7.8 M_w earthquake and tsunami of 16 April 2016 in Ecuador and based on the above stated partial data, the present study postulates that the excessive volume and weight of flood-waters retained in the coastal crustal layers following the cataclysmic rains of late 2015 and early 2016, triggered an earlier rupture of the already strained offshore fault near the city of Muisne. As an additional contributing mechanism of earthquake and tsunami generation, the evaluation proposes that the extreme volume and weight of floodwaters may have also altered temporarily the crustal buoyancy characteristics of the intersecting Carnegie Ridge with the South America continent along

the central part of the country. Additionally examined and evaluated are the unusual clusters of the 16 April 2016 event(s) and the three-dimensional and temporal anomalous distribution of aftershocks - which did not follow a typical pattern as would have been expected. Similarly atypical was the distribution of observed Modified Mercalli high intensities of this earthquake over a rather large and separated geographical area that stretched more than 200 km along the Ecuadorian coastline.

Keywords: *Climatic Anomalies; El Niño Southern Oscillation (ENSO); Triggering Earthquakes; Precursor Events; Earthquake and Tsunami of 16th April 2016 in Ecuador.*

1. INTRODUCTION

The Colombia/Ecuador subduction zone is a region where high seismic stress has been accumulating and where the rupture of two or more offshore fault segments - as in 1906 (Mw=8.8, total rupture 600 km.) - could generate a tsunami with a very destructive near and far-field impacts in Ecuador, in South Colombia and in the entire Pacific Basin (Pararas-Carayannis, 1980, 2012; Beck & Ruff, 1984). Fig. 1 shows the major tectonic features along northwestern South America, parallel to the convergence direction of the Ecuador-Colombia trench where such events frequently occur.

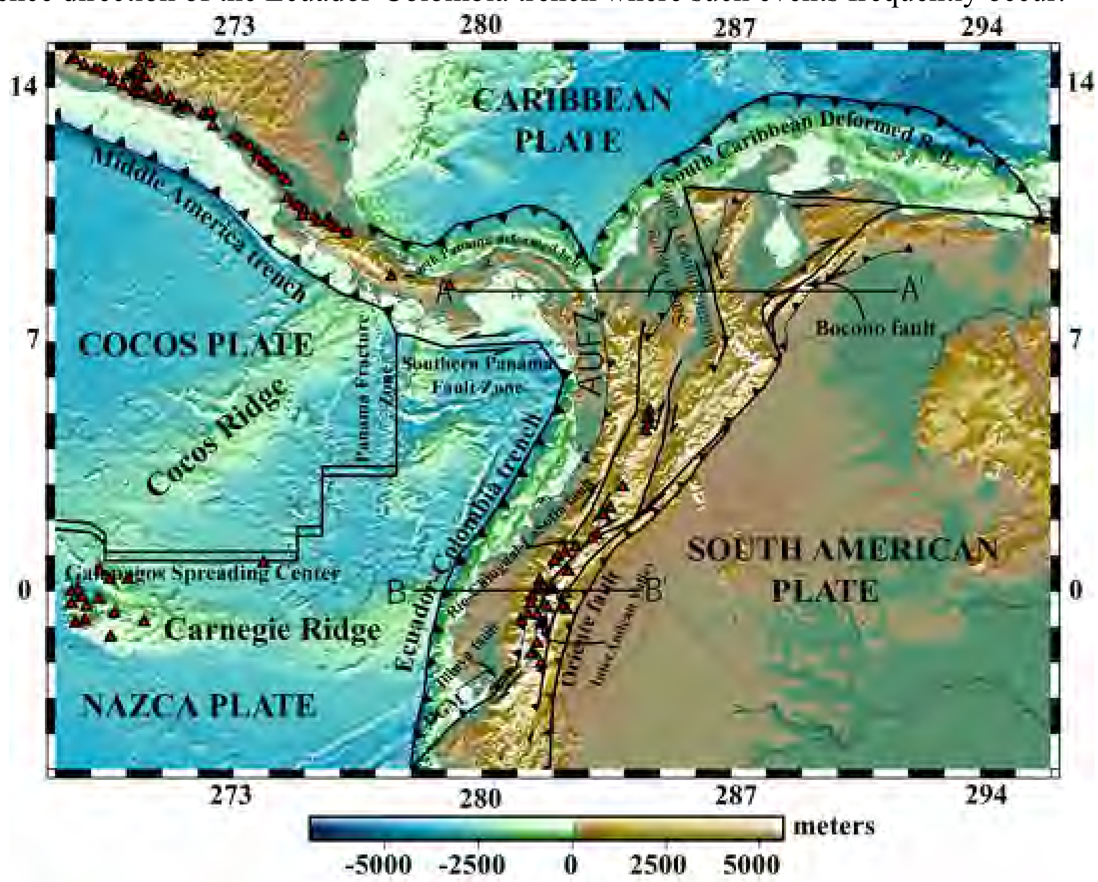

Figure 1. Major Tectonic Features along northwestern South America parallel to the convergence direction (Pararas-Carayannis 2012, after Trenkamp et al. 2002).

Statistical probability studies and subsequent GPS measurements of crustal deformation after the survey of the 1979 Tumaco earthquake and tsunami along Southern Colombia near Ecuador clearly indicated that the region still had a great deal of stress remaining and there was an increased potential for the recurrence of a great tsunamigenic earthquake similar to that of 1906. Furthermore, all three fault segments 1942, 1958 and of the 1979 events represented seismic gaps where a major earthquake was expected (Pararas-Carayannis, 1980, 2012). Fig. 2 shows the major faults that ruptured in 1942, 1958, 1979 and the continuous rupture of all three-fault segments in 1906.

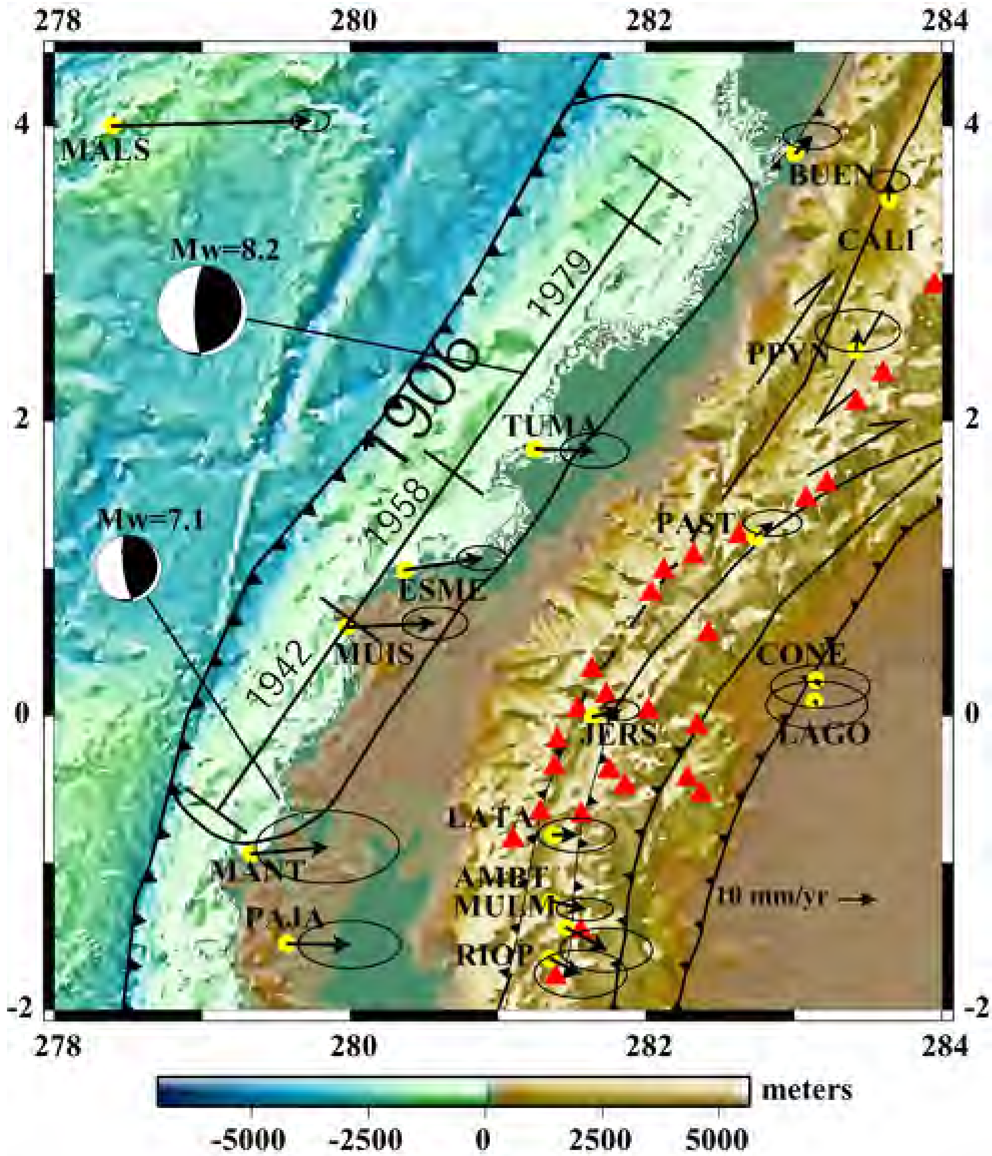

Figure 2. Ruptures of the 1906, 1942, 1958 and 1979 tsunamigenic earthquakes (Pararas-Carayannis, 2012, after Trenkamp et al. 2002)

More recent evaluation of the seismicity of Ecuador and of the potential for recurrence of significant earthquakes, included a review of controlling inter-plate coupling mechanisms, changes in the tectonic regime of the margin, ongoing lithospheric structure deformations, changes in sea-floor relief and on the impact of ongoing subduction or accretion of highly folded, hydrated sediments along the South American continent (Pararas-Carayannis, 2012 a, b, c). Also evaluated were the seismo-dynamics and role in earthquake and tsunami generation, as affected by the Carnegie Ridge's oblique subduction beneath the South American continent and by its resulting buoyancy effects on both sides of the region of interjection and underthrusting that control the magnitudes and tsunami-genesis of earthquakes. Based on this analysis, it was concluded that there was still a lot of tectonic stress remaining in the region both to the north and to the south of the Carnegie Ridge intersection, but principally to the north along the faults of the 1942 and 1955 earthquakes. Also the clustering of aftershocks of the 1979 Tumaco earthquake in Southern Colombia indicated that two major faults offshore from the Esmeraldas/Muisne coastal region in Ecuador had been nucleated and, as previously stated, another major earthquake was very possible along these zones (Pararas-Carayannis, 1980, 2012). Furthermore, the recent analysis concluded that a repeat of the 31 January 1906 event with more than the two fault segments rupturing for about 500-600 km, was also possible, and that such an event could generate a tsunami with very destructive near and far field impacts (Pararas-Carayannis, 2012). What was not considered previously was whether climatic changes and heavy rainfalls in the Andes and in the coastal peninsula – related to the El Niño Southern Oscillation (ENSO) may have contributed to an early triggering of tsunamigenic earthquakes along the Colombia/Ecuador subduction zone.

Fortunately, a great earthquake such as that of the 31 January 1906 did not recur but - as predicted - on 16 April 2016 a 7.8 M_w earthquake ruptured the already strained fault offshore from Muisne in Ecuador, causing great destruction and a local destructive tsunami. This event occurred on the same fault as the one in 1942 (see Fig. 2) where a seismic gap had been identified - with no significant activity for 75 years (Pararas-Carayannis, 2012). However, the epicenter of this event occurred near the northeast end of the 200 km. fault, closer to the city of Muisne. As stated, what was unusual about this quake was that it occurred following prolonged rainfall and flooding of coastal valleys near Guayaquil and Esmeraldas in December 2015, as well as in late January and February 2016. The question was then raised on whether the prevailing anomalous seasonal climatic conditions had some influence in perhaps triggering earlier this and other earthquakes in the region. Thus, using the 16 April 2016 earthquake as a case study, the present paper examines and provides an incipient evaluation of the unusually strong 2015-2016 El Niño's Southern Oscillation (ENSO) and of the quasi-periodic fluctuation and anomalies of sea surface temperature (SST) across the equatorial Pacific, as being the cause for the prolonged rainfall and flooding, not only in Ecuador but elsewhere along the western side of South America. A prolonged drought followed by intense rainfall is very hazardous. This preliminary evaluation postulates that the excessive volume and weight of flood-waters from the prolonged rainfall and flooding of coastal valleys were retained in the coastal crustal layers, thus increasing significantly the weight of the continental coastal crust and triggering an earlier-than-expected rupture of the already-strained fault offshore from Muisne, causing the tsunamigenic earthquake of 16 April 2016. Thus, the present paper reviews and evaluates:

a) The Earthquake and Tsunami of 16th April 2016 in Ecuador, as well as the focal depths and time history of aftershock clusters and whether the quake was a single event or two events in close sequence.
b) The speed of the rupture as well as any bridging of asperities on one or more offshore/onshore zones of the 1942 and 1958 earthquakes.
c) The anomalous distribution of Modified Mercalli intensities of the 16 April 2016 earthquake.
d) A 4.8 quake which may or may not be characterized as a foreshock associated with the major event(s) of 16 in April quake(s) because of its large separation in the spatial/time distribution and the initiation point of rupture(s).
e) Satellite measurements which may be indicative of changes of crustal movements along the known tectonic boundaries.

Another study under preparation will examine in detail the seasonality of recent tsunamigenic and non-tsunamigenic earthquakes in Ecuador and elsewhere in South America, in relation to strong El Niño Southern Oscillations and documented SST Anomalies - that may be causing them. The forthcoming study will also examine selectively the possible correlation of the El Niño Southern Oscillations in Ecuador and elsewhere, with climatic changes induced by the global impact of volcanic explosions and of other terrestrial and extraterrestrial events, as to what impact they may have on the geostrophic circulation of oceanic currents in both in the North and South Pacific, as well as on similar circulation in the Atlantic Ocean - perhaps associated with the observed cycles of Atlantic Multidecadal Oscillations (AMO's) of small surface water temperatures, which may also result in nucleating periodic clusters of sequential hurricanes.

1. TSUNAMIGENIC AND NO-TSUNAMIGENIC EARTHQUAKE PRECURSORY PHENOMENA

There is not a single geophysical instrument that can measure any direct parameter of an earthquake and give a warning in advance. It is only secondary precursor parameters that are being monitored - which are primarily byproducts of the subsurface tectonic stress. Magnetic field changes, strain, tilt, subsidence, and bulging of the earth's surface, are being studied as primary precursors. For example, "dilatancy" (granular volume change due to shear deformation (Reynolds, 1886; Pararas-Carayannis, 2000)) occurs when the rocks on a fault are stressed and the ground "dilates" or swells. Symmetric tilting of the ground can be expected in a uniform pattern away from the potential earthquake epicenter. Asymmetric tilting of the ground around the earthquake source area can occur also from no uniform stresses on the rocks, which eventually will result in strike-slip type of faulting when the earthquake finally occurs (Pararas-Carayannis, 2000). Micro fracturing prior to an earthquake is responsible for some of the precursor events, which are thought to result from the preliminary stages of failure of the subsurface rocks preceding a major earthquake. A few of the precursory phenomena may be indicative of imminent rock failure, while others may be longer-term manifestations of such failure.

There are many other precursor phenomena observed prior to an earthquake. Several of the short-term, physical and geochemical precursors of earthquakes that can be measured with instruments, include: a) Increase in the rate of a seismic creep and the slow movement along the fault; b) Unusual straining and gradual tilting of the ground near the fault zone; c) Drop or rise in the water level within wells; d) Increase of hydrogen gas in the soil; e) Release of radioactive radon gas from wells; f) Decrease in the number of micro quakes and foreshocks; g) Lessening of electrical resistance in the rocks; h) Flashes and other lights in the sky; i) Appearance of a ring-like pattern of micro quakes surrounding the epicenter of a future quake, called “Mogi’s donut”, and many other physical and chemical manifestations (Pararas-Carayannis, 2000).

As stated, most of the precursor phenomena are believed to be caused by imminent or longer-term manifestations of subsurface rock failure before a major earthquake occurs. When crustal blocks are stressed along a fault - by tectonic plate interaction - the rocks begin to break and crack at some depth below the fault area, thus losing their strength. This initial stage of rock failure is a mechanical process. Part of this mechanical energy is stored in the fault-rock as potential energy, while the rest becomes either thermal, chemical, or electrical energy. In turn, these forms of energy may result in all sorts of accompanying, chemical/physical effects and manifestations - precursory phenomena that may be measurable and indicative of an impending earthquake (Pararas-Carayannis, 2000). The initial stage of rock failure may also change the pressure/temperature phase relationship or release of gases. Methane hydrate may generate methane, which may catch fire on the surface of the earth before or during an earthquake. Such extensive fires occurred during the 1945 Makran earthquake in the North Arabian Sea (Pararas-Carayannis, 2006). Underground water may fill in the cracks of the failing rocks and change their electrical resistance. Such chemical and physical changes may continue as failing rocks contract and crack further by the constant, tectonically-induced strain. Rise in the temperature of the water often results from such crust alterations (Pararas-Carayannis, 2000).

1a. Terrestrial and Extraterrestrial Factors of Climate Change, Global Warming and Precursory Phenomena Affecting Major Oceanic Currents’ Circulation and Temperature Anomalies

The sun is the primary source of energy that affects climate. During long periods of geologic time, the Earth's climate has been an unstable dynamic system that has undergone short and long term cycles of change - heating up or cooling down - with corresponding rises and falls in sea level. Important natural drivers of climatic change include both astronomical and terrestrial factors. Since climate change on Earth is a dynamic process affected by such factors, the impact of the Greenhouse Effect has also varied during long periods of geologic time. The effect of global warming on weather patterns is frequently blamed for an apparent increase in weather-related disasters. Continuing global warming can be expected to contribute significantly to future disasters (Pararas-Carayannis, 2003, 2004 a, b, c). Also, it is very possible that climatic disasters can collaterally influence local tectonic conditions of crustal isostacy and buoyancy near stressed fault zones, and thus influence the triggering of earthquakes. The present study presents a cursory review of such phenomena, focusing primarily on recent quakes in Ecuador, Colombia and Peru.

1b. Triggering of SSTA and ENSO Anomalies

For triggering mechanisms of precursory phenomena associated with earthquakes (tsunamigenic or not) we must also consider not only the chemical/physical effects and manifestations of crustal failures along seismically active regions, but also larger scale phenomena that may have an impact. Specifically, we must also examine the possible correlation of the El Niño Southern Oscillations in Ecuador and elsewhere, with other climatic changes induced by the global impact of volcanic explosions or by other terrestrial or extraterrestrial events. For example, we know that some of these phenomena, such as solar storms, changes of incoming solar radiation, holes in the ozone layer, migrating hot spots in the earth's mantle and many other seemingly unrelated causes, may have an effect on the ocean temperatures and on the geostrophic circulation of oceanic currents in both the North and South Pacific, as well as on similar geostrophic circulation of ocean currents in the Atlantic and other of the world's oceans and seas. These are also associated with the observed Atlantic Multidecadal Oscillations (AMO's) (Schlesinger, 1994) - small changes of surface water temperatures (SST) in the Northern Atlantic influenced by both natural and anthropogenic factors - which also result in climate cycles and the nucleation of periodic clusters of severe historical hurricanes (Pararas-Carayannis, 1975).

In relation to strong ENSO and documented SST Anomalies in the Pacific - as well as to the differently proposed mechanisms that may cause them along the coasts of Ecuador and elsewhere, we may also need to examine climatic changes induced by the global impact of volcanic explosions, in causing nuclear winters or small changes in oceanic surface water temperatures which interact with atmospheric air masses - conditions which may be also responsible for the observed periodic clusters of storm systems generated near the earth's oceanic equatorial zones.

1c. The Strong 2015-2016 El Niño-Southern Oscillation (ENSO) in South America

As earlier mentioned, a reversal in atmospheric circulation known as the Southern Oscillation (ENSO) is a periodic phenomenon which may be caused by a variety of influences on the geostrophic flow of major equatorial ocean currents in the Pacific (See Fig. 3). When an El Niño occurs, the entire equatorial and atmospheric circulation pattern reverses. Currents and winds reverse and bring warm water and air from the western Pacific to the Galapagos and the coastal regions of South America. In the Southern hemisphere of the Pacific, the Peru or Humbolt Current carries an enormous volume of cold water northward from the Antarctic region, thus keeping the western coast of South America temperate and dry. As it passes northern Peru, the Humbolt current continues in a counterclockwise direction and joins the Equatorial Current which flows westward across the Pacific, thus causing upwelling of cooler water near Peru, Ecuador and the Galapagos region. However, small changes in the temperature of surface waters near the equator result in strong El Niño-Southern Oscillations (ENSO's) and have a significant climatic effect on South America and possibly on the overall earth's weather.

A similar oceanic flow of currents occurs in the northerns hemisphere of the Pacific where the Kuroshio current turns in a clockwise direction into the North Pacific current then joins the California current, which warms and moderates California's climate. Both the Humbolt and the California currents are parts of such large gyres - known as geostrophic currents - as they relate to the earth's rotation, the Coriolis force and the varying spherical angular velocities of the earth at different latitudes. The circulation of ocean currents is also affected by strong winds and the resulting Ekman Spiral flow of surface waters forces up cooler, nutrient rich water to the surface (Pararas-Carayannis, 1991). Similar current systems operate in the Atlantic, the Indian Oceans - although the currents in the Indian Ocean are complicated by the seasonal monsoons.

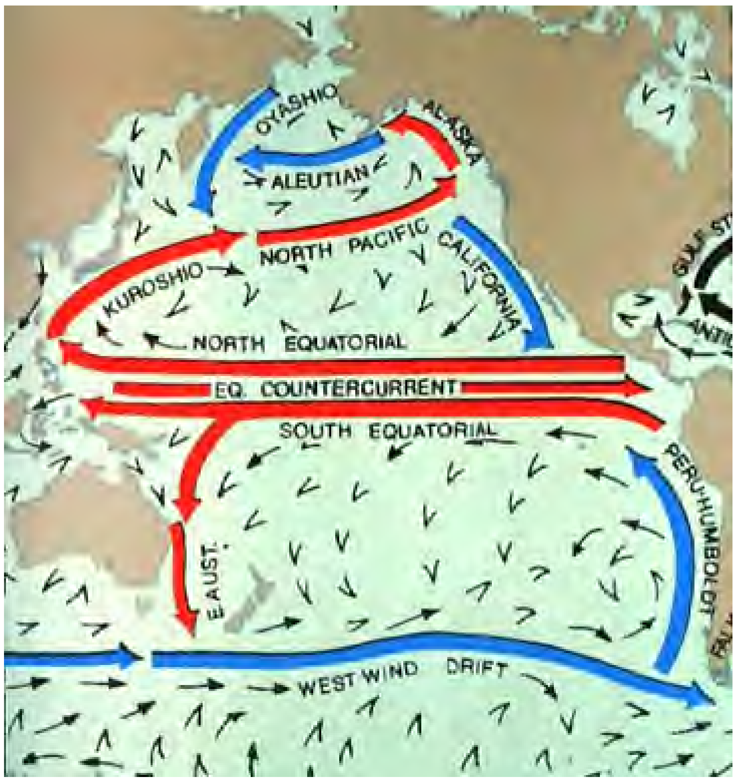

Fig. 3. Geostrophic currents in the North and South Pacific.

In brief, the temperatures of surface oceanic water masses near the equator in the Pacific generally fluctuate between a warmer than normal state along the central and eastern equatorial Pacific (El Niño) and the second state which is cooler than normal on the central and eastern equatorial Pacific (characterized as La Niña). Fig. 4 shows the monthly sea surface temperature in the Niño 3.4 region of the tropical Pacific compared to the long-term average for all moderate-to-strong El Niño years since 1950, and how the 2015/16 (black line) compared.

1d. Severe El Niño events since 1950

As shown in Fig. 4 below, a particularly severe El Niño occurred in 1982-1983. Another severe El Niño occurred in 1997-1998 and it was one of the strongest events of the 20th century. Indonesia and Australia suffered drought and wildfires while western North and South America suffered from floods and heavy snows. In the Galapagos there were heavy rains between March and June of 1997, and again in the wet season of 1998. Sea and air temperatures were 4 to 5° C above normal. The event had an adverse impact on marine life, since upwelling and hence ocean nutrient levels, were significantly reduced.

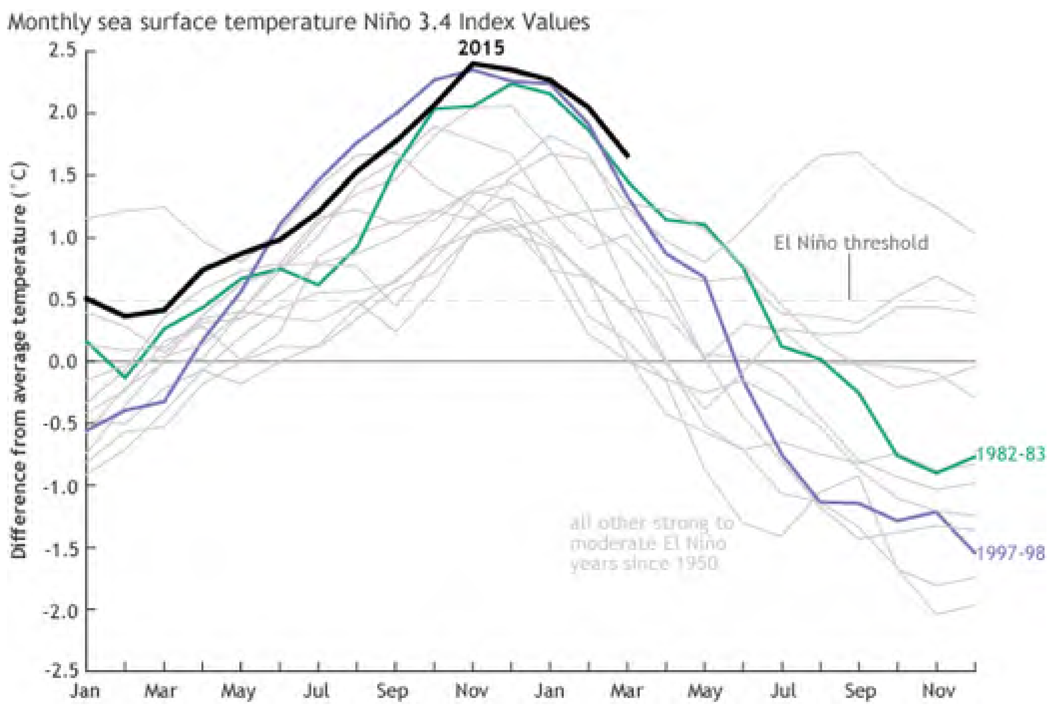

Fig. 4. Monthly sea surface temperature in the Niño 3.4 region of the tropical Pacific compared to the long-term average for all moderate-to-strong El Niño years since 1950, showing how 2015/16 (black line) compares to other strong previous events. (Climate.gov graph based on ERSSTv4 temperature)

1e. SST Anomalies in January 2016

In January 2016, the strong El Niño Southern Oscillation phenomenon appeared to be weakening, indicating a trend towards neutral conditions for the May – June 2016 period. However, a sea surface temperature anomaly was observed and associated with the 2015-2016 El Niño in the Pacific. Fig. 5 shows the SST Anomalies on 6 January 2016. Extreme SST anomalies (up to 3 degrees C.) were recorded in the central Pacific, with values higher than the records for the El Niño 1982-1983 and the 1997-1998 seasons.

However, in March of 2016, the U.S. National Oceanic and Atmospheric Administration (NOAA) issued a report on the El Niño's Southern Oscillation (ENSO), based on the sea surface temperature (SST) anomalies across the equatorial Pacific – noting a decrease since January. Nevertheless, NOAA indicated that during the decreasing phase of ENSO, significant prolonged rainfall and flood events could still occur – as indeed it happened in Ecuador as well as in Peru, Bolivia and elsewhere. As indicated, the overall conclusion was that the strong 2015-2016 El Niño Southern Oscillation phenomenon was weakening and the NOAA models indicated a transition to neutral conditions for the May – June 2016 period. More specifically, the NOAA model (Fig. 6) shows the Average SST anomalies for the period 21 February to 19 March 2016 prior to the 16 April 2016 Ecuador Earthquake.

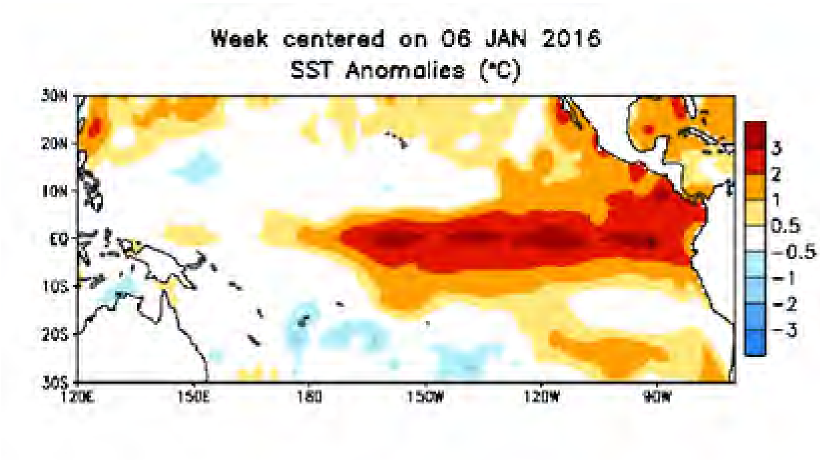

Fig. 5. 6 January 2016 SST Anomalies (NOAA graphic).

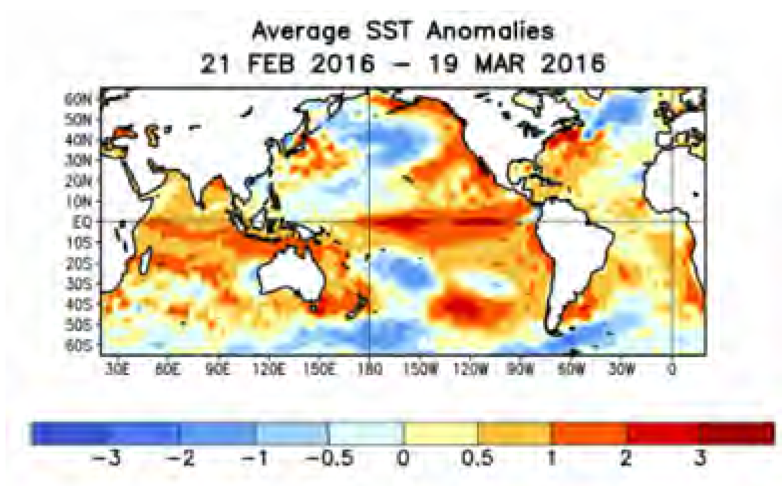

Fig. 6. Average SST Anomalies 21 February to 19 March 2016 prior to the 16 April 2016 Ecuador Earthquake (NOAA graphic).

1f. Heavy Rainfall in January 2016 in Ecuador and in South America

Indeed, and as predicted, significant prolonged rainfall and flood events resulted in Ecuador and elsewhere in South America (Fig. 7). Extensive flooding and landslides after torrential rainfall in late January 2016 occurred in Guayaquil (Fig 9) and elsewhere in Ecuador, Peru and even in Bolivia, Brazil and Argentina. Heavy rains between 19 and 20 January 2016 in Ecuador caused severe flooding in the provinces of Manabi and Guayas. The cities of Chone and Portoviejo were some of the worst affected in Manabí. In Guayaquil, there was extensive flood damage to houses and roads. In the Muisne Province, the Esmeraldas rain station recorded 244.5 mm of rainfall in 24 hours, while in Muisne (50 km to the west) the rain station recorded 88.5 mm (Source: INAMHI).

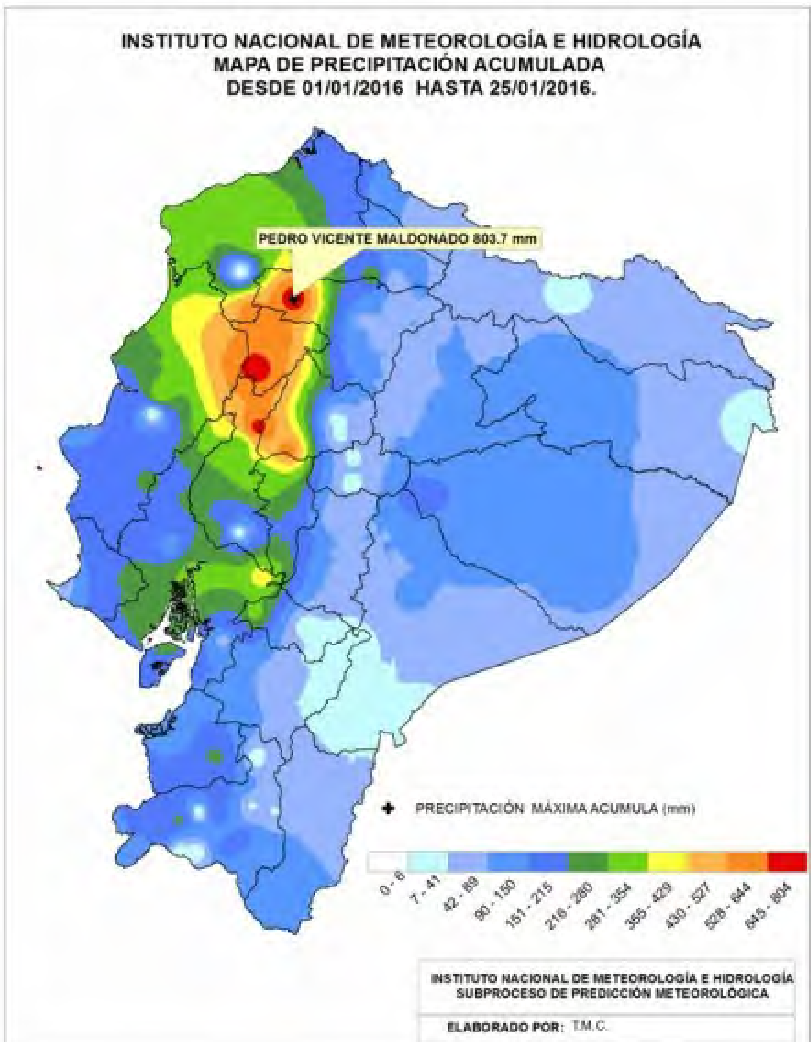

Fig. 7. Rainfall for January 2016 in Ecuador. (Image: INAMHI)

As shown in Figure 8, the rainfall was heavy at 22:00 on 24 January 2016, intensified at around 23:00 and lasted through the night, causing severe flooding by 24:00 early on 25 January and many landslides. The heavy flooding caused a state of emergency for the region and particularly for the city of Esmeraldas (Fig. 9)(Secretaría de Gestión de Riesgo – SGR).

Fig. 8. Rainfall, Esmeraldas, Ecuador, 22:00 on 24 January 2016 (Japanese Aerospace Agency)

Fig. 9. Floods in Esmeraldas. (Photo: Municipio Esmeraldas)

1g. El Niño-Southern Oscillations (ENSO's) impact on the frequency of earthquakes.

Whether El Niño-Southern Oscillations (ENSO's) have an impact on the frequency of earthquakes in South America remains to be investigated. As shown in Fig. 10 below, the strong 2015-2016 ENSO was accompanied by a large number of earthquakes of intensities with Richter magnitudes of 5.0 or greater since 1/1/2016 in Ecuador, Colombia and Peru.

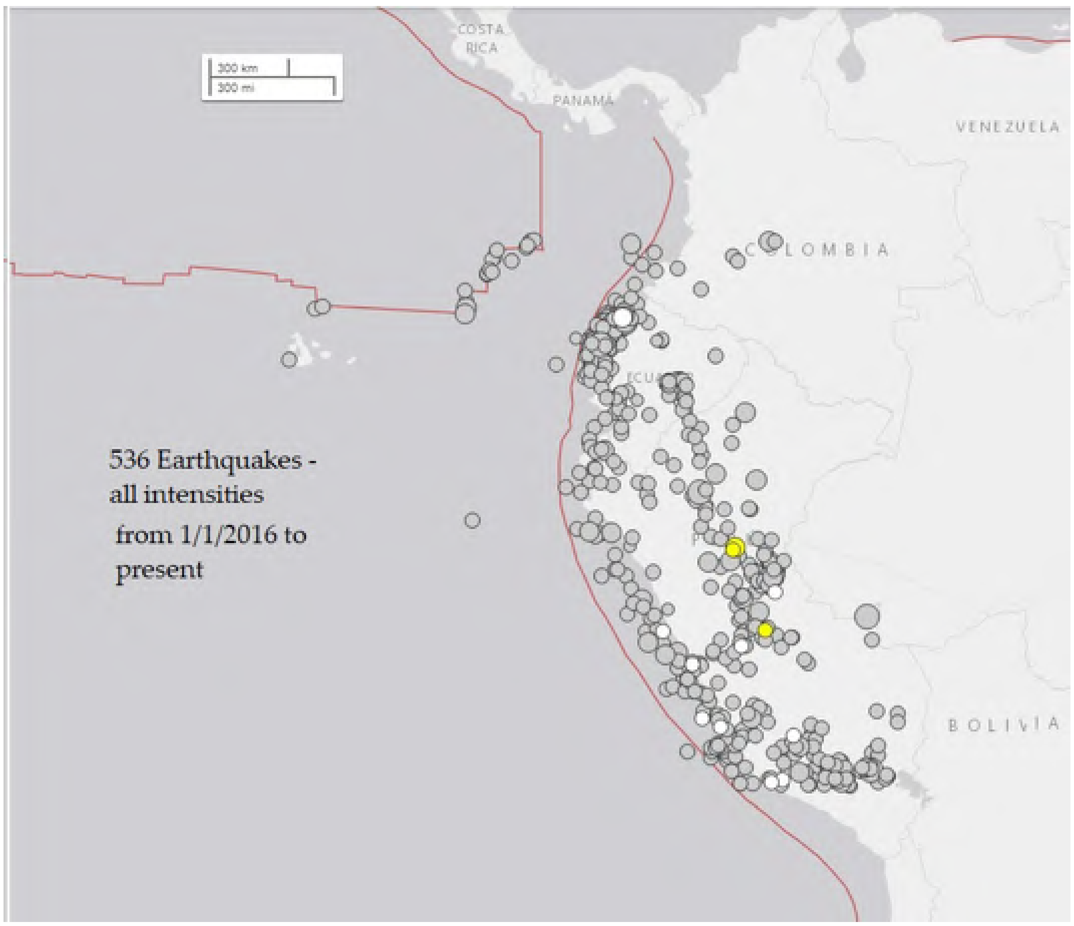

Fig. 10. Earthquakes with Richter magnitudes of 5.0 or greater since 1/1/2016 in Ecuador, Colombia and Peru.

It remains to be examined whether some of the large historical earthquakes (Fig. 10) along the west coast of South America (Colombia, Ecuador and Peru) since 1906, with the exception of a Richter 8.0 event in 1970 - occurred during periods of strong El Niño-Southern Oscillations (ENSO's)

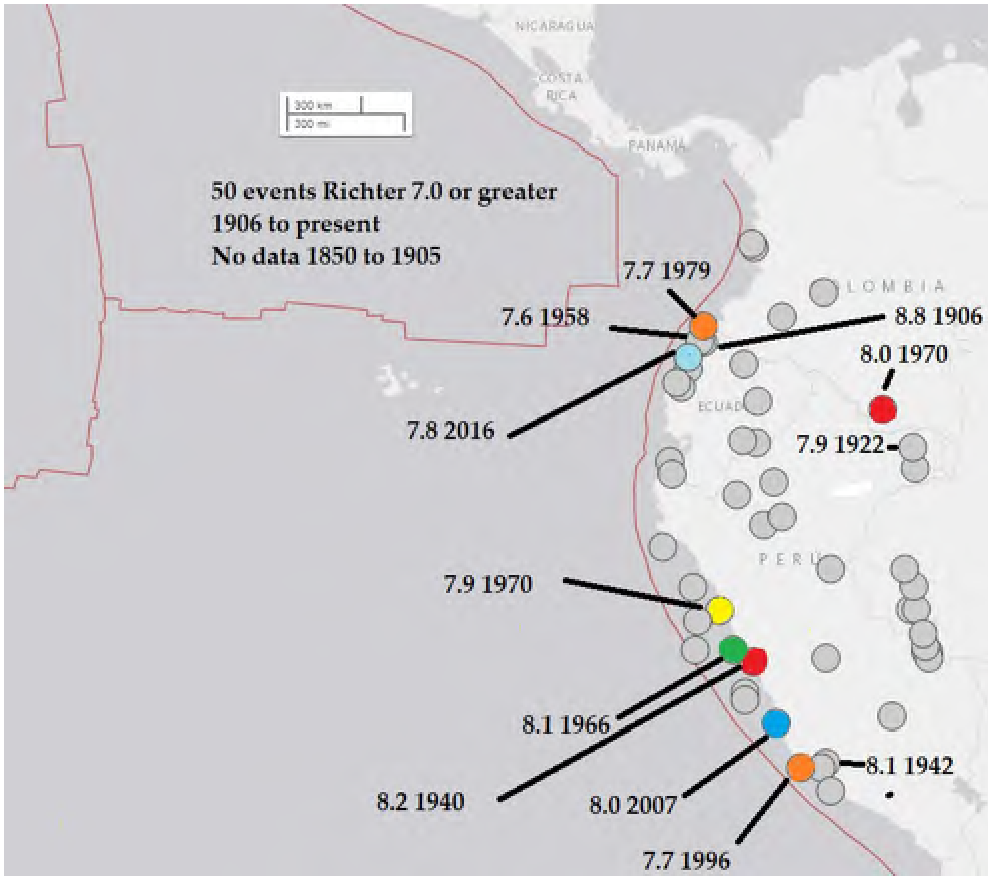

Fig. 11. Epicenters and Magnitudes of Fifty Richter 7.0 or greater, historic earthquakes most along the west coast of South America (Colombia, Ecuador and Peru) since 1906 – with the exception of a Richter 8.0 event event in 1970. No data exists for the period of 1850 to 1905.

2. ECUADOR EARTHQUAKE AND TSUNAMI OF 16 APRIL 2016

The floods, landslides and the destruction in Ecuador were followed by a major tsunamigenic earthquake on 17 April 2016 (local date). According to Ecuadorian government reports, more than 650 people were killed and there was widespread destruction. The town of Portoviejo, close to the epicenter, was devastated. The quake generated a locally damaging tsunami. Fig. 12 shows the epicenter of this tsunamigenic earthquake, as well as the epicenters, dates and magnitudes of significant historic earthquakes since 1906 in the region (as in Fig. 2)(Swenson & Beck, 1996). Fig. 13 shows the epicenter of the 2016 earthquake (blue circle) in relation to other recent significant historical earthquakes in Ecuador and Colombia.

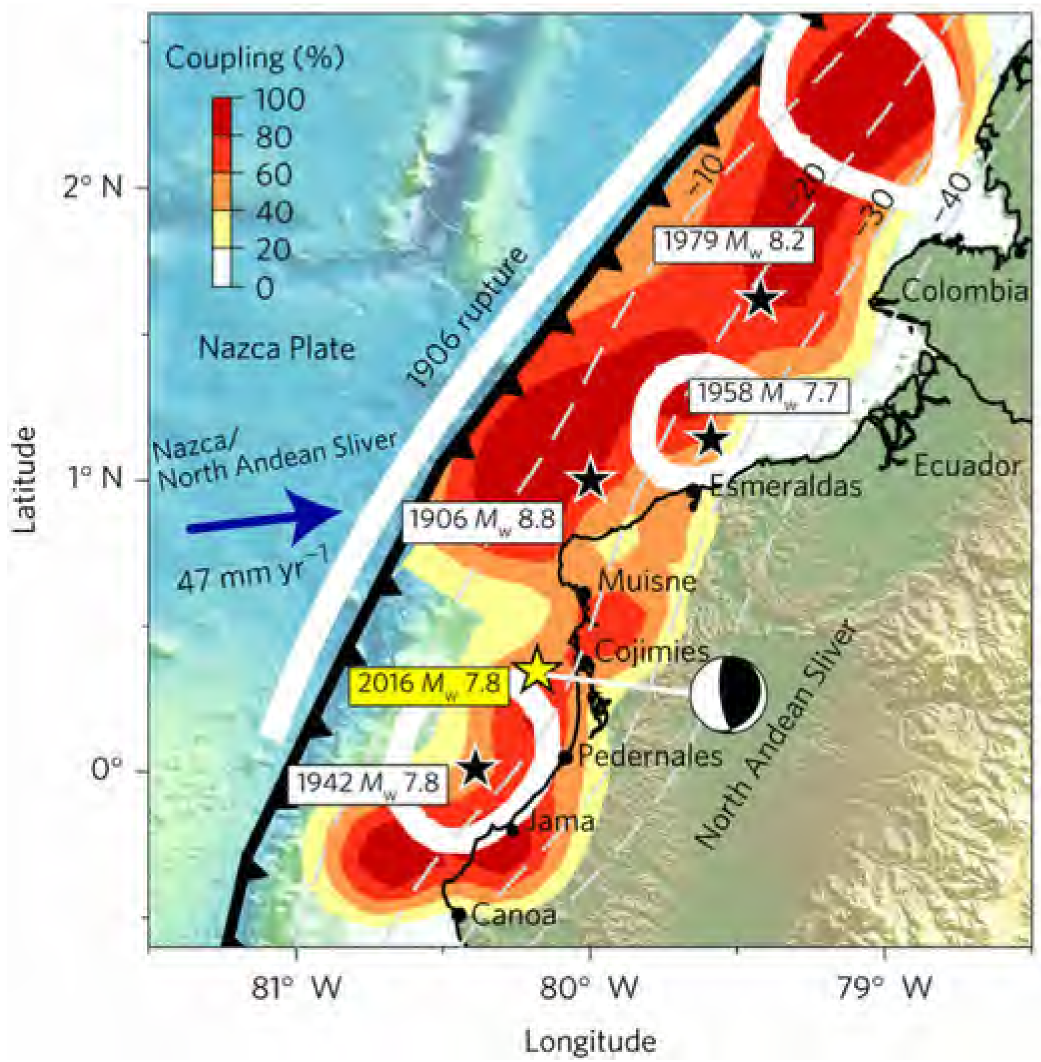

Fig. 12. Epicenter and mechanism of the 17 April 2016 earthquake and of other major historical tsunamigenic earthquakes in Northern Ecuador and Southern Colombia since the great 1906 earthquake (Internet graphic after Gabriel Lotto, 2016).

As established and reported, the 7.8 M_w magnitude earthquake of 17 April 2016 in Ecuador (local date) (2016-04-16T23:58:36.980Z) had its epicenter at 0.3819 N. and –79.9218 W., about 29 km SSE of the city of Muisne in the Esmeraldas Province, but somewhat NE of the epicenter of the 1942 quake which also had a magnitude (M_w7.8 revised) and apparently involved the same offshore fault. The focal depth of the quake was estimated at 20.59 km (about 12 miles). The 2016 quake had many similarities with the 1942 event.

Based on recent evaluations of Ecuador's seismicity, this earthquake was not a surprise. Since 2013 a major event was expected to occur in the region, given the fact that the Ecuador–Colombia plate boundary is being obliquely underthrust by the Nazca plate at the rate of ~ 4.6 cm/yr, with the upper plate being a fragment of the South American plate known as the North Andean Sliver (Nocquet et al., 2014; Chlieh et al., 2014). The Nazca tectonic plate moves slightly eastwards at a varying rate which ranges from 80 mm/yr in the south to about 65 mm/yr in the north (Pararas-Carayannis, 2012). Although of large magnitude, the 2016 earthquake was not as large as it could have been if its rupture extended beyond the existing 1942 fault asperity and included all or part of the rupture of the 1958 quake (M_w 7.7), or that of the catastrophic 1906 quake (M_w 8.8). Furthermore the 2016 quake may not have been a single event as reported. As postulated in this evaluation - its impact may have been somewhat ameliorated by the 2015 – 2016 El Niño climatic conditions that preceeded it. However, what was also perplexing about this event was the clustering of its aftershocks and their spatial distribution, as well as the possible contributing triggering mechanism, following the strong 2015-16 El Nino period - associated specifically with heavy rainfalls in the Andes and extensive flooding of Ecuador's coastal peninsula.

An extensive and detailed survey of the earthquake was conducted by scientists in Ecuador and their report is included in this issue of the journal (Chunga et. al. 2016; Toulkeridis et. al., 2017 a, b). The report reviews the literature on the country's geodynamic setting and seismogenic origin, the volcanism of the region, the geologic setting of the earthquake's epicentral area and a statistical evaluation and geophysical clustering of the main earthquake and of the aftershocks. Thus - and to avoid redundancy - the present section of this study mainly avoids reporting on details of the social and economic impact this earthquake had in Ecuador and concnctrates only on non-reported anomalies and further analytical evaluation of this event.

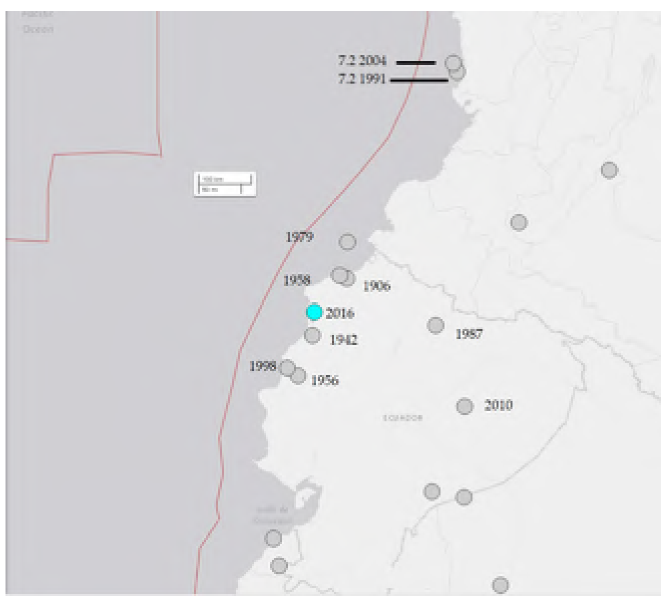

Fig. 13. Epicenter of the 2016 earthquake (blue circle) in relation to Recent Significant Historical Earthquakes in Ecuador and Colombia.

2a. Crustal Mechanism

The mechanism and location of the 2016 earthquake was consistent with a subduction type of seismic events that occur along the Colombia/Ecuador Trench but also with the coastal structure of the continental margin of southern Ecuador and northwest Peru (Shepperd, G.L. and Moberly, R., 1981). According to the post-disaster survey of the earthquake, the crustal displacements involved an area which was approximately 160 km long and 60 km wide (Toulkeridis et. al., 2017 c). The main quake was followed for weeks by numerous aftershocks – some of which appeared to have an anomalous spatial distribution.

2b. Rupture of the 16 April 2016 Earthquake in Ecuador.

The M_w 7.8 earthquake of 16 April 2016 ruptured along the zone where the Nazca plate interfaces with the South America. As illustrated in Fig. 12 and as previously stated, it occurred along the same fault where a similar M_w 7.8 earthquake occurred in 1942, a region where a seimic gap had been identified. It was along a part of the segmented zone which the great tsunamigenic earthquake of 1906 had ruptured in much greater length. This is a tectonic interface belt, north of the Carnegie Ridge intersection with the South America continent - a zone characterized by variable rupture modes, heavy sedimentation and tranversed by transform faults, which have formed mechanical barriers (asperities), thus preventing a continuous rupture similar to that caused by the great 1906 earthquake (Ruff & Kanamori, 1980; Kanamori & McNally, 1982; Beck & Ruff, 1984; Pararas-Carayannis 1980, 2012; Ye et. al., 2016). This heavy sedimentation along this zone is attributed to the heavy erosion caused by heavy rainfalls on the western slope of the Andes. Large amounts of sediments of heterogeneous density structure are deposited on Ecuador's coastal plains and subsequently find their way to the offshore areas and to the trench's fore-arc zone. The heterogeneous density structure of the decoupled Ecuador fore-arc could explain the propagation of the rupture zone of the April 2016 Ecuador earthquake. In particular, this rupture zone developed through a relatively low-density zone of the fore-arc sliver. Seismic and tsunami observations indicated a rupture of about 120 km length, north of the 1998 earthquake's rupture (Ye, et. al., 2016) and overlapping with that of the 1942 earthquake.

Something similar occurred with the 2 September 1992 tsunamigenic earthquake in Nicaragua near the Middle America Trench along the intra-oceanic convergent margins of the Cocos and Caribbean plates - a zone of active, oblique, shallow subduction. Also, Nazca Ridge's oblique subduction and migration along central and southern Peru had a similar effect on generating the tsunami of 23 June 2001 (Pararas-Carayannis, 2001 b). The quantity and thickness of subducted sediments along certain sections of such margins alter the seismic focal mechanisms and the geometry and velocity of ruptures. Certain large earthquakes, along such zones, can be expected to be "slow" - that is to have lower rupture velocities and to generate seismic waves of longer periods. The greater tsunamigenic potential of such earthquakes - along such zones of oblique shallow subduction - is not only the result of greater energy release but of the contribution of subducted sediments to the geometry of ocean floor deformation and volumes of displacements (Pararas-Carayannis, G. 1992; 2014).

2c. Unusual Clustering of Aftershoks

'The 2016 earthquake was also unusual in that it involved separate clusters of aftershocks from April to July 2016, with peculiar distribution over a great areal distance and widely separated in time, which indicated that this was not just the Mw 7.8 event with some aftershocks. (see Fig. 14 below). The unusual clustering was also discussed in the report by Toulkeridis et al. (2017).

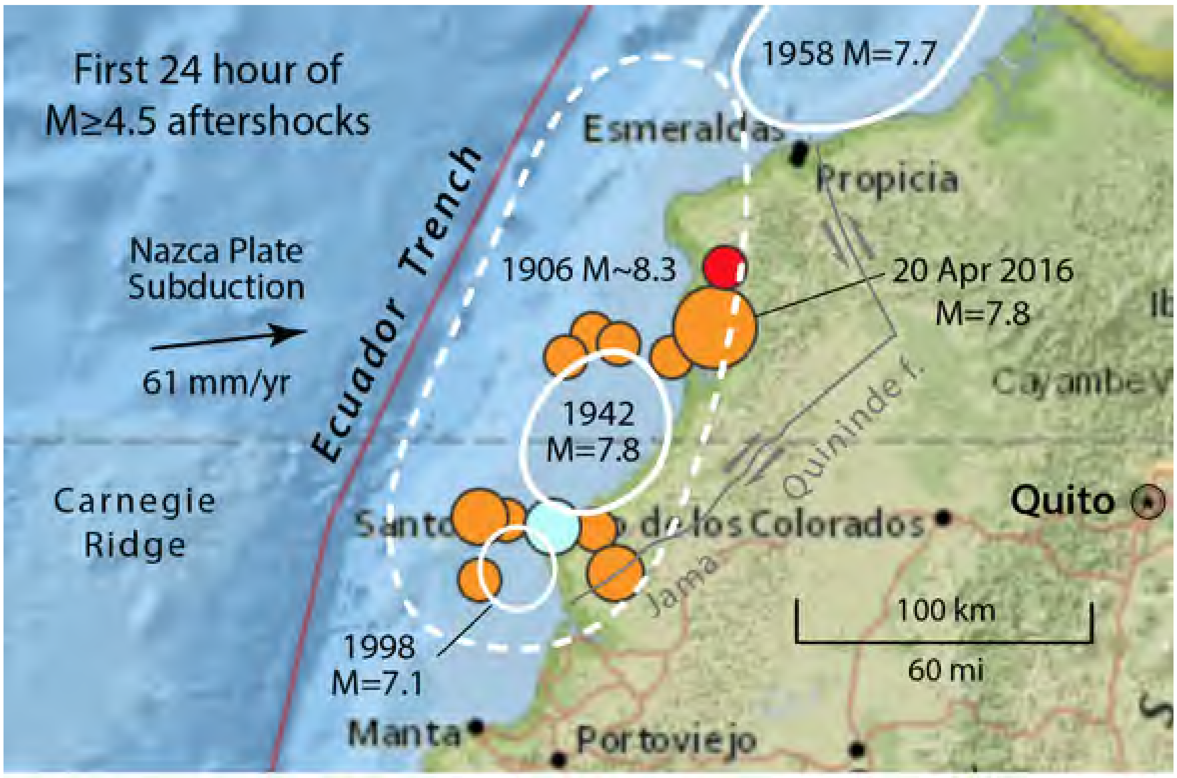

Fig. 14. Epicenters of Historic Earthquakes and Unusual Clustering of Major Aftershocks of the 1906 and 1942 earthquakes.

Figure 15 is a time series chart of major 25 aftershocks with Richter magnitudes 5.0 or greater to 8/1/2017 (marked as present in the figure) which followed the 16 April, 2016, quake (focal depth 20.6km) 27 km SSE of Muisne Ecuador (note the two separate clusters). Figure 16 shows three additional aftershoks until 28 November 2017. What was unusual about the three afterhocks of Richter 5s magnitudes is that they occurred close in time and space near the largest and most economically important city of Ecuador, particularly since the only other Richter 5 or greater in that time was a 5.2 magnitude far inland aftershock on October 7, 2017 represented by the gray dot in Figure 16. Actually, this October 5.2 event was part of a cluster of four including a 4.9 magnitude event which occurred on 9 October 2017.

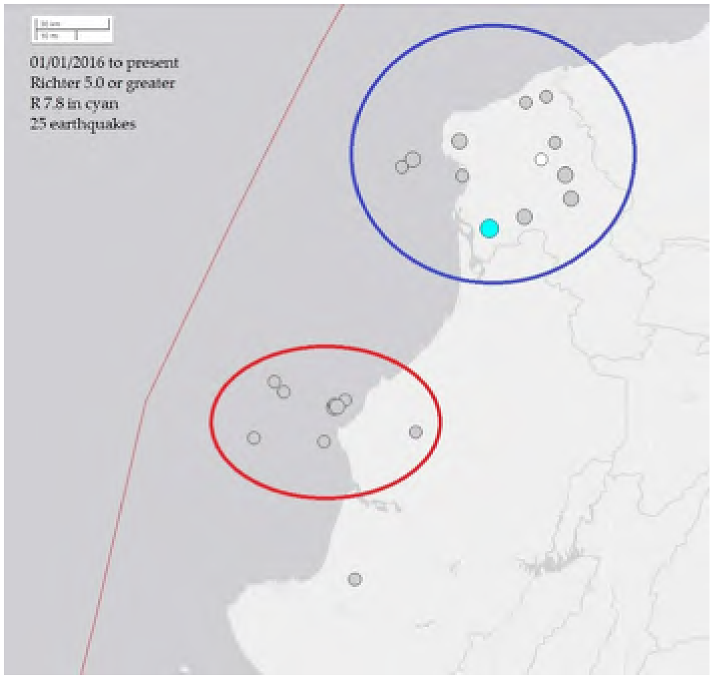

Fig. 15. Twenty-five major aftershocks of Richter magnitudes 5.0 or greater to 8/1/2017 (marked as "present") following the 16 April, 2016 quake (note the two separate clusters)(Source: USGS).

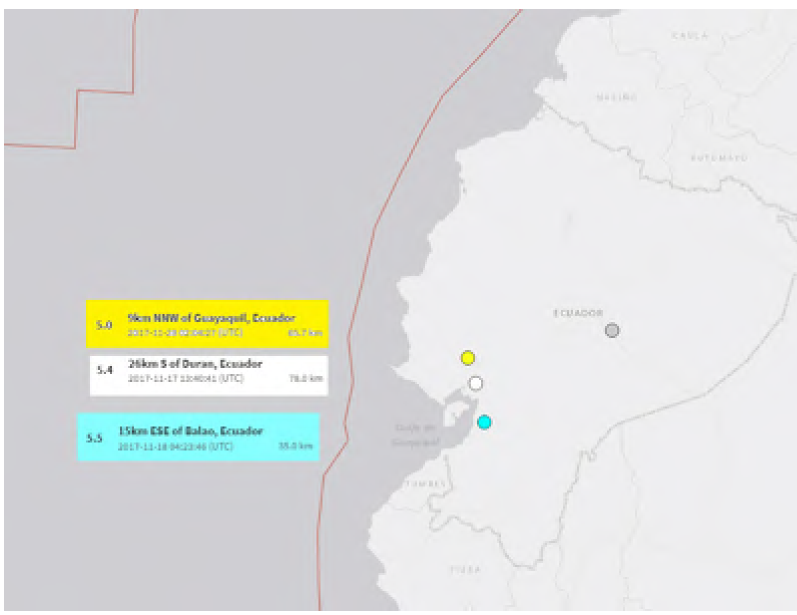

Figure 16. Three additional aftershocks until 28 November 2017.

As indicated in Figure 17 below, the leftmost (earliest) event marked by a green arrow was pretty far apart in time so it is difficult to say that it was a precursor event without conducting a new fault analysis. Then with essentially no warning, a 6.2 (red arrow) event occurred and subsequent aftershocks started declining in a classical pattern. Then a surprising 6.0 occurred which looks like a separate cluster – with its aftershocks also declining in the expected way. The three events to the right of the orange arrow might be a separate cluster. Then all is quiet for a while giving the impression that all stress on the fault has diminished, when all of a sudden a magnitude 7.0 (purple arrow) occurs that is just way out of pattern. The subsequent sequence of the aftershocks (black arrows) are also out of expected normal pattern.

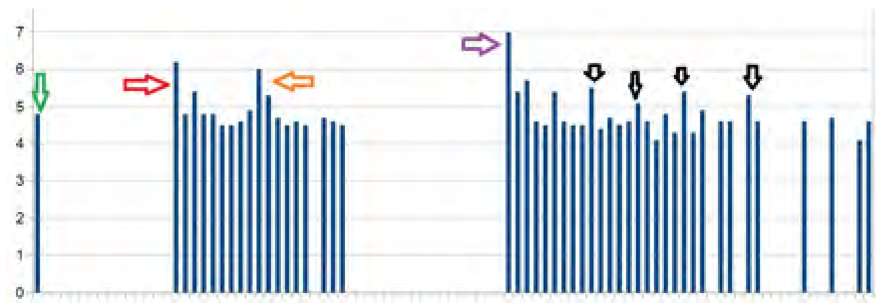

Fig. 17. Clustering of major aftershocks of the Ecuador Earthquake from April 16-23.

Figure 18 shows quake clusters from April 16-23, 2016, clusters on May 18 and clusters from July 8-11, 2016. As shown, two large events occurred on May 18, 2016. The clusters depend a bit on the size of the region involved as well the intensity of the earthquakes. For a large region with all earthquakes you would get the six clusters. A statistical argument can be made for breaking the blue cluster into 2 pieces and for breaking the orange cluster into three pieces as shown. Overall, the aftershock sequence and the subsequent clusters appear to have nucleated around the area of maximum slips in the rupture zone, and that suggests that asperities can be persistent features which can be determined by the spatial variations of the mechanical properties of the subduction megathrust zone. This observation implies that the heterogeneous density structure of the fore-arc can be determined from gravity data - whch could be used to forecast zones of future potential damage.

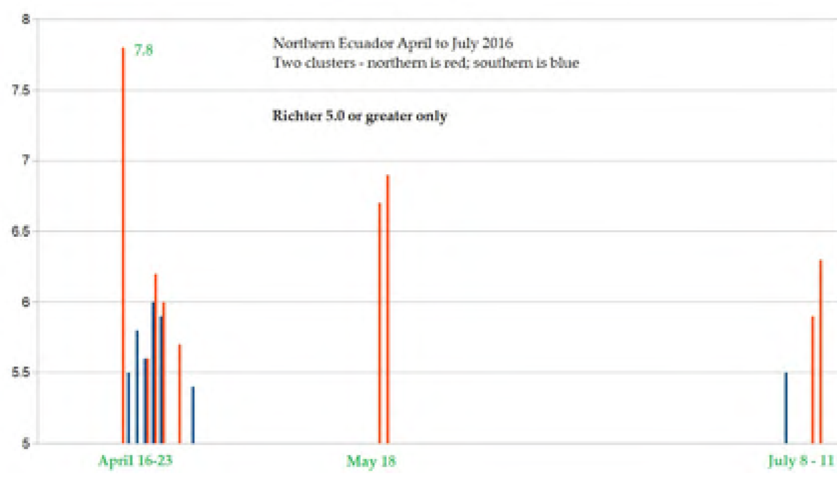

Fig. 18. Unusual occurrence of two more quakes on May 18 and more significant aftershocks from July 8-11, 2016.

2d. Distribution of Earthquake Intensities

Post-disaster evaluation indicated a large areal distribution of ground effects and intensities of the 2016 earthquake (Chunga et. al. 2016). Fig. 19 below shows the extensive and unusual distribution of the earthquake's high intesities and destruction.

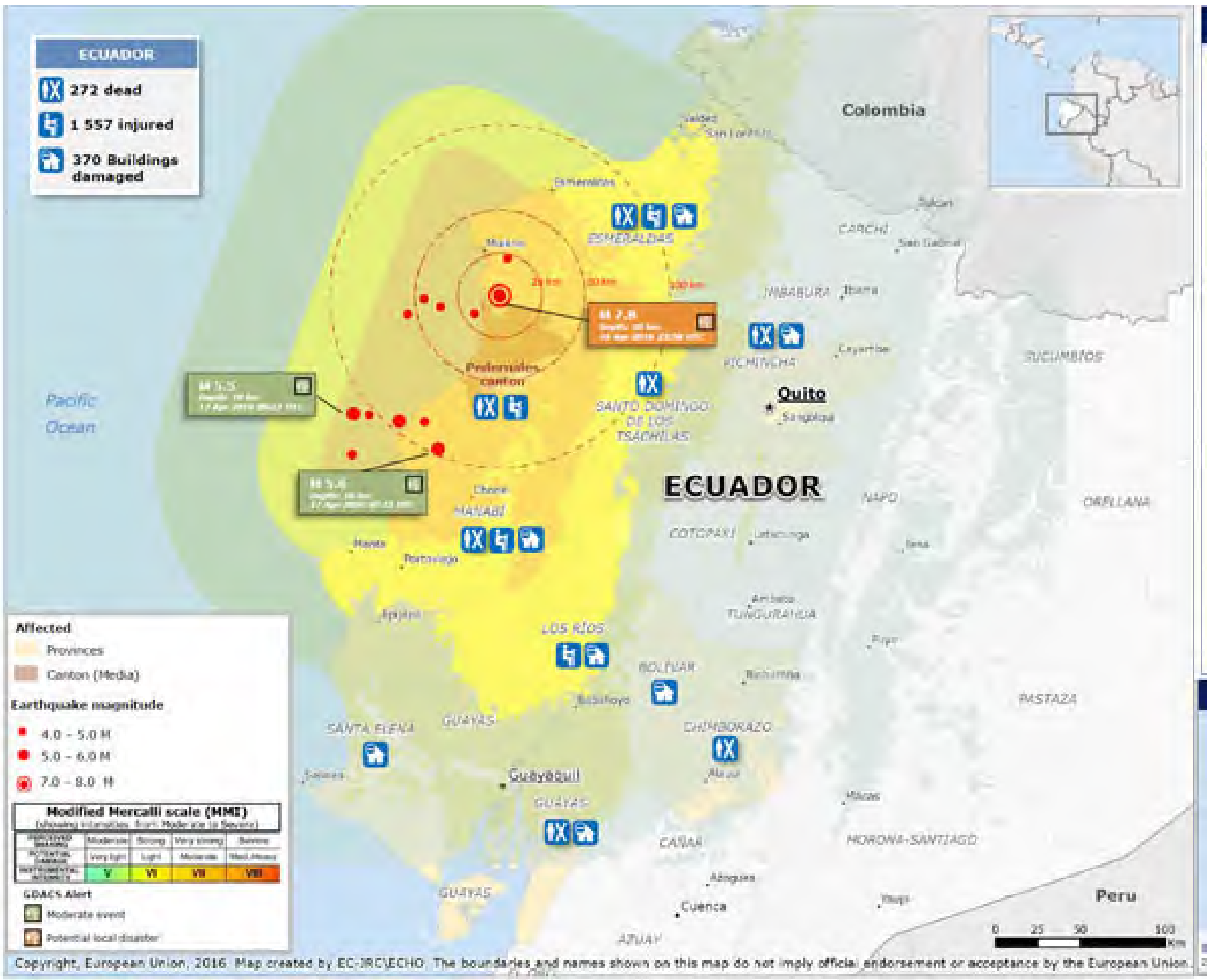

Figure 19. Unusual distribution of the earthquake's high Modified Mercalli intesities and destruction.

2e. The Tsunami

Based on data from the INOCAR-DATA buoy, INOCAR issued a Tsunami Warning for coastal areas of Ecuador and the Galapagos Islands. The warning lasted for four hours. According to eyewitnesses, there were significant changes in the level of the sea but not an extreme runup – because the tsunami ocurred at low tide. A much higher runup and damage would have occurred if the quake had occurred at high tide. As shown in Fig. 20 below, the INOCAR tide gauge at the Port of Esmeraldas begun recording a recession of sea water level at 19:00 and within a short period of about three minutes the arrival of the tsunami crest with subsequent fluctuations of about ~50 cm/min (Toulkeridis et al., 2017). Note that the crest of the first wave of the tsunami arrived 6 minutes after the quake. The tsunami resulted in lasting currents within the port of Esmeraldas which were strong enough to displace some small boats and buoys from their anchorage sites.

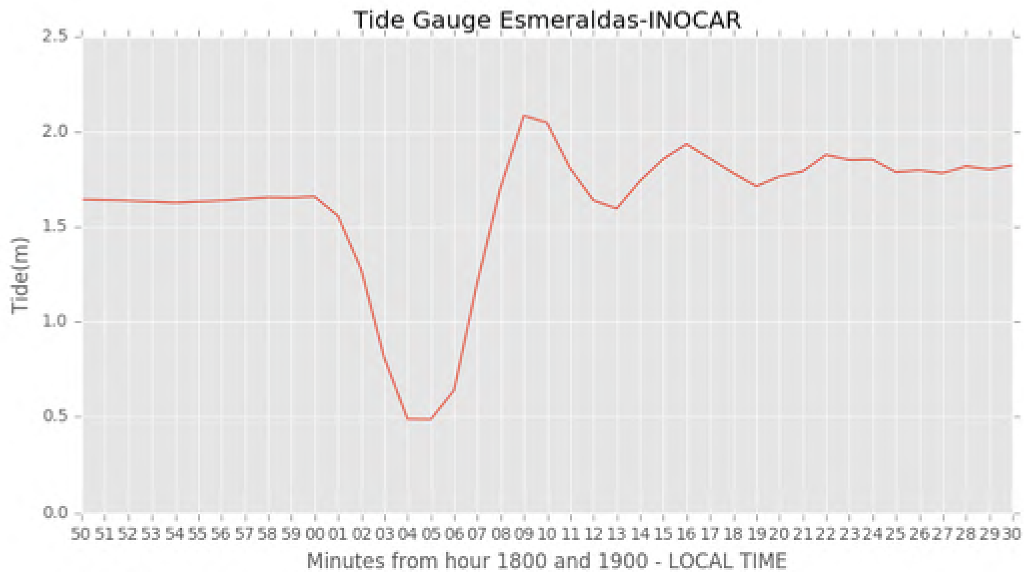

Fig. 20. Mareogram of the Tsunami Recorded at the Port of Esmeraldas tide station. (Toulkeridis et al., 2017; Source: INOCAR)

3. SEASONALITY OF HISTORICAL EARTHQUAKES ALONG THE ECUADOR TRENCH AND THE WEST COAST OF SOUTH AMERICA.

As previously mentioned, Ecuador is very vulnerable to earthquakes. Although infrequent, large earthquakes as that of 1906 can occur from time to time along the subduction zone of Colombia/Ecuador and generate destructive Pacific-wide tsunamis. The historic record shows that large earthquakes in the region are often preceded by increasing activity of smaller events. The morphology of the offshore region is further complicated by the extensive sedimentation which takes place as a result of erosion of the Andes mountain ranges and the numerous rivers flowing into the sea. A very thick sedimentatry column enters the subduction zone, so part of the trench associated with the present accretionary front in the offshore region of Ecuador has been buried and does not have much of a morphological relief as other subduction-caused trenches around the world oceans.

There is little historical data on earthquakes for Ecuador and the rest of the west coast of South America on which to base a correlation of the seasonality of the El Nino phenomenon and possible mechanism(s) that may be contributing to their triggering. A search for historical earthquakes for a catalogs of tsunamis for South America by the Internarional Tsunami Information Center (Pararas-Carayannis, 1975) included all available literature and historical letters and data of the Archives of Seville in Spain, the records of the British Museum in London and of the Bishop Museum in Hawaii.

The historic record for Ecuador was found to be incomplete but some cursory documentation for South America earthquakes was found in a publication by the French mathematician Fernard Montessus De Ballore, for events beginning in 1441 after the Pizzaro brothers conquered Peru. In continuing the search for older historical earthquakes in Ecuador, nothing much was found for events prior to 1906. Many more quake events – some of which may have been significant - were also missing for the period from 1905 to 1940 for the coasts of northern Peru, Ecuador and Southern Colombia. Figure 21 provides epicenters of 298 earthquakes of Richter 6.0 or greater that ocurred in the northwestern region of South America (between 1850 and 1906). Most of these events occurred along the West Coast of Colombia, Ecuador and Peru and some of the coastal quakes generated small local tsunamis, but no details are available.

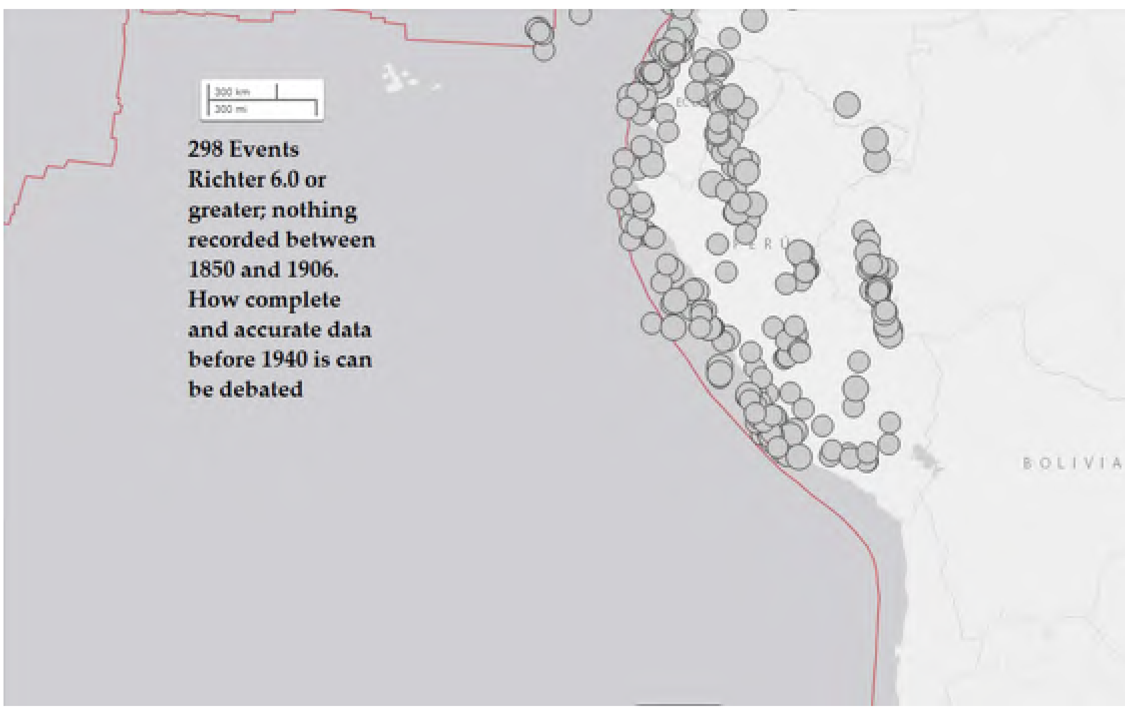

Fig. 21 Epicenters of 298 Historical Earthquakes with Magnitudes 6.0 or greater in the northwestern region of South America (between 1850 and 1906).

Figure 22 shows 187 earthquakes of Richter 6 and above as well as some details for the Richter 7's in the region since 1906. Given the small size of the region and the short times between powerful events, it is concludethat a lot of stress was imposed by the eastward moving Nazca Plate (See also Fig.12).

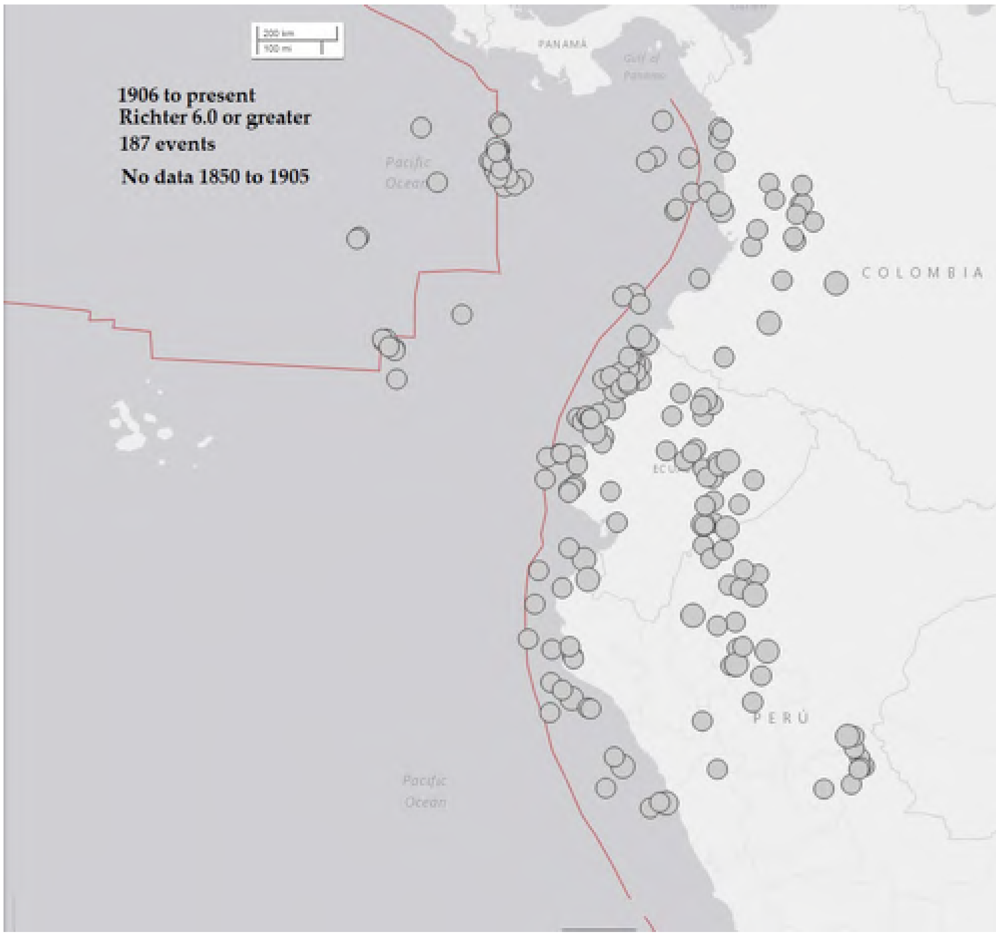

Fig. 22 Recent Historical Earthquakes along the Colombia, Ecuador and Peru (since 1906) with Magnitudes 6.0 or greater.

The seasonality of historical earthquakes along the Ecuador/Colombia and Peru subduction zones and their possible correlation to recent known periods of strong El Niño-Southern Oscillations (ENSO's) remains to be examined in order to determine if indeed there is a contributing factor to the triggering such events - at least along coastal margin regions with high thickness of subducted and greatly hydrated sediments.

3. VOLCANIC IMPACTS ON CLIMATE CHANGES AND IN TRIGGERING EARTHQUAKES

Convergent, compressional and collisional tectonic activity is responsible for zones of subduction, the formation of island arcs and the evolution of particular volcanic centers on the overlying plates. The inter-plate tectonic interaction and deformation along such marginal boundaries result in moderate seismic and volcanic events that not only can generate tsunamis by a number of different mechanisms but also result in significant climatic changes - based on the geochemical consistency and viscocity of the material in their magmatic chambers which control the intensities and explosivity of eruptions. Such active geo-dynamic processes have created volcanoes characterized by both effusive and explosive activity for both continental and oceanic volcanoes (Pararas-Carayannis, 2006).

Eruption mechanisms of volcanoes are complex and often anomalous. Earthquakes precede collapses of lava domes often prior to major eruptions, which may vary in intensity from Strombolian to Plinian. Locally catastrophic, short-period tsunami-like waves can be generated directly by lateral, direct or channelized volcanic blast episodes, or in combination with collateral air pressure perturbations, nuess ardentes, pyroclastic flows, lahars, or cascading debris avalanches. All these occurrences – depending on their severity – affect climatic conditions both locally and globally. Submarine volcanic eruptions can also alter the temperature of the overlying waters and create climatic changes as well as changes in the circulation of geostrophic ocean currents. Studies of intensive volcanic eruptions and their impact on climate changes have been made for numerous volcanoes in Hawaii, Alaska, Kuril Islands, Indonsesia, Japan, the Cascade Range, South America, Reunion Island, the Lesser Antilles, the Canaries, the Mediterranean Sea, the Northern Arabian Sea and other regions of the world (Pararas-Carayannis, 2001a; 2002; 2003; 2004 b, c, d; 2006).

Specically, the volcanoes of Ecuador are the result of subduction of the Pacific tectonic plate under the continental plate of South America. Four rows of volcanoes can be identified in Ecuador compared to a single line in Colombia to the north. The volcanoes of the Galapagos Islands have been thoroughly described in a book by Toulkeridis (2011).

One of the largest eruptions in the world in the past 1000 years was that of the Quilotoa Volcano in 1280 A.D. (80 km SSW from Quito). This eruption came after 14,000 years of dormancy. It was a Plinian eruption which discharged ~11 cubic km of magma during four eruptive phases. Although not adequately documented, this eruption must have had a global impact on climate change and severe reduction of incoming solar radiation. Such large explosive eruptions of this volcano in Ecuador occur every 10,000-14,000 years.

Also, the Cotopaxi stratovolcano's eruptions (60 km. South of Quito) of 1744, 1768, 1877, 1880 and 2015, the eruptions of volcanoes in the Galapagos, the 1600 Huaynaputina volcano's explosion in Southern Peru (Volcanic Explosivity Index [VEI] 6), and of the cataclysmic 1991 eruption of Mount Pinatubo volcano in the Phillipines must have a significant impact on climate. Also, the thermal impact of undersea volcanoes such Kick-Them-Jenny, will be examined in a subsequent study.

REFERENCES

Beck, S.L. and Ruff, L.J., 1984: The rupture process of the great 1979 Colombia earthquake: evidence for the asperity model. J.Geophys. Res., 89: 9281–9291

Chunga, K., Besenzon, D., Mulas, M., Loayza, G. and Pindo JC., 2016: Areal distribution of Ground effects induced by the 2016 Mw 7.8 Pedernales earthquake (Ecuador). 88° Congresso della Societa' Geologica Italiana. S1. Earthquakes and Active Tectonics: a multidisciplinary approach. Napoli, 7/9 Sept. 2016.

Kanamori, H. and McNally, K.C., 1982. Variable rupture mode of the subduction zone along the Ecuador-Colombia coast. Bulletin of the Seismological Society of America, 72(4): 1241-1253.

Ye Lingling , Kanamori Hiroo , Avouac Jean-Philippe , Li Linyan , Cheung Kwok Fai, Lay Thorne , 2016. The 16 April 2016, *M W* 7 . 8(*M S* 7 . 5) Ecuador earthquake: A quasi-repeat of the 1942 *MS* 7.5 earthquake and partial re-rupture of the 1906 *MS* 8.6 Colombia–Ecuador earthquake. Earth and Planetary Science Letters, 2016 Elsevier.

J-M. Nocquet, J. C. Villegas-Lanza, M. Chlieh, P. A. Mothes, F. Rolandone, P. Jarrin, D. Cisneros, A. Alvarado, L. Audin, F. Bondoux, X. Martin, Y. Font, M. Régnier, M. Vallée, T. Tran, C. Beauval, J. M. Maguiña Mendoza, W. Martinez, H. Tavera & H. Yepes, 2014. Motion of continental slivers and creeping subduction in the northern Andes, ***Nature Geoscience*** 7**, 287–291 (2014) doi:10.1038/ngeo2099**

Pararas-Carayannis, G., 1975. "Verification Study of a Bathystrophic Storm Surge Model". A study prepared for the U.S. Nuclear Regulatory Commission under contract with the U.S. Army, Corps of Engineers Coastal Engineering Research Center, Washington, D.C., Technical Memorandum No. 50, May 1975.

Pararas-Carayannis, G. 1980: The Earthquake and Tsunami of December 12, 1979, in Colombia. Intern. Tsunami Information Center Report, Abstracted article in Tsunami Newsletter, Vol. XIII, No. 1, January 1980. Also: http://www.drgeorgepc.com/Tsunami1979Colombia.html

Pararas-Carayannis, G., 1988. The Tsunami Generated from the Eruption of the Volcano of Santorini in the Bronze Age. Science of Tsunami Hazards, Vol16/N1/1988. http://tsunamisociety.org/STHVol6N1Y1988.pdf

Pararas-Carayannis, G. 1991. Tsunami Glossary – UNESCO Intergovernemental Oceanographic Commission, Technical Memorandum 37, 136 pp., 1991 http://unesdoc.unesco.org/images/0008/000885/088538eb.pdf

Pararas-Carayannis, G. 1992. The Earthquake and Tsunami of 2 September 1992 in Nicaragua http://drgeorgepc.com/Tsunami1992Nicaragua.html

Pararas-Carayannis, G., 2000. “The Big One – The Next Great California Earthquake”, 385pp. Forbes Press, 2000. http://www.drgeorgepc.com/BookTheBigOne.html

Pararas-Carayannis, G., 2001a, "The Earthquake and Tsunami of 28 November 1945 in Southern Pakistan" http://www.drgeorgepc.com/Tsunami1945Pakistan.html

Pararas-Carayannis, G., 2001b. GEODYNAMICS OF NAZCA RIDGE'S OBLIQUE SUBDUCTION AND MIGRATION - IMPLICATIONS FOR TSUNAMI GENERATION ALONG CENTRAL AND SOUTHERN PERU: Earthquake and Tsunami of 23 June 2001. Science of Tsunami Hazards, Vol. 31/N2/2001. http://tsunamisociety.org/312GPCc.pdf

Pararas-Carayannis G., 2002. Evaluation of the Threat of Mega Tsunami Generation from Postulated Massive Slope Failures of Island Stratovolcanoes on La Palma, Canary Islands, and on the Island of Hawaii, Science of Tsunami Hazards. Vol 20 (5). pages 251-277, 2002 http://tsunamisociety.org/STHVol20N5Y2002.pdf

Pararas-Carayannis G., 2003. Near and Far-Field Effects of Tsunamis Generated by the Paroxysmal Eruptions, Explosions, Caldera Collapses and Slope Failures of the Krakatau Volcano in Indonesia, on August 26-27, 1883, Presentation for the International Seminar/Workshop on Tsunami "In Memoriam 120 Years Of Krakatau Eruption Tsunami And Lesson Learned From Large Tsunami" August 26th 29th 2003, Jakarta and Anyer, Indonesia. Also published in the Journal of Tsunami Hazards, Volume 21, Number 4. 2003. http://tsunamisociety.org/STHVol21N4Y2003.pdf

Pararas-Carayannis G., 2004a. Ocean Governance and Sustainability - Present Trends - Future Challenges, Plenary Lecture - 30th Pacem in Maribus (PEACE IN THE OCEANS). A Year after Johannesburg. Ocean Governance and Sustainable Development: Ocean and Coasts - a Glimpse into the Future, Organized by National Academy of Sciences of Ukraine, IOI, and National Commission of Ukraine for UNESCO, Kiev, Ukraine, October 26-30, 2003 / Published in "A Gateway to Sustainable Development" - pp. 90-101, Proceedings of the 30 International Conference Pacem in Maribus, International Ocean Institute, Sevastopol 2004. http://www.drgeorgepc.com/OceanGovernance.html

Pararas-Carayannis, G., 2006. THE POTENTIAL OF TSUNAMI GENERATION ALONG THE MAKRAN SUBDUCTION ZONE IN THE NORTHERN ARABIAN SEA. CASE STUDY: THE EARTHQUAKE AND TSUNAMI OF NOVEMBER 28, 1945. Volume 24, N5, pp- 358-384. http://library.lanl.gov/tsunami/ts245.pdf http://drgeorgepc.com/TsunamiPotentialMakranSZ.html

Pararas-Carayannis G., 2004a - Climate Change, Natural and Man-Made Disasters - Assessment of Risks, Preparedness and Mitigation, Keynote Presentation CLIMATE CHANGE DISASTER PREPAREDNESS, 30th Pacem in Maribus (PEACE IN THE OCEANS). A Year after Johannesburg. Ocean Governance and Sustainable Development: Ocean and Coasts - a Glimpse into the Future, Organized by the National Academy of Sciences of Ukraine, IOI, and National Commission of Ukraine for UNESCO, Kiev, Ukraine, October 26-30, 2003 / Published in "A Gateway to Sustainable Development" - pp. 606 - 612, Proceedings of the 30 International Conference Pacem in Maribus, International Ocean Institute, Sevastopol 2004. http://www.drgeorgepc.com/ClimateChange.html

Pararas-Carayannis G., 2004b. INDONESIA 1883: Near and Far-Field Effects of Tsunamis Generated by the Paroxysmal Eruptions, Explosions, Caldera Collapses and Slope Failures of the Krakatau Volcano in Indonesia, on August 26-27, 1883 http://drgeorgepc.com/Tsunami2004Indonesia.html

Pararas-Carayannis G., 2004c. Natural Disasters in Oceania, Chapter 10, in International Perspectives on Natural Disasters: Occurence, Mitigation, and Consequences - Book Series: ADVANCES IN NATURAL AND TECHNOLOGICAL HAZARDS RESEARCH, Western Michigan University, ISBN: 1-4020-2850-4, Nov. 2004, Springer Publishing.

Pararas-Carayannis, G. 2004d. Volcanic Tsunami Generating Source Mechanisms in the Eastern Caribbean Region. Science of Tsunami Hazards, 22(2), 74-114/2004. http://tsunamisociety.org/STHVol22N2Y2004.pdf

Pararas-Carayannis G., 2006. Risk Assessment of Tsunami Generation from Active Volcanic Sources in the Eastern Caribbean Region - In "CARIBBEAN TSUNAMI HAZARDS"- Proceedings of National Science Foundation Caribean Tsunami Workshop, March 30-31, 2004, Puerto Rico, Aurelio Mercado-Irizarry - Philip Liu, Editors. ISBN 981-256-545-3, 341 pp. 2006, Hard Cover Book. World Scientific Publishing Co. Pte.Ltd., Singapore

Pararas-Carayannis, G. 2012a. Evaluation of Potential Tsunami Generation along the Colombia/Ecuador Subduction Margin - Examination of Historical Tsunamis – 5th International Tsunami Symposium, European Commision Joint Research Centre, Ispra, Italy, 2012.

Pararas-Carayannis, G., 2012b: Potential of tsunami generation along the Colombia/Ecuador subduction margin and the Dolores-Guayaquil Mega-Thrust. Science of Tsunami Hazards, 31, 3: 209-230.http://tsunamisociety.org/313gpcC.pdf

Pararas-Carayannis, G., 2012c. Geodynamics of Nazca Ridge's Oblique Subduction and Migration - Implications for Future Tsuanmi Generation Along Central and Southern Peru: Earthquake and Tsunami of 23 June 2001. Science of Tsunami Hazards, 31, 2, 2012. http://tsunamisociety.org/312GPCc.pdf

Pararas-Carayannis, G., 2014. The Great Tohoku-Oki Earthquake and Tsunami of March 11, 2011 in Japan: A Critical Review and Evaluation of the Tsunami Source Mechanism. Pure and Applied Geophysics, December 2014, Volume 171, Issue 12, pp 3257–3278.

Reynolds, O., 1886. "Experiments showing dilatancy, a property of granular material, possibly connected with gravitation," Proc. Royal Institution of Great Britain, February 12, 1886.

Ruff, L.J., and Kanamori, H., 1980, Seismicity and the subduction process: Physics of the Earth and Planetary Interiors, v. 23: 240–252, doi: 10.1016/0031–9201(80)90117-X.

Shepperd, G.L. and Moberly, R., 1981: Coastal structure of the continental margin, northwest Peru and southwest Ecuador. Geological Society of America Memoirs, 154: 351-392.

Schlesinger, M. E. (1994). "An oscillation in the global climate system of period 65-70 years". *Nature*. **367** (6465): 723–726. *Bibcode*:*1994Natur.367..723S*. *doi*:*10.1038/367723a0*.

Swenson, J.L. and Beck, S.L., 1996: Historical 1942 Ecuador and 1942 Peru subduction earthquakes, and earthquake cycles along Colombia–Ecuador and Peru subduction segments. Pure Appl. Geophys.146 (1): 67–101.

Toulkeridis, T., Parra, H., Mato, F., Cruz D´Howitt, M., Sandoval, W., Padilla Almeida, O., Rentería, W., Rodríguez Espinosa, F., Salazar Martinez, R., Cueva Girón, J., Taipe Quispe, A. and Vernaza Quiñonez, L., 2017a: Contrasting results of potential tsunami hazards in Muisne, central coast of Ecuador. J. Tsunami Soc. Int, 36: 13-40.

Toulkeridis et al., 2017b; Real-Time Radioactive Precursor of the April 16, 2016 Mw 7.8 Earthquake in Ecuador. Submitted

Toulkeridis, 2011: Volcanic Galápagos Volcánico. Ediecuatorial, Quito, Ecuador: 364 pp

Theofilos Toulkeridis, Kervin Chunga, Willington Rentería, Fabian Rodriguez, Fernando Mato, Sissy Nikolaou, Mario Cruz D´Howitt, Davide Besenzon, Hugo Ruiz, Humberto Parra and Xavier Vera-Grunauer 2017c, THE 7.8 M_w EARTHQUAKE AND TSUNAMI OF 16th April 2016 IN ECUADOR:Seismic Evaluation, Geological Field Survey and Economic Implications. Science of Tsunami Hazards, Vol.36, No. 4, 2017.

Trenkamp, R., Kellogg, J. N. Jeffrey T. Freymueller, Hector P. Mora, 2002. Wide plate margin deformation, southern Central America and northwestern South America, CASA GPS observations, Journal of South American Earth Sciences, Volume 15, Issue 2, June 2002, Pages 157-171.

Ye Lingling , Kanamori Hiroo , Avouac Jean-Philippe , Li Linyan , Cheung Kwok Fai , & Thorne Lay, 2017. The 16 April 2016, *M W* 7 . 8(*M S* 7 . 5) Ecuador earthquake: Aquasi-repeat of the 1942 *M S* 7.5 earthquake and partial re-rupture of the 1906 *M S* 8 . 6 Colombia–Ecuador earthquake Earth and Planetary Science Letters

USGS SOURCES:

USGS (United States Geological Service), 2016a: Historic Earthquakes, 1906 January 31st. (http://earthquake.usgs.gov/earthquakes/world/events/1906_01_31.php)

USGS (United States Geological Service), 2016b: M7.8 - 29km SSE of Muisne, Ecuador.http://earthquake.usgs.gov/earthquakes/eventpage/us20005j32#general

USGS (United States Geological Service), 2016c: Earthquake Glossary - aftershocks.https://earthquake.usgs.gov/learn/glossary/?term=aftershocks

USGS (United States Geological Service), 2016d: Earthquake Catalog Search.https://earthquake.usgs.gov/earthquakes/search/

ISSN 8755-6839

SCIENCE OF TSUNAMI HAZARDS

Journal of Tsunami Society International

Volume 36 Number 4 2017

ECONOMIC EVALUATION OF RECOVERING NATURAL PROTECTION WITH CONCURRENT RELOCATION OF THE POPULATION THREATENED BY TSUMANI HAZARDS IN CENTRAL COASTAL ECUADOR

Fabián Rodríguez Espinosa[1,2]; Theofilos Toulkeridis[1]*, Rodolfo Salazar Martínez[1,3]; Jessica Cueva Girón[1], Adriana Taipe Quispe[1], Lucía Vernaza Quiñonez[4], Oswaldo Padilla Almeida[1], Fernando Mato[1], Mario Cruz D'Howitt[1], Humberto Parra[1], Washington Sandoval[1] and Willington Rentería[5]

*Corresponding author: ttoulkeridis@espe.edu.ec

[1]Universidad de las Fuerzas Armadas ESPE, Sangolquí, **ECUADOR**.
[2]Facultad de Economía, Pontificia Universidad Católica del Ecuador, Quito, **ECUADOR**.
[3]Laboratorio do Territorio, Universidad de Santiago de Compostela, Lugo, **ESPAÑA**.
[4]Pontificia Universidad Católica del Ecuador Sede Esmeraldas – PUCESE, Esmeraldas, **ECUADOR**.
[5]Instituto Oceanográfico de la Armada INOCAR, Guayaquil, **ECUADOR**.

ABSTRACT

Tsunamis are destructive forces which threaten life, social infrastructure and production, resulting in enormous economic losses. In the last two decades destructive tsunamis as those in Indonesia (2004), Japan (2011) and Chile (2010 and 2015), caused more than 366,353 deaths and economic losses over 355 billions US$. Our present study focuses on a theoretical case of economic and human losses that tsunami impact can have in Muisne, along the central Ecuadorian coast. Using a cost benefit analysis (BCA) framework, we estimate the cost of recovery of a mangrove ecosystem in Muisne, where earthquakes with magnitudes up to 8.8 Mw can generate tsunamis with run-ups up to 43 meters. Economic benefits of environmental goods and services from Muisne mangroves are estimated to reach 16.7 US$ million/year. To maintain local wellbeing and businesses in the region, it is estimated that the mangrove recovery costs may reach up to 7.3 million US$. In terms of preventing loss human loss of life and maintaining human wellbeing, we calculate the value of community relocation to be approximately 93.2 million US$. Therefore, the total economic benefits from a recovering the Muisne ecosystem would be around 109.9 million US$ and the benefit/cost ratio is B⁄C=1.16, meaning that the recovery of the Muisne mangroves has a higher value than resettlement costs, and that makes good public policy sense.

Keywords: *Tsunami strike, Resettlement, Mangrove ecosystem recovery, Benefit / cost ratio, Ecuador*

1. INTRODUCTION

There is a thin line in the evaluation of the economic implications of maintaining or leaving a disaster threatened area, of recovering a naturally protected area and of considering the costs of relocating people in more secure zones, while preserving their jobs, way of life and the needed commerce and business infrastructure. However, destructive tsunamis can cause high economic losses, which can impact enormously the infrastructure of a region and result in high losses of human lives. For example, the 2011 tsunami in Japanw generated from a 9.0 M_w earthquake, caused 15,853 deaths, injured 6,023 and of 3,282 people missing (Chen and Sato, 2013). According to Japan's National Policy Agency 300,000 building were destroyed, as well as 4,000 roads, 78 bridges, and 29 railways were affected. The economic damage reached 210 billion US$, of which some 66.9 billion were insured lost (Aon Benfield, 2015). One year earlier another tsunami from an 8.8 Mw earthquake in Concepcion Chile, resulted in catastrophic damages throughout the country. About 500 people lost their lives, at least 1,5 million homes were damaged, of which one third were completed destroyed. The economic cost of the disaster was estimated at 30 billion US$, with 8.5 insured lost (Barcená *et al*., 2010). A more recent 8.3 Mw tsunamigenic earthquake in 2015 near Coquimbo, Chile, resulted in an estimated loss ranging between 100 million US$ and up to 1 billion US$(CEDIM, 2015; Aránquiz et al., 2016; Ye et al., 2016). On Christmas 2004, a devastating tsunami struck Indonesia and Thailand causing 350,000 deaths and an estimated 15 billion US$ of immediate economic losses (Athukorala & Resosudarmo, 2005; Jayatilleke and Naranpanawa, 2007).

Due to enormous financial damages the recovery of natural defense habitats and community resettlement should be considered as part of any mitigation plan. Resettling the population requires of a very considered, careful and detailed planning, as the International Finance Corporation (IFC) pointed out in their resettlement handbook published in 2002 (English and Brusberg, 2002). A resettlement process implies displacement of human population which may cause disturbance as well, as it affects housing, employment, commerce and often the way of life. However, if the damage costs are overwhelming higher, governments should consider resettlement as an alternative before a disaster strikes.

On the other hand, natural habitats such as mangroves play an important role of reducing the impact of a tsunami (Mazda et al., 2006; Tanaka et al., 2007; Chatenoux and Peduzzi, 2007; Tanaka, 2009; Osti et al., 2009). A report from the Environmental Justice Foundation points out the overall importance of mangroves as natural barriers against typhoons, cyclones, hurricanes, and tsunamis (EJF, 2006). Mangroves help minimize the loss of human life and damage to property by reducing the heights and speed of tsunami waves, as well as redistributing the incoming water flow throughout channels and creeks (EJF, 2006). Therefore, governments as well as regional or even local authorities should consider mangroves in recovering or reforestation costs as part of a useful disaster mitigation investment.

Ecuador has been in past particularly vulnerable to a variety of natural hazards (Charvériat, 2000; Guha-Sapir et al., 2004; Cavallo and Noy, 2009; Toulkeridis, 2011; 2013; Toulkeridis and Zach, 2016; Mato and Toulkeridis, 2017). Ecuador´s extensive coastlines are vulnerable to tsunamis and earthquakes because of the region's geodynamic location on the continental shelf and the proximity to the Ecuadorian trench, where the Nazca oceanic plate subducts below the Caribbean and South American continental plates (Kellogg and Vega, 1995; Gutscher et al., 1999; Gusiakov, 2005; Egbue and Kellog, 2010; Pararas-Carayannis, 2012). At least six notable tsunamis occurred in the Ecuadorian coasts. A magnitude 8.8 M_w earthquake and destructive tsunami in 1906 struck the Esmeraldas Province, causing up to 1,500 deaths and the destruction of 450 houses (Kanamori and McNally, 1982; USGS, 2016; Chunga et al., 2017). In this context, a recent study demonstrated a small coastal village named San Vicente to be highly vulnerable to tsunamis, flooding, landslides and mud flows. Due to the village's vulnerability, it was documented that recovery of the habitat with mangroves and resettlement may be relatively cheap and efficient mitigation investment to draw up for public policy attention (Cruz D' Howitt et al., 2010; Rodriguez et al., 2016).

2. TSUNAMI HAZARDS IN THE AREA OF MUISNE AND SURROUNDING

Tsunamis can an enormous impact on coastal areas. Abe et al. (2012) determined that Japan's 2011 tsunami inundation reached a maximum of 4 km inland, but based on measurements of debris deposits it was determined that 90 percent of the inland inundations reached less than 2.5 km. Once the transects for the determination of inundation were settled, they added the topography (elevation) features using RTK GPS instruments. This allowed for a more accurated determination of the extent of tsunami deposits and inundation distance in the field (Abe et al., 2012).

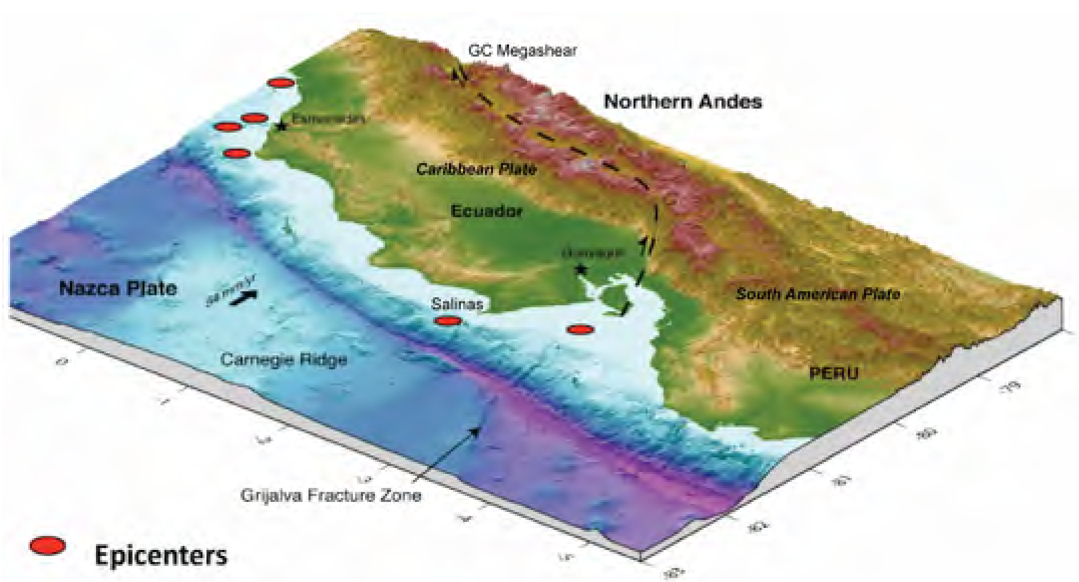

Fig. 1: Panoramic view of the morphology of western Ecuador and location of seismic epicenters, which generated tsunamis in the last 110 years. (Adapted and modified from Collot et al., 2004).

The specific geodynamics and the geological setting of Muisne and its surrounding have been analyzed and presented in Toulkeridis et al. (2017a; Fig. 1). The area of Muisne is threatened by a variety of tsunami scenarios (Fig. 1, 2, 3), all of which would affect severely this part of the Ecuadorian coastline. Extremely destructive tsunamis may be generated by earthquakes with magnitudes of up to 8.8 M_w and wave run-ups may have runups of up to 43 meters (Toulkeridis et al., 2017a). These parameters have been based on the modeling of tsunamis along the coast taking into consideration past tsunamis of local origins during the last two centuries (Rudolph and Szirtes, 1911; Kelleher, 1972; Beck and Ruff, 1984; Kanamori and McNally, 1982; Swenson and Beck, 1996; Pararas-Carayannis, 2012; Toulkeridis et al., 2017b; 2017c; Rodriguez et al., 2016), while evidences of paleo-tsunami deposits are scarce (Chunga and Toulkeridis, 2014; Chunga et al., 2017).

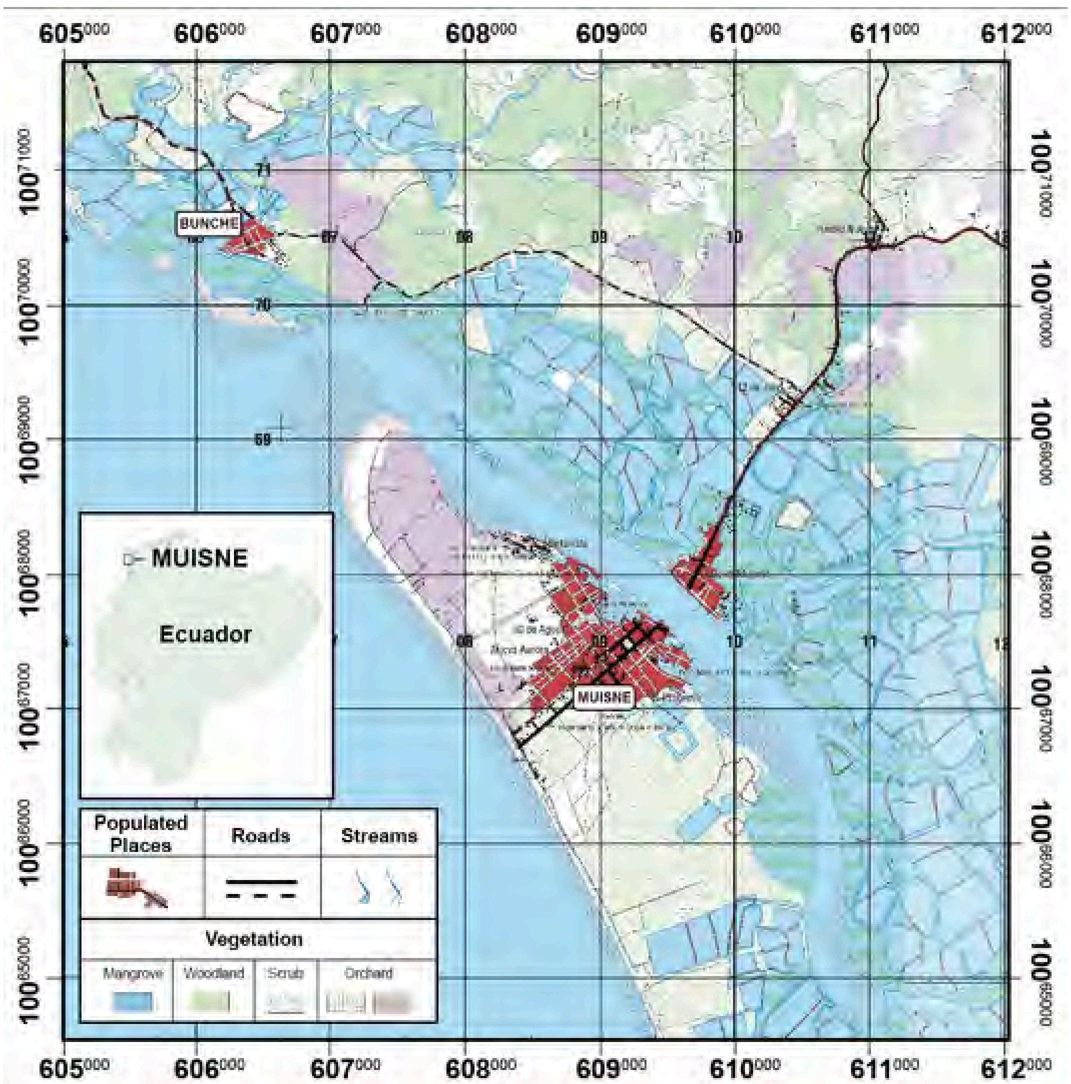

Fig. 2: Location of Muisne and Bunche within Ecuador and topographic area of the mentioned sites

The most prominent examples of tsunamis along the Ecuador–Colombia subduction zone include those generated from earthquakes in 1906 (M_w=8.8), in 1942 (M_w=7.8), in 1958 (M_w=7.7), in 1979 (M_w=8.2) and in 2016 (M_w=7.8) within the 600-km long rupture area of the great 1906 event (Collot et al., 2004; Toulkeridis et al., 2017b; 2017c). While the 1906 event caused the death of up to 1500 persons in Ecuador and Colombia, the 1979 tsunami killed in Colombia at least 807 persons (Pararas-Carayannis, 1980).

Fig. 3: Tsunami hazard modeling of three different scenarios, based on Toulkeridis et al. (2017). Location of Muisne, Bunche and proposed relocation site (in yellow).

3. COSTS OF HABITAT RECOVERY AND COMMUNITY RELOCATION

The economic analyses for mangroves habitat recovering and community resettlement has been based on a cost benefit analysis (BCA) framework. BCA framework is perfectly suited to analyze public investment, which is the essential in our analysis (Zerbe et al., 2010; Hanly and Spash, 1993). We have used a benefit cost ratio to set up a comparison between potential economic damages due to the impact of a tsunami, habitat recovering and community resettlement costs in Muisne. The benefit cost ratio has been expressed as follows:

$$\frac{B}{C} = \frac{\sum_{t=0}^{T} \frac{b_t}{(1+r)^t}}{\sum_{t=0}^{T} \frac{c_t}{(1+r)^t}} \qquad (1)$$

Where, bt are benefits of the project over time, ct are the costs over time, r is the discount rate, and t is the time period. In this study, benefits are denoted by bypassed cost of potential tsunami economic damages on the infrastructure of Muisne only. We did not take into account other potential economic damages on commerce, fisheries, agriculture, livestock production as well as human life through potential householders' income loss as Rodriguez *et. al* (2016) pointed out in their study on potential effects of a tsunami in another coastal town in Ecuador. The resettlement costs of the entire community of Muisne, includes land acquisition cost.

Resettlement costs (RC) have two major components, land acquisition (L) and housing, public services and infrastructure costs for a new community (Cn). Land acquisition has been a relatively straightforward estimation, price of land at the area (average price paid in historical land transactions in the area) and land's area, which has been estimated using SIG tools ($L=p\times Q$). Resettlement costs of a new community (Cn) has been more difficult since we had to include values for each public services, housing for householder, public buildings, open spaces, schools, hospitals, communication networks, commercial buildings among others. There has been a lack of information regarding towns' planning and development from Ecuador; instead we have used guidelines and regulations from Communities of Granada and Galicia (Spain) for urban land and use planning. We have used such information as these communities share a similar vision of how to display the man-land relationship with towns in Ecuador. These guidelines and regulations relate people with building areas and these with the minimum required space that it should take into account to build a sustainable space. Resettlement costs have been defined as:

$$Rs=i=1nL,Cn \qquad (2)$$

In addition, we included as part of the total costs, all recovering costs needed to a mangrove habitat functioning. Recovering costs included mangle tree planting, recovering natural hydrological function. Furthermore, recovering costs included soil recuperation costs that included recovering soil natural functioning from abandoned shrimp's farms, as well as recovering of soil functioning from areas where the city of Muisne is currently located and soil contamination related to the city (Table 1). The values of these different costs were estimated from different mangle recuperating studies

(Bayraktarov et al., 2016; GreenFlash Technologies, 2015; Shinde and Donde, 2015; Qadir et al., 2014; Dominati and Mackay, 2013; Marchand, 2008; Goldstein and Ritterling, 2001; Lewis, 2001).

Table 1: Estimates of costs implied in the recovery of the mangrove ecosystem of Muisne

MANGROVE RECOVERING COSTS	AREA (ha)	COSTS/UNIT (US$/ha)	TOTAL COSTS (US$)
PLANTING MANGLE TREES	591,3	8961	5.298.639,30
RECOVERING TIDAL FLOW	591,3	700	413.910,00
RECOVERING SALT-SOIL	290,8	1191	346.342,80
RECOVERING COMPACTED-SOIL	68,9	300	20.670,00
RECOVERING SOIL CONTAMINATION	300,5	4200	1.262.100,00
TOTAL	1842,8	15352	7.341.662,10

The total costs now may be defined as:

$$TC=Rs,Rc \qquad (3)$$

where,

$Rs=Resettlement\ cost\ in\ US\$$

$Rc=Mangrove\ recovering\ cost\ \ in\ US\$$

The total costs of the city of Muisne resettlement reached a value of about 93.15 million US$, being approximately 5 million US$ more than the Ecuadorean´s governmental estimation of its resettlement program of Muisne in Bunche.

Furthermore, the Muisne mangrove ecosystem benefits have been defined as the sum of all benefits from a healthy and well-functioning ecosystem and the avoided costs of housing and infrastructure. Therefore, the total benefits of Muisne' mangrove ecosystem may be defined as:

$$TB=i,jnBi,ACj \qquad (4)$$

where
$Bi=$ *Economic benefits from ecosystem goods and services in US$*
$ACj=$ *Avoided cost of Muisne housing and infrastructure in US$*

Economic values of total benefits have been estimated from studies regarding environmental services in mangrove forests and potential earnings and/or ecosystem services monetary value assessment (Malik et al., 2015; UNEP, 2011; UNEP, 2014; Giri et al., 2008; Corbishley and Pearce, 2007; Shuichi, 2004; Rivera, 2001; Sathirathai, 2000; Cabrera et al., 1998; Gammage, 1997; Barbier et al., 1997; Padilla and Janssen, 1996; Pearce, 1993; Ruitenbeek, 1992). Based on these studies, we have estimated the value of Muisne's mangrove ecosystem and its services. The highest value has been calculated from fisheries (Table 2) and it is estimated from all efforts to capture fish species that use mangrove forest as a nursery area, being some 93,149,958.06 million US$.

Table 2: Economic benefits estimation of Muisne's mangrove good and services

MANGROVE SERVICES	US$/ha/yr	Total Benefits
FLOOD MITIGATION	911,00	1.678.790,80
FILTERING NUTRIENTS AND CONTAMINANTS	1.800,00	3.317.040,00
DECOMPOSITION OF WASTE	127,00	234.035,60
SOIL CARBON STORAGE (937 Tc-ha-1)	327,95	604.346,26
MANGROVE CARBON STORAGE (2,42 Tc/ha)	0,93	1.709,20
FISHERIES	5.500,00	10.135.400,00
COASTLINE PROTECTION	238,93	440.305,36
RESEARCH VALUE	184,40	339.812,32
TOTAL	9090,21	16.751.439,54

Flood mitigation, which is the environmental service provided by a mangrove forest in case of an impact by a tsunami, is also important in economic terms with an estimated 1.7 million US$. Even though table 2 lists just a few of goods and services that a mangrove may provide, the total amount of 16.7 million US$ per year is a significant economic benefit.

Furthermore, potential losses of housing and infrastructure in the Island of Muisne and of "Nuevo Muisne", an illegitimate settlement the continent just in front of the main city of Muisne, has been estimated to strike some 93,149,958.06 million US$. The analysis did not take into account several costs such as market losses, commerce, potential earnings losses and personal consumption offsets. We did not consider both local and government taxes such as property taxes and income tax, value-added tax, neither income increases throughout time, and worklife discounts. Thus, these estimates certainly will be much higher.

The total economic benefits from recovering the ecosystem of Muisne would be some 109.9 million US$. Additionally, we calculated the benefit/cost ratio to observe if this resettlement proposal makes an economic sense, resulting to a $BC=1.16$, which indicates an economic benefit. Therefore, the ratio allows us to conclude that in terms of human life, housing, and infrastructure and business relocation of Muisne should be severely considered by the state, regional and local authorities as well as policy makers.

4. CONCLUSIONS

We estimated the value of a mangrove ecosystem recovery to influence policy decision making, as such reforestation helps to protect or mitigate susceptible areas of tsunamis in Muisne, along the central coast of Ecuador. The estimated mangrove recovery raised to some 109.9 million US$, which is significant, and hereby higher than the resettlement costs of the actual site of Musine Recovering Muisne mangrove will provide an estimate of 16 US$ million annually and secure ways of living of approximately 60% of the actual population. The B/C ratio of 1.16 demonstrates that such a project as proposed is of high efficiency. This calculated ratio also allows to conclude, that recovering of the Muisne mangrove at any scenario has a higher value than the potential resettlement costs. Therefore, the mangrove recovering means in terms of ways of living, housing, infrastructure and business relocation of Muisne needs to be considered by the policy makers. As resettlement usually occurs after a disaster stroke, our study suggests a preventing public policy, by using well-known evaluation tools such as BCA, SIG and other analysis tools.

ACKNOWLEDGMENTS

We thank the Universidad de las Fuerzas Armadas ESPE for logistic and financial support. Fernando Mato acknowledges support from the Prometeo Project of the National Secretariat of Higher Education, Science, Technology and Innovation (SENESCYT), Ecuador.

REFERENCES

Abe, T., Goto, K. and Sugawara, D. 2012: Relationship between the maximum extent of tsunami sand and the inundation limit of the 2011 Tohoku-oki tsunami on the Sendai Plain, Japan. Sedimentary Geology 282: 142-150.

Aon Benfield, 2015. 2014 Annual Global Climate and Catastrophe Report, Impact Forecasting. Aon Benfield Risk, Reinsurance and Human Resources. Aon plc.: 68pp

Aránguiz, R., González, G., González, J., Catalán, P.A., Cienfuegos, R., Yagi, Y., Okuwaki, R., Urra, L., Contreras, K., Del Rio, I. and Rojas, C., 2016. The 16 September 2015 Chile tsunami from the post-tsunami survey and numerical modeling perspectives. Pure and Applied Geophysics, 173(2), pp.333-348.

Athukorala, P.C. and Resosudarmo, B.P., 2005. The Indian Ocean tsunami: Economic impact, disaster management, and lessons. Asian Economic Papers, 4(1): 1-39.

Barbier, E.B., Acreman, M. and Knowler, D., 1997: Economic valuation of wetlands: A guide for policymakers and planners, the Ramsar Convention Bureau, Gland, Switzerland: 116-149.

Barcená, A., Prado, A., López, L. and Samaniego, J.L., 2010. The Chilean earthquake of 27 of February 2010: an overview. Disaster Assessment Unit of ECLAC, United Nations Publications, Santiago, Chile: 32pp.

Bayraktarov, E., Saunders, M.I., Abdullah, S., Mills, M., Beher, J., PossIngham, H.P., MumBy, P.J. and Lovelock, C.E., 2016. The cost and feasibility of marine coastal restoration. Ecological Applications, 26(4): 1055–1074.

Beck, S.L. and Ruff, L.J., 1984: The rupture process of the great 1979 Colombia earthquake: evidence for the asperity model. J.Geophys. Res.89: 9281–9291

Cabrera, M.A. Seijo, J.C., Euan, J. and Pérez, E., 1998: Economic Values of Ecological Services from a Mangrove Ecosystem. Intercoast Network, International Newsletter of Coastal Management # 32. Focus on: Coastal Economics. Narragansett, Rhode Island: 1-2.

Cavallo, E.A. and Noy, I., 2009: The economics of natural disasters: a survey. IDB WORKING PAPER SERIES No. IDB-WP-124: 49pp

CEDIM, 2015: Massive deadly earthquake near Illapel (Coquimbo coast), Chile - at least 16 people killed - Pacific Ocean tsunami. At http://earthquake-report.com/2015/09/16/massive-earthquake-near-coast-of-central-chile-on-september-16-2015/

Charvériat, C., 2000: Natural disasters in Latin America and the Caribbean: An overview of risk. Research Department Working papers series, 434: 104pp

Chatenoux, B. and Peduzzi, P., 2007. Impacts from the 2004 Indian Ocean Tsunami: analysing the potential protecting role of environmental features. Natural Hazards, 40(2): 289-304.

Chen, S.W. and Sato, M., 2013. Tsunami damage investigation of built-up areas using multitemporal spaceborne full polarimetric SAR images. IEEE Transactions on Geoscience and Remote Sensing, 51(4), pp.1985-1997.

Chunga, K. and Toulkeridis, T. (2014). First evidence of paleo-tsunami deposits of a major historic event in Ecuador. Science of Tsunami Hazards, 33: 55-69.

Chunga, K., Toulkeridis, T., Vera-Grunauer, X., Gutierrez, M., Cahuana, N. And Alvarez, A., 2017: A review of earthquakes and tsunami records and characterization of capable faults on the northwestern coast of Ecuador. Science of Tsunami Hazards, 36: 100-127.

Collot, J.Y., Marcaillou, B., Sage, F., Michaud, F., Agudelo, W., Charvis, P., Graindorge, D., Gutscher, M.A. and Spence, G., 2004. Are rupture zone limits of great subduction earthquakes controlled by upper plate structures? Evidence from multichannel seismic reflection data acquired across the northern Ecuador–southwest Colombia margin. Journal of Geophysical Research: Solid Earth, 109(B11).

Corbishley, J. and Pearce, D., 2007: Growing trees on salt-affected land, ACIAR Impact Assessment Series Report No. 51: 46 pp.

Cruz D'Howitt, M., M.C, Acosta, and N.E. Vásquez. 2010. Riesgo por Tsunami en la Costa Ecuatoriana. Instituto Panamericano de Geografía e Historia, Sección Nacional del Ecuador , Organización de los Estados Americanos – OEA. Publicaciones.15pp.

Dominati, E. and Mackay, A., 2013: An Ecosystem Services Approach to the Cost of Soil Erosion and Value of Soil Conservation, Report prepared for: Hawke's Bay Regional Council, Land and Environment, AgResearch Limited-Grasslands Research Centre, Palmerston North, New Zealand: 50 pp.

Egbue, O. and Kellogg, J., 2010: Pleistocene to Present North Andean "escape". Tectonophysics 489: 248-257.

EJF, 2006: Mangroves: Nature's defence against Tsunamis—A report on the impact of mangrove loss and shrimp farmdevelopment on coastal defences. Environmental Justice Foundation, London, UK. 33 pp.

English, R., and Brusberg, F.E., 2002. Handbook for Preparing a Resettlement Action Plan. International Finance Corporation, Environmental and Social Development Department. Washington DC. 93 pp.

Gammage, S., 1997: Estimating the Returns to Mangrove Conversion: Sustainable Management or Short Term Gain?, Environmental Economics Programme Discussion Paper DP 97-02, International Institute for Environment and Development IIED, London UK: 56 pp.

Giri, C., Zhu, Z., Tieszen, L.L., Singh, A., Gillette, S. and Kelmelis, J.A., 2008: Mangrove forest distributions and dynamics (1975–2005) of the tsunami-affected region of Asia, Journal of Biogeography 35: 519–528.

Goldstein, M. and Ritterling, J., 2001: A Practical Guide to Estimating Cleanup Costs, U.S. Environmental Protection Agency Papers. Paper 30: 103-121

GreenFlash Technologies LLC, 2015: Saline-Sodic Soils Remediation, GreenFlash Technologies LLC-Solutions Driven by Nature, Costa Mesa CA: 7 pp.

Guha-Sapir, D., Hargitt, D. and Hoyois, P., 2004. Thirty years of natural disasters 1974-2003: The numbers. Presses univ. de Louvain, Belgium: 190pp

Gusiakov, V.K., 2005: Tsunami generation potential of different tsunamigenic regions in the Pacific. Marine Geology, 215, 1-2: 3-9.

Gutscher, M.A., Malavieille, J.S.L. and Collot, J.-Y., 1999: Tectonic segmentation of the North Andean margin: impact of the Carnegie ridge collision. Earth Planet. Sci. Lett. 168: 255–270.

Hanley, N. and Spash. C.L., 1993: Cost-benefit Analysis and the Environment.Aldershot, Hants, England: E. Elgar: 288pp

Jayatilleke, B. and Naranpanawa, A., 2007. The economic effects of the Asian tsunami on the tear drop in the Indian Ocean: a general equilibrium analysis. South Asia Economic Journal, 8(1): 65-85.

Kanamori, H. and McNally, K.C., 1982. Variable rupture mode of the subduction zone along the Ecuador-Colombia coast. Bulletin of the Seismological Society of America, 72(4), pp.1241-1253.

Kanamori, H. and McNally, K.C., 1982. Variable rupture mode of the subduction zone along the Ecuador-Colombia coast. Bulletin of the Seismological Society of America, 72(4), pp.1241-1253.

Kelleher, J.A., 1972: Ruptures zones of large South American earthquakes and some predictions. Journal of Geophysical Research, 77, 11: 2087-2103.

Kellogg, J.N. and Vega, V., 1995: Tectonic development of Panama, Costa Rica and the Colombian Andes: Constraints from Global Positioning System geodetic studies and gravity. Geol. Soc. Am. Special Paper 295, 75–90.

Lewis III, R.R., 2001: Mangrove Restoration - Costs and Benefits of Successful Ecological Restoration, In: Proceedings of the Mangrove Valuation Workshop, Universiti Sains Malaysia, Penang, 4-8 April, 2001. Beijer International Institute of Ecological Economics, Stockholm, Sweden: 18 pp.

Malik, A., Fensholt, R., and Mertz, O., 2015: Economic Valuation of Mangroves for Comparison with Commercial Aquaculture in South Sulawesi, Indonesia, Forests, 6: 3028-3044.

Marchand, M. 2008: Mangrove restoration in Vietnam: Key considerations and a practical guide. Report prepared for WRU / TUD, T2666. Deltares: 42 pp.

Mato, F. and Toulkeridis, T., 2017: The missing Link in El Niño's phenomenon generation. Science of Tsunami Hazards, 36: 128-144.

Mazda, Y., Magi, M., Ikeda, Y., Kurokawa, T. and Asano, T., 2006. Wave reduction in a mangrove forest dominated by Sonneratia sp. Wetlands Ecology and Management, 14(4): 365-378.

Osti, R., Tanaka, S. and Tokioka, T., 2009. The importance of mangrove forest in tsunami disaster mitigation. Disasters, 33(2): 203-213.

Padilla, J.E. and Janssen, R., 1996: Extended benefit-cost analysis of management alternatives: Pagbilao mangrove forest, Journal of Philippine Development, 42, XXII No. 2: 339-363.

Pararas-Carayannis, G. 1980: The Earthquake and Tsunami of December 12, 1979, in Colombia. Intern. Tsunami Information Center Report, Abstracted article in Tsunami Newsletter, Vol. XIII, No. 1.

Pararas-Carayannis, G., 2012: Potential of tsunami generation along the Colombia/Ecuador subduction margin and the Dolores-Guayaquil Mega-Thrust. Science of Tsunami Hazards, 31, 3: 209-230.

Pearce, D.W., 1993: Economic Values and the Natural World, The MIT Press. Cambridge, Massachusetts: 143pp

Qadir, M., Quillerou, E., Nangia, V., Murtaza, G., Singh, M., Thomas, R. J., Drechsel, P. and Noble, A.D., 2014: Economics of salt-induced land degradation and restoration. Natural Resources Forum, 38: 282-295. doi: http://dx.doi.org/10.1111/1477-8947.12054

Rivera, E.S., 2001: Valoración Económica de Servicios Ambientales Prestados por Ecosistemas: Humedales en México, Estudios PEA-RI-2001-001 Instituto Nacional de Ecología, Dirección General de Investigación en Política y Economía Ambiental, Secretaría de Medio Ambiente y Recursos Naturales SEMARNAT, México DF: 45 pp.

Rodriguez, F., D'Howitt, M.C., Toulkeridis, T., Salazar, R., Romero, G.R., Moya, V.R. and Padilla, O., 2016: Economic evaluation and significance of early relocation vs. complete destruction by a potential tsunami of a coastal city in Ecuador, Science of Tsunami Hazards., 35 (1): 18-33.

Rudolph E. and Szirtes S., 1911: Das kolumbianische Erdbeben am 31 Januar 1906, Gerlands Beitr. z. Geophysik, 2: 132- 275.

Ruitenbeek, H.J., 1992: Mangrove Management: An Economic Analysis of Management Options with a Focus on Bintuni Bay, Irian Jaya, EMDI Environmental Reports 8, Dalhousie University, Halifax, Nova Scotia: 53 pp.

Sathirathai, S., 2000: Economic Valuation of Mangroves and the Roles of Local Communities in the Conservation of Natural Resources: Case Study of Surat Thani, South of Thailand, Research Reports-International Development Research Centre, Ottawa, Canada: 38 pp.
Shinde, P. S. and Donde, S.S., 2015: Impact of mangrove pollution and devastation: a study for sustainable measures, International Research Journal of Natural and Applied Sciences, 2, (6): 178-185.
Shuichi, I., Kiyoshi, F., Motohiro, K., Ryo, W., and Shinji, T., 2004: Relationship between mangrove vegetation and micro-topography, and carbon storage of Kandelia candel (L.) Druce forests in Amami-ohshima Island, southwestern Japan, Japanese Journal of Forest Environment, 46:1 9-19.
Tanaka, N., 2009. Vegetation bioshields for tsunami mitigation: review of effectiveness, limitations, construction, and sustainable management. Landscape and Ecological Engineering, 5(1): 71-79.
Tanaka, N., Sasaki, Y., Mowjood, M.I.M., Jinadasa, K.B.S.N. and Homchuen, S., 2007. Coastal vegetation structures and their functions in tsunami protection: experience of the recent Indian Ocean tsunami. Landscape and Ecological Engineering, 3(1): 33-45.
Toulkeridis, T., 2011: Volcanic Galápagos Volcánico. Ediecuatorial, Quito, Ecuador: 364 pp
Toulkeridis, T., 2013: Volcanes Activos Ecuador. Santa Rita, Quito, Ecuador: 156pp
Toulkeridis, T. and Zach, I., 2016: Wind directions of volcanic ash-charged clouds in Ecuador – Implications for the public and flight safety. Geomatics, Natural Hazards and Risks, DOI:10.1080/19475705.2016.1199445
Toulkeridis, T., Parra, H., Mato, F., Cruz D´Howitt, M., Sandoval, W., Padilla Almeida, O., Rentería, W., Rodríguez Espinosa, F., Salazar martinez, R., Cueva Girón, J., Taipe Quispe, A. and Bernaza Quiñonez, L., 2017a: Contrasting results of potential tsunami hazards in Muisne, central coast of Ecuador. Science of Tsunami Hazards, 36: 13-40.
Toulkeridis, T., Mato, F., Toulkeridis-Estrella, K., Perez Salinas, J.C., Tapia, S. and Fuertes, W., 2017b: Real-Time Radioactive Precursor of the April 16, 2016 Mw 7.8 Earthquake in Ecuador. Lecture Notes in Computer Science, Proceedings ITISE 2017, Granada, Spain: 207-219.
Toulkeridis, T., Chunga, K., Rentería, W., Rodriguez, F., Mato, F., Nikolaou, S., Cruz D´Howitt, M., Besenzon, D., Ruiz, H., Parra, H. and Vera-Grunauer, X., 2017c: The 7.8 M_w Earthquake and Tsunami of the 16th April 2016 in Ecuador - Seismic evaluation, geological field survey and economic implications. Science of Tsuanami Hazards, in press
UNEP (United Nations Environment Programme), 2011: Economic Analysis of Mangrove Forests: A case study in Gazi Bay, Kenya, UNEP, iii+: 42 pp.
UNEP (United Nations Environment Programme), 2014: The Importance of Mangroves to People: A Call to Action. van Bochove, J., Sullivan, E., Nakamura, T. (Eds). United Nations Environment Programme World Conservation Monitoring Centre, Cambridge: 128 pp.
USGS (United States Geological Survey), 2016: Earthquake Hazards Program. http://http://web.archive.org/web/20130502223428/http://earthquake.usgs.gov/earthquakes/recenteqsww/Quakes/usc0001xgp.php

Ye, L., Lay, T., Kanamori, H. and Koper, K.D., 2016. Rapidly estimated seismic source parameters for the 16 September 2015 Illapel, Chile M w 8.3 earthquake. Pure and Applied Geophysics, 173(2), pp.321-332.

Zerbe, R.O Jr, T.B. Davis, N. Garland, and T. Scott. 2010. Toward Principles and Standards in the Use of Benefit-Cost Analysis. Benefit Cost Analysis Center, University of Washington. Seattle WA: 115 pp.

ISSN 8755-6839

SCIENCE OF **TSUNAMI HAZARDS**

Journal of Tsunami Society International

Volume 36 **Number 4** **2017**

TSUNAMI SOCIETY INTERNATIONAL, 1741 Ala Moana Blvd. #70, Honolulu, HI 96815, USA.

WWW.TSUNAMISOCIETY.ORG